ARIZONA DEPARTMENT OF WATER RESOURCES

2021 Prescott AMA Groundwater Flow Model Update

June 2021

Acknowledgments

Arizona Department of Water Resources staff contributing to this report include John Mawarura, Keith Nelson, Olga Hart, Dianne Yunker and Jeff Inwood. For insightful discussions about the area hydrology, the authors would like to thank Bill Remick, Don Pool, Frank Corkhill, Justin Clark, Abe Springer and Doug McMillan.

Cover photo – View of Del Rio Springs (facing east), circa 2000. Photo courtesy of Jim Holt.

Table of Contents

Acronyms and Abbreviations

Acronym	Description
ACM	Alternative conceptual model
ADWR	Arizona Department of Water Resources
AF	Acre-feet
AF/yr	Acre-feet per year
AMA	Active Management Area
BIC	Big Chino
cfs	Cubic feet per second
CI	Confidence interval
CSS	Composite-scaled sensitivity
CVID	Chino Valley Irrigation District
EVT	Evapotranspiration
ft	Feet
GHB	General head boundaries
GWSI	Groundwater Site Inventory
HOB	Head observation
K_x	Horizontal hydraulic conductivity
LIC	Little Chino
LVU	Lower Volcanic Unit - Layer 2
MFR	Mountain Front Recharge
NAU	Northern Arizona University
ROGR	Registry of Groundwater Rights
standev	Standard deviation
UAF	Upper Agua Fria
UAU	Upper Alluvial Unit -Layer 1
USF	Underground storage facility
USGS	United States Geological Survey

Executive Summary

The 2021 Prescott Active Management Area (AMA) groundwater flow model was updated and recalibrated to represent hydrologic conditions in the Little Chino (LIC) and Upper Agua Fria (UAF) sub-basin from 1939 to 2019. The model simulates groundwater flow dynamics associated with the Upper Alluvial Unit (UAU) and Lower Volcanic Unit (LVU) aquifers. As part of the model update process, numerous alternative conceptual models (ACMs) were developed and tested for plausibility. Each ACM was optimized using non-linear regression by constraining core model parameters (hydraulic conductivities, aquifer storage terms, and recharge rates) to available target data including observed groundwater levels and regional groundwater discharge. The calibration was consistent with the methods and guidelines established by the USGS (Hill, 1998). Although the 2021 updated model is generally consistent with the previous release (Nelson and Yunker, 2014), in the 2021 update several portions of the model were refined, including the Santa Fe Well field, the northern and southern model boundaries, the Williamson Valley area, as well as locations near present-day underground storage facilities (USF).

Many ACMs were investigated during this model update. Each ACM was optimized using inverse modeling techniques by constraining the acceptable solution to best fit the available 3,962 head and 248 flow targets. Head and flow targets serve as guideposts for tracking basin behavior over time. However, they are secondary (or indirect) measurements of groundwater flow through an aquifer. Further, they are composite metrics which reflect the response of the basin to unknown (or imperfectly known) stresses to a similarly imperfectly known 'mesh' or underlying hydrogeologic structure. The more observations of heads and flow that are available, the more tightly the possible combination of stress/structure pairings can be constrained. Because there exists uncertainty both with respect to the exact spatially varying geohydrologic structure of the basin, and with respect to the temporally varying historic stresses imposed on it, there will, likewise, exist a range of multiple possible solutions that satisfy the observations and any other prior conceptual knowledge of the basin. Thus, it is unreasonable to assume any one single ACM fully and exactly captures the regional-scale groundwater flow system, its structure, or the stresses imposed on it during the historic period.

As a result, head solutions for plausible ACMs were grouped together to form ensembles. The ensemble results are presented for selected sites throughout the model area. The ensemble distributions provide a more comprehensive estimate of uncertainty: areas of the model in which results show wider head distributions reflect areas that are simulated with lesser certainty. The converse is also true: in areas where the ensemble results are more self-consistent and the range in simulated heads is narrower, a greater degree of certainty can be expected. Analyzing ensemble results consisting of equally likely ACM's in combination with potential boundary conditions may assist in developing a more complete understanding of future groundwater conditions. This is particularly true for locations where future groundwater conditions (heads and flows) are anticipated to extend far beyond the calibration range. The resulting head and flow solutions, thus, form a distribution that can be used to better understand the groundwater flow system and associated uncertainty.

One ACM (referred to as the 'base model') was selected for release and used for the presentation of model-error statistics and water budgets. The base model was calibrated to produce mean and absolute mean head errors of -1.2 ft and 12 ft, respectively, where the error is calculated as observed minus simulated heads. The base model accurately represents regional-scale groundwater discharge patterns in the LIC and UAF sub-basins, both in trend and magnitude. At the groundwater-fed Del Rio Springs, long-term pumping in the LIC Sub-basin has significantly reduced the rate of spring discharge. Pumping in the UAF sub-basin has also impacted groundwater discharge to the stream along the Agua Fria River. Capture along the Agua Fria River has, historically, induced additional recharge to the aquifer by facilitating greater infiltration of streamflow during episodic flood events. Because the Agua Fria River is in direct hydraulic connection with the stream-aquifer system of limited storage capacity, sustained stream-induced recharge from groundwater pumping may result in the retraction of downgradient streamflow, all else equal.

Between 1939 and 2019, the model simulated 1.4 million acre-feet (AF) of groundwater pumping, corresponding to a long-term annualized average rate of 17,571 acre-feet per year (AF/yr). The cumulative net change-in-storage was simulated at 583,038 AF; thus, the long-term aquifer storage-loss rate simulated between 1939 and 2019 was 7,300 AF/yr.

1. Introduction

1.1. Objective and Scope

The objective of this report is to document the latest update and recalibration of the 2021 Prescott Active Management Area (AMA) groundwater flow model (the model). The Prescott AMA covers portions of the Little Chino (LIC) and Upper Agua Fria (UAF) sub-basins, and the model simulates groundwater flow conditions associated with the Layer 1 - Upper Alluvial Unit (UAU) and Layer 2 - Lower Volcanic Unit (LVU) aquifers between 1939 and 2019. Refer to **Figure 1** for the 2021 Prescott AMA model location map.

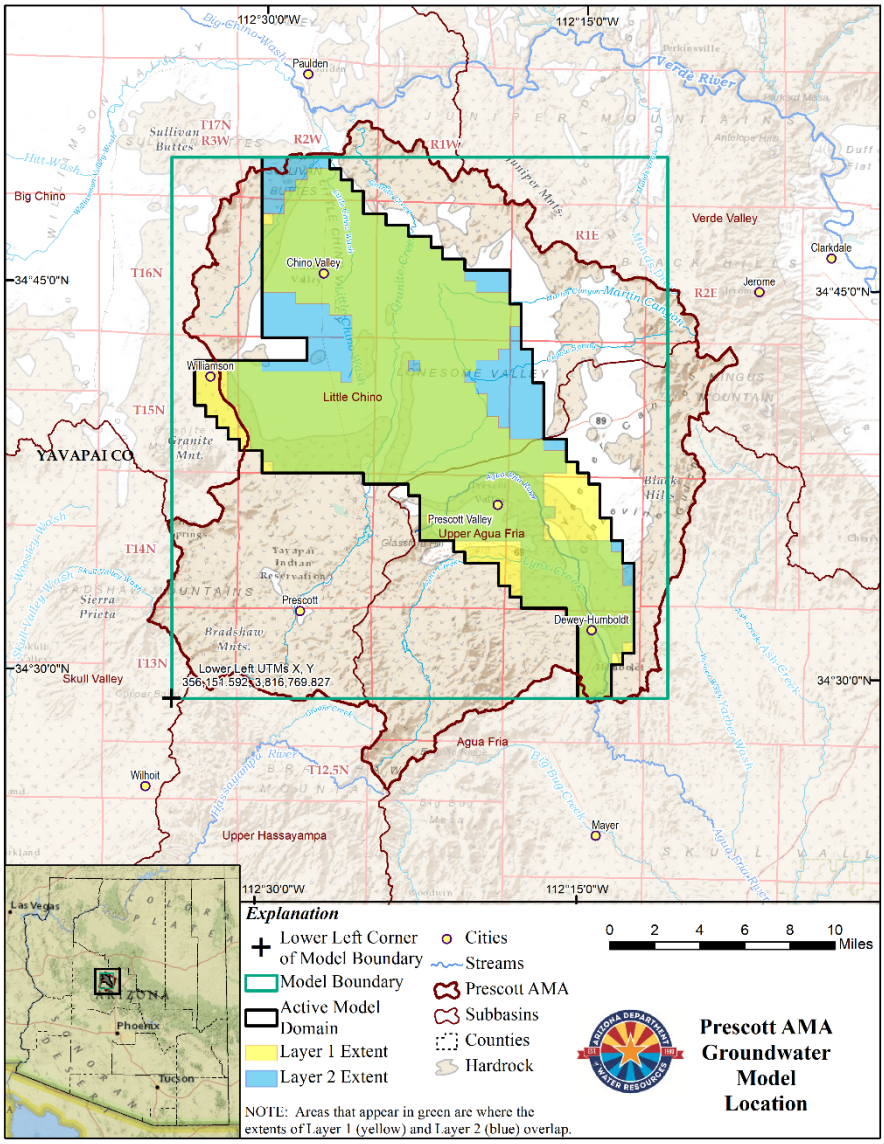

Figure 1. *Prescott AMA groundwater model location map*

In general, the 2021 model retains a similar conceptualization as the previous release, which simulated groundwater flow conditions from 1939 to 2011 (Nelson and Yunker, 2014). However, several areas of the model were refined in the 2021 update. These include: 1) the Santa Fe Well Field, 2) the Williamson Valley area, 3) the southern portion of LIC Sub-basin near the City of Prescott's USF, 4) the area near the Town of Prescott Valley's USF, and 5) both the northern and southern model boundaries.

As with the previous (Nelson and Yunker, 2014) release, attention in the 2021 model update was focused on developing and evaluating alternative conceptual models (ACMs). This consisted of defining specific model assumptions, calibrating the model parameters to available data, and evaluating the results. Each ACM was calibrated using non-linear regression techniques based on minimizing the sum of weighted squared residuals. For this model, residuals represent the difference between simulated and observed groundwater levels (heads) and regional-scale groundwater discharge (flows) in the LIC and UAF Sub-basins, represented by Del Rio Springs and baseflow along the Agua Fria River, respectively.

Model results are presented for groundwater flow conditions in the UAU and LVU aquifers from 1939 to 2019 in the LIC and UAF Sub-basins in the form of a comparison between simulated and observed heads (HOB) and flows for selected, high-ranking ACMs. One ACM (referred to as the 'base model') was selected for release and used for the presentation of model-error statistics and water budgets. The base model simulated water budget is presented to show the various components of the groundwater flow system including simulated pumping, recharge, and net change-in-storage between 1939 and 2019. Additional information regarding inferential statistics about model parameters, including composite sensitivities and information about estimated parameter reliability, is presented in **Appendix A.**

1.2. Background and Previous Work

The Prescott AMA groundwater flow model, originally developed by the Arizona Department of Water Resources (ADWR) in 1995, was a two-layer model comprised of a heterogeneous upper alluvial aquifer and a fractured, lower volcanic unit aquifer, exclusive to the LIC Sub-basin (Mason and Corkhill, 1995). The 1995 model simulated groundwater flow conditions between 1940 and 1994 in parts of the UAF and LIC sub basins within the Prescott AMA.

In 2002, ADWR updated the Prescott model to simulate groundwater flow conditions between 1939 and 1999 (Nelson, 2002). The 2002 update included the addition of a lower volcanic unit aquifer (LVU) in the northern portion of the UAF Sub-basin (the Santa Fe Well Field), an increased underflow from the LIC to the Big Chino (BIC) Sub-basin, and an improved representation of episodic natural recharge along Granite and Lynx Creeks. A single (deterministic) projection was developed, covering the period between 2000 and 2025.

In 2006, Northern Arizona University (NAU) was contracted by ADWR to update the calibration of ADWR's 2002 Prescott model through 2006 (Timmons and Springer, 2006). The 2006 NAU model update included the activation of model cells in the Williamson Valley area, as well as an updated geology based on exploratory drilling (refer to ADWR, 2001 for details).

A third model update was completed in 2014 (Nelson and Yunker, 2014), extending the simulation period from 1939 to 2011. Some of the model changes associated with the 2014 model update include the extension of the aquitard between the UAU and LVU aquifers in the southern LIC sub-basin and an improved spatial and temporal distribution of natural recharge.

In 2015 the USGS completed a large, regional-scale groundwater flow model (the NARGFM) covering much of northern and central Arizona, including the Prescott AMA (Pool, 2016). With respect to ADWR's Prescott AMA model's northern boundary, conjunctive use of the NARGFM eliminates the need to simulate groundwater flow through the artificial boundary representing flow between the LIC and BIC Sub-basins.

2. 2021 Model Update

As part of the 2021 update, model packages were modified to simulate the updated period through 2019. Consistent with ADWR's previous Prescott AMA models, the historic model period starts November 1, 1939 and completes 80 years later October 11, 2019, without accounting for offsets during leap years.

2.1. Simulated Pumping

The MODFLOW well package was extended to include new pumping data reported to ADWR and logged in ADWR's Registry of Groundwater Rights (ROGR) database through 2019. Well pumping data from a total of 130 wells was appended to previous model update and thus constitutes the "*base*" pumping distribution. The model retains the seasonality of previous ADWR Prescott AMA models, with a summer (April-October) and a non-summer (November-March) stress period recurring each year. The annual lump-sum pumping reported to ROGR was split 70/30, with 70 percent of the annual pumping assumed to occur between April and October and 30 percent between November and March. Due to incomplete records for 2019 at the time of initial model development, it was assumed that the distribution of groundwater pumping for 2019 was consistent with 2018.

In some model cells, model-based pumping represents "effective" (rather than "exact") pumping, due to: 1) the regional-scale scope of the model (model cells = 0.25 square miles); 2) potentially having multiple wells per cell, each having distinct pumping rates and screened intervals; and 3) model pumping being constrained to cell centers, which is generally not consistent with actual groundwater withdrawal locations. Thus, because of inherent structural model errors associated with simulated pumping (see above) and imperfect and/or incomplete historical pumping records, a collection of ACMs was developed by scaling *base* pumping rates by factors of 0.9, 0.95, 1.05 and 1.1. This was done to better "bracket" the most likely upper and lower bounds of actual historic pumping behaviors and to solve for, using inverse methods, correspondingly adjusted aquifer parameters which would be required to arrive at the same head and flow observations. The pumping-scaled ACMs were then optimized to available head and flow target data and evaluated. Despite a twenty percent range in the net pumping imposed on the modeled basin, the final

optimized solutions of each of the ACMs provided similar head-error statistics and were deemed plausible and thus included in the ensemble.

2.2. Simulated Recharge

The recharge package was extended through 2019, with some recharge terms ultimately estimated by inverse regression and treated as independent model parameters. The inclusion of recharge components in the non-linear regression process allows recharge to be optimized while providing information about their properties and relationships to other system parameters, such as hydraulic conductivity and storage. Due to the regional scope of the model and auto spatial correlation, there are individual model cells that receive multiple types of recharge, and thus the rates specified in the MODFLOW recharge package for these cells represents an "effective" or "net" recharge. For example, there are two USF sites that are located adjacent to major ephemeral tributaries. In additional to managed recharge, these model cells also receive periodic flood recharge (refer to photos B1and B2 in **Appendix B**). In cases where multiple types of recharge overlap individual model cells, the effective recharge rates were optimized.

2.3. Northern Boundary

During the calibration of the 2021 model, higher-ranking (more plausible) ACMs optimized to higher underflow rates out of the Prescott AMA model domain along the northern boundary than previously estimated in earlier model releases (Nelson and Yunker, 2014; Nelson, 2002; Mason and Corkhill, 1995). Inspection of groundwater level data in previously inactive model cells, including at Groundwater Site Inventory (GWSI) wells (B-17-03)29CAC and (B-17-02)29ADC, showed water table elevations (4,280 feet (ft) above sea level) consistent with patterns observed in the lower BIC Sub-basin, including the general Verde River headwaters area. This area is located about one mile west of Del Rio Springs (elevation 4,465 ft above sea level), and the resulting east-to-west hydraulic gradient of 0.035 is high enough to support significant underflow, even with modest values of hydraulic conductivity. This underflow component is assumed to be in addition to previously simulated underflow directed to the north and northeast. Refer to **Appendix C** for additional details.

2.4. Southern Boundary

In the southern portion of the model, two additional model rows were activated in UAF Sub-basin to increase the distance between the southern boundary and simulated model stresses (pumping and recharge) to the north. Furthermore, to better represent potential regional influences in the lower UAF Sub-basin, selected model cells in layer 2 (LVU) were activated. These modifications are thought to provide more flexibility to the calibration and are expected to attenuate potential adverse boundary condition influences when evaluating upgradient groundwater pumping. Refer to **Appendix C** for additional details.

2.5. Santa Fe Well Field

The availability of new hydrogeologic information near the LIC / UAF Sub-basin divide resulted in the reconfiguration of horizontal hydraulic conductivity zone K_x26, which is associated with the productive LVU aquifer and includes the Santa Fe Well Field. In order to simulate the significant declines and occasional recoveries observed in wells perforated in the LVU, the extent of K_x26 was necessarily bounded by much less transmissive material, which is represented in the model by the horizontal hydraulic conductivity parameter, K_x4. With respect to the previous model update (Nelson and Yunker, 2014), the reconfiguration and re-calibration resulted in a contraction in the areal extent of K_x26 (**Figure 2**).

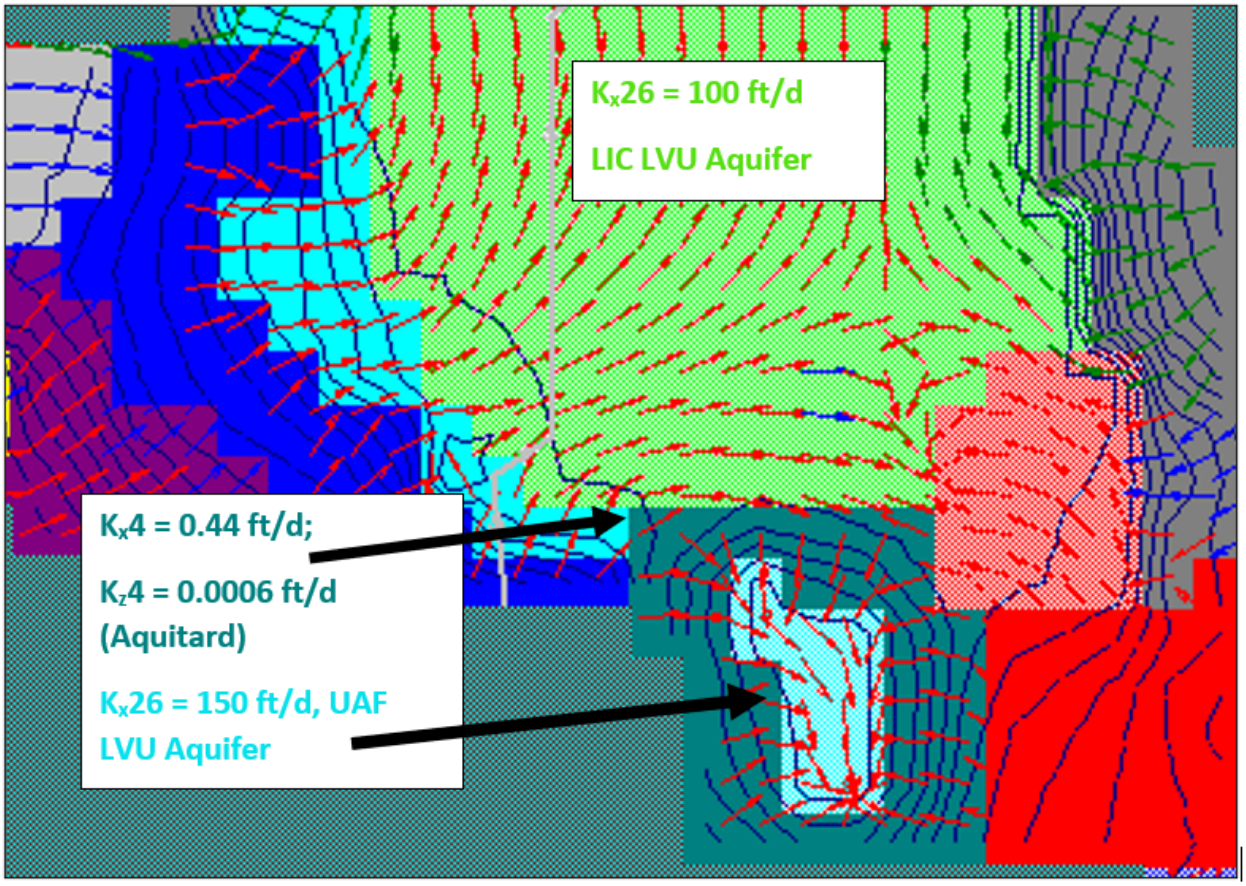

Figure 2. *Simulated groundwater flow in model layer 2, 2019. Figure shows concentric ovals representing the cone-of-depression. The composite-scaled sensitivity (CSS) of model parameters K_x4 is very high, reflecting its importance in simulating observed declines associated with intensive pumping. The CSS of K_x26, the primary aquifer supplying municipal demand in the area, is much lower than the "bounding" zone, K_x4.*

2.6. Williamson Valley

Additional groundwater level observations throughout Williamson Valley were added to the non-linear regression as head calibration targets. The spatial resolution of zones associated with hydraulic conductivity, storage, and recharge in the area was refined to improve simulated head fit to the significant declines observed in the field.

3. Model Calibration

To a large extent, the calibration of the model consisted of optimizing ACMs and evaluating the resulting solutions for plausibility with respect to aquifer properties and flow budgets. Each ACM was optimized using non-linear regression techniques and generally followed methods and guidelines established by the USGS (Hill, 1998).

Testing ACMs consisted of defining specific modeling assumptions, calibrating each ACM to available groundwater level and regional-scale flow data using non-linear regression, and evaluating the optimized solutions. These modeling assumptions included 1) the spatial distribution of fundamental model parameters, including hydraulic conductivity and storage; 2) the spatial and temporal distribution of recharge, including boundary conditions; and 3) other assumptions, including plausible ranges of assigned pumping assumptions, alternative weighting, etc.

To minimize potential bias (such that preconceived, possibly imperfect, assumptions about the structure of the basin or groundwater flow system would overshadow the signal embedded in the raw observation data), no regularization or *a priori* constraints were used in the non-linear regression calibration. Furthermore, use of head-dependent boundaries was largely limited to the northern and southern model boundaries. The availability of a combination of both head and flow targets provided excellent constraints for the non-linear regression. Refer to **Appendix A** for additional information regarding the non-linear regression.

A total of 3,692 head targets were included in the updated calibration using water level elevation data from ADWR's Groundwater Site Inventory (GWSI) database. In addition, 248 regional-scale flow targets of groundwater discharge rates feeding Del Rio Springs and baseflow along the Agua Fria River were included in the non-linear regression as proxies for groundwater discharge patterns in the LIC and UAF Sub-basins. Note that regional-scale groundwater flow remaining in the subsurface along boundaries cannot be directly measured. As a result, underflow rates along the northern and southern boundaries were not assigned as calibration targets, but rather as model parameters, subject to estimation by non-linear regression and subsequent optimization.

For most ACMs, head residuals were assigned weights equal to 0.1 ft^{-1}, representing a standard deviation of 10 ft. Flow residuals were assigned weights of 2.3E-5 $(ft^3/d)^{-1}$, representing a standard deviation of 0.5 cubic feet per second (CFS), for most ACMs including the base model. Evaluation of the standard error of regression was also used to guide weighting to ensure that neither heads nor flows dominate the objective function. Note that high streamflow events along Granite Creek and the Agua Fria River were not used directly as model calibration targets because transmission

losses during large runoff events are difficult to quantify due to data gaps, uncertainty associated with high flow measurements, unmeasured tributary contributions, and other factors. However, stream recharge is an important model constraint, and was honored by calibrating the model to groundwater level changes in response to positive or negative stresses such as pumping or recharge.

4. Calibrated Model Results

This section documents model results including, comparison of simulated and observed heads and flows, presentation of model-error statistics, simulated water budgets, major trends and associated implications. More details about the model conceptualization are provided in **Appendix D**. Unless otherwise indicated, all references to "feet" in the figures in this section refer to "feet above sea level."

4.1. Summary of Simulated Heads

A total of 3,692 observed groundwater levels were used as head calibration targets. For the base model, the residual mean, absolute mean, and root mean squared were -1.2 ft, 12.1 ft, and 18 ft, respectively. There were 1,687 head targets screened in layer 1 (UAU aquifer), and the residual mean, absolute mean, and root mean squared were +2.2 ft, 13 ft, and 19 ft, respectively. There were 2,005 head targets screened in layer 2 (mostly the LVU aquifer), and the residual mean, absolute mean, and root mean squared were -4.1 ft, 11 ft, and 18 ft, respectively. All plausible ACMs had comparable absolute residual mean ranging from 10 to 13 ft. The X-Y plot displaying total head residual statistics is presented below (**Figure 3**).

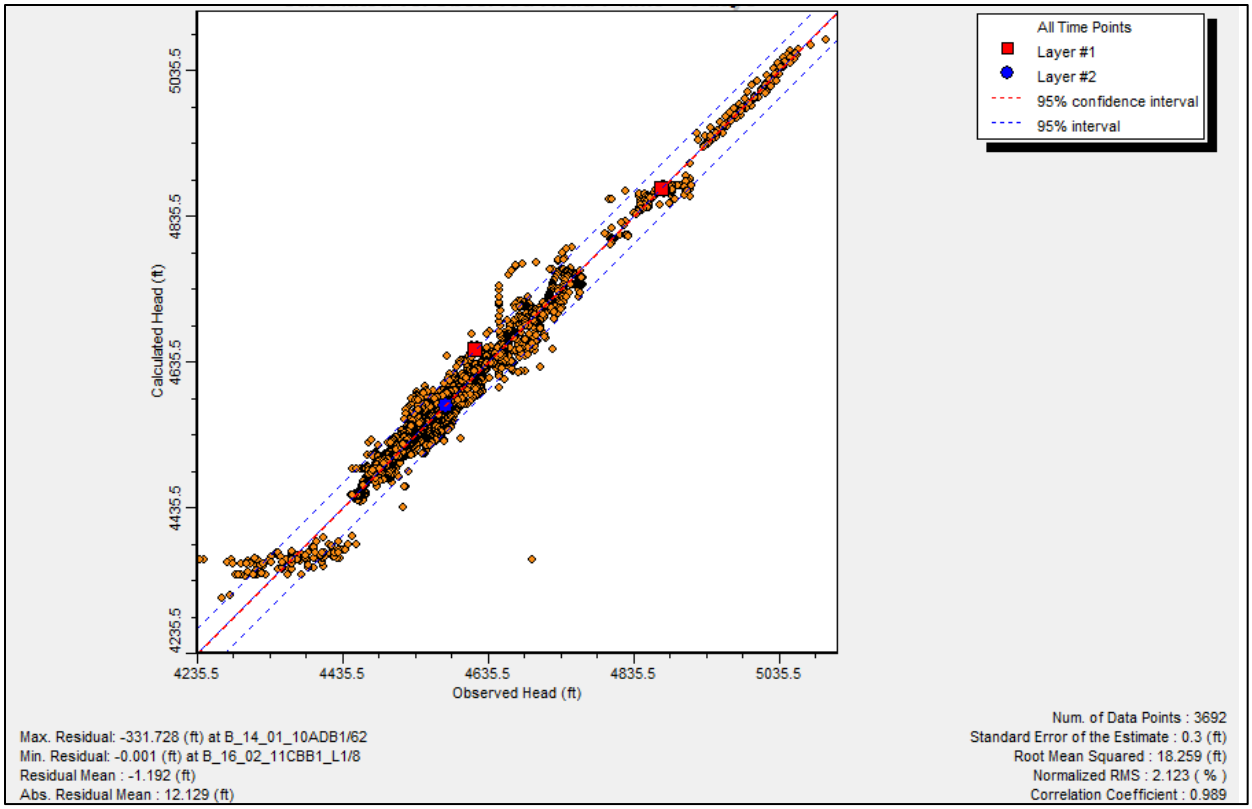

Figure 3. *X-Y Plot showing head residual statistics summary.*

Comparing simulated and observed heads show that the model accurately represents regional-scale groundwater level elevations over space and time in the LIC and UAF Sub-basins for both the UAU and LVU aquifers. The absolute mean residual head error represents about 1.5% of the system head change.

4.2. Simulated and Observed Heads at Select Locations

Information about simulated heads for different areas within the model are presented in several different ways in this report, including: 1) direct, time-series comparisons between simulated and observed heads (hydrographs) for five locations using the base model, and 2) simulated head ranges, based on an ensemble of plausible ACMs. To provide a broader representation of hydrologic conditions within local areas, simulated and observed groundwater levels are presented for seven different areas in **Appendix E**. The different areas are identified in **Figure 4**.

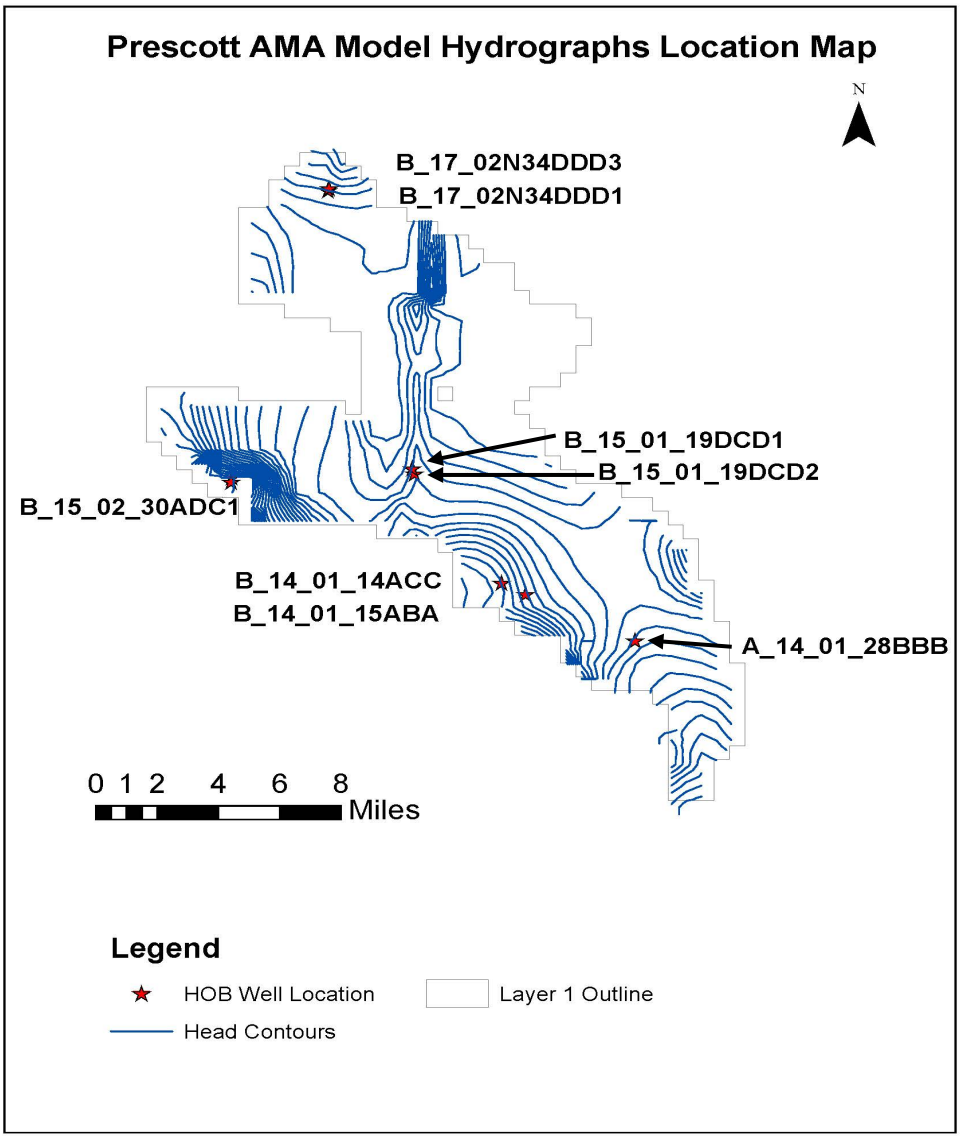

Figure 4. *Location of selected hydrographs.*

4.2.1. Little Chino Sub-basin, North

Figures 5a and **5b** below show simulated and observed heads for well (B-17-02)N34DDD1 and the ensemble in the LIC Sub-basin, north location.

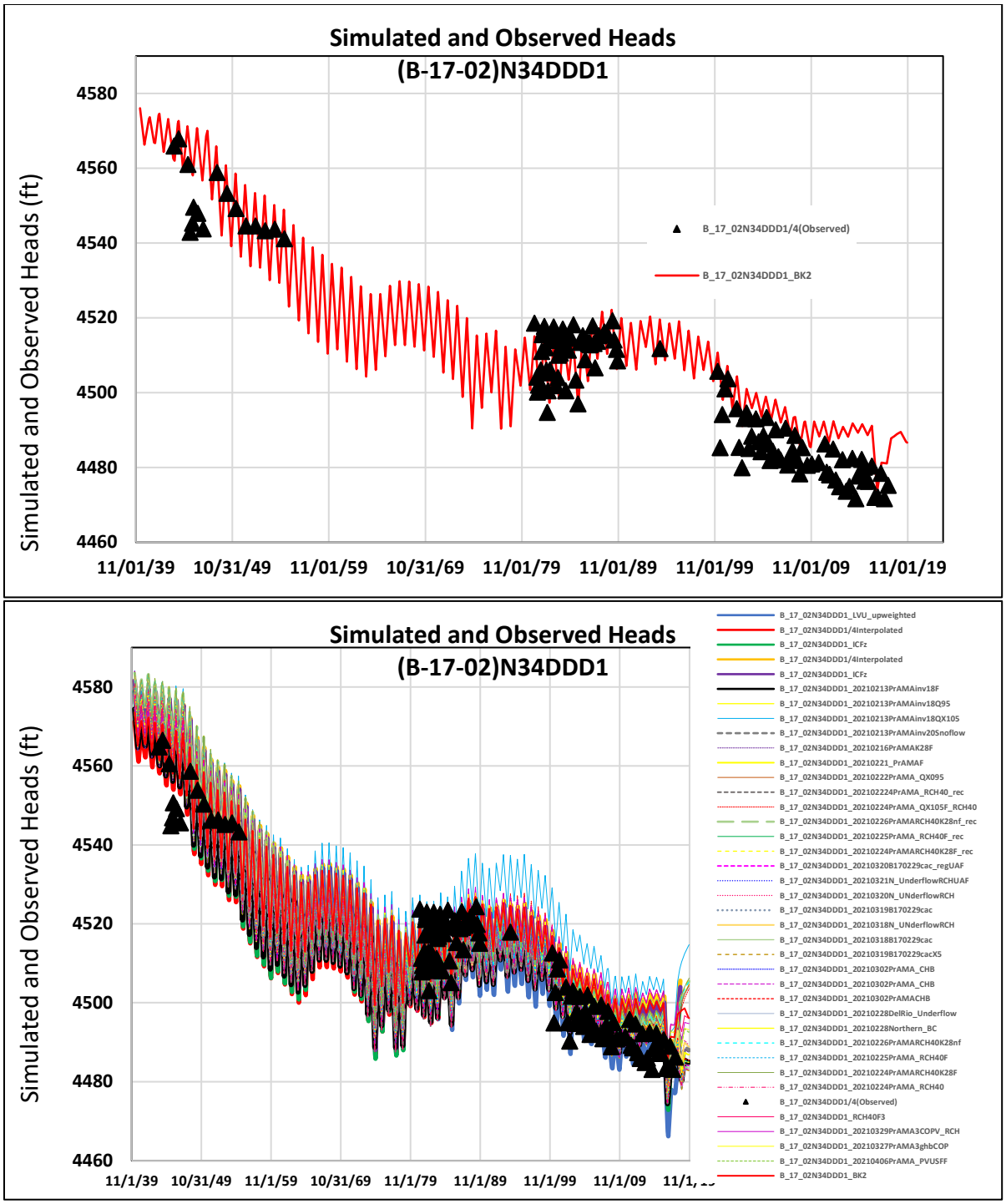

Figures 5a and **5b.** *Simulated and observed groundwater levels at (B-17-02)N34DDD1. (a) Base model (top), and (b) ensemble showing range of plausible ACM solutions (bottom).*

4.2.2. Little Chino Sub-basin, South

Figures 6a and **6b** below show simulated and observed heads for well (B-15-01)19DCD1&2 and the ensemble in the LIC Sub-basin, south location. In the figure immediately below, the simulated head for Layer 1 is represented by the blue line and the simulated head for Layer 2 is represented by the red line.

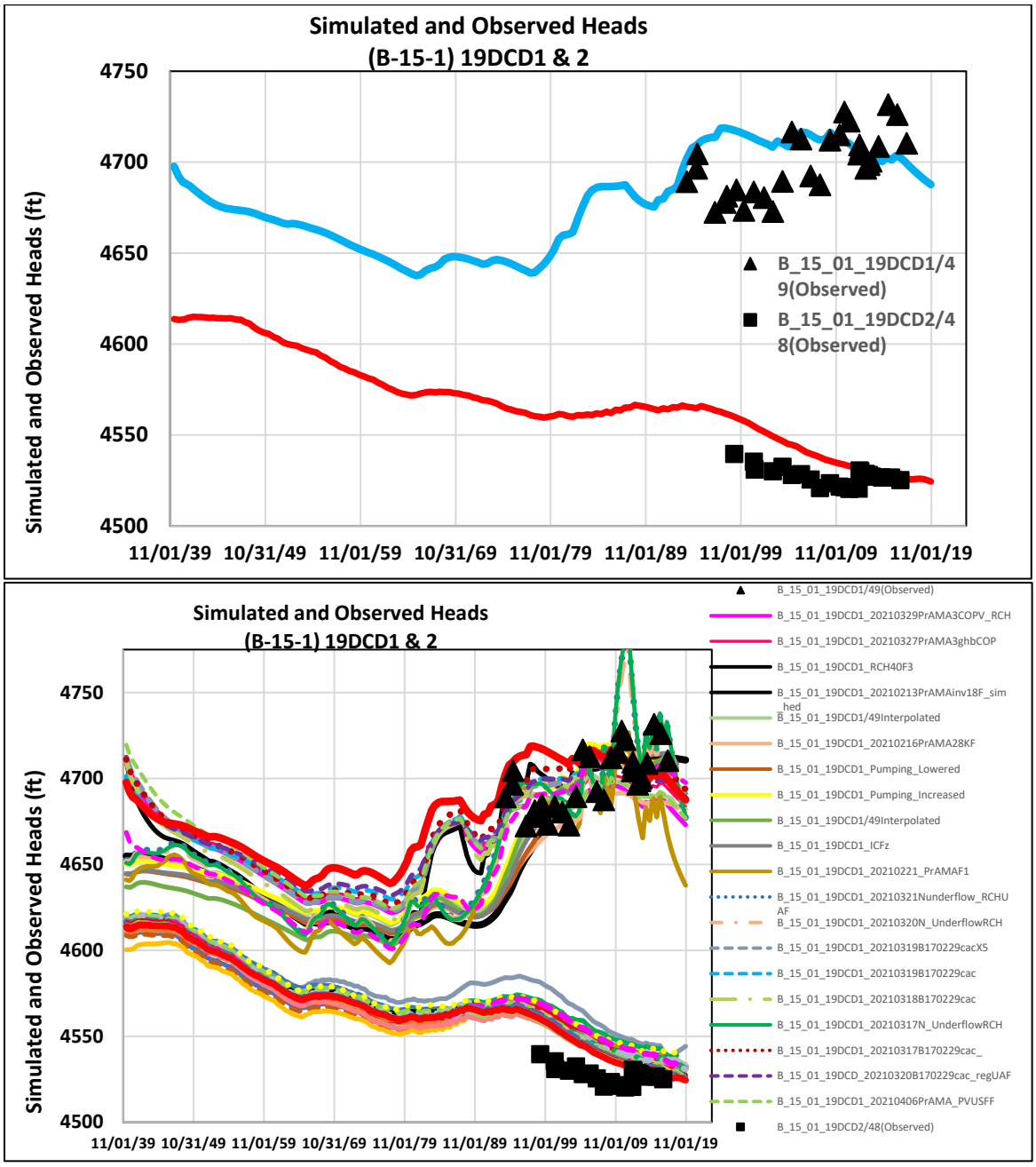

Figures 6a and **6b.** *Simulated and Observed UAU and LVU Heads Southern LIC Sub-basin; (a) Base model (top) and (b) ensemble showing range of plausible ACM solutions (bottom).*

One region of the model where there was considerable spread in the ensemble was in model layer 1, near the City of Prescott USF and Granite Creek (Southern LIC/UAU aquifer). It is assumed that the wider distribution of simulated heads are the result of: 1) having fewer head-constraining calibration targets with respect to the LVU aquifer; 2) heterogenous distribution of both horizontal and vertical hydraulic conductivity associated with the UAU aquifer; 3) imperfect application of "effective" recharge from multiple sources including artificial recharge and periodic flood recharge along Granite Creek; and 4) the attenuation of regional-scale flow "information," originating from Del Rio Springs and baseflow along the Agua Fria River, with distance, towards central portions of the model.

Compared to the spread of simulated LVU aquifer heads, **Figure 6b** above shows a greater range of plausible simulated water levels associated with the UAU aquifer. Hence the simulation of groundwater flow in the UAU Aquifer near the Prescott Airport is subject to greater levels of uncertainty than the LVU aquifer solutions.

4.2.3. Upper Agua Fria Sub-basin, North (Santa Fe Well Field)

Significant declines have been associated with the productive Santa Fe Well Field (K_x26) in the northern UAF Sub-basin. Decline rates of this magnitude can only be simulated when the highly transmissive aquifer, K_x26, is bounded by much less transmissive material. In other words, the surrounding low-K zone (K_x4), limits the cone-of-depression originating from zone K_x26 from propagating into adjacent materials; thus, high resistance to hydraulic flow outside of K_x26, results in the concentrated removal of groundwater (and pressure head reduction) within the productive aquifer, K_x26.

Figures 7a and **7b** below show simulated and observed heads for two wells and the ensemble in the LIC Sub-basin, south location.

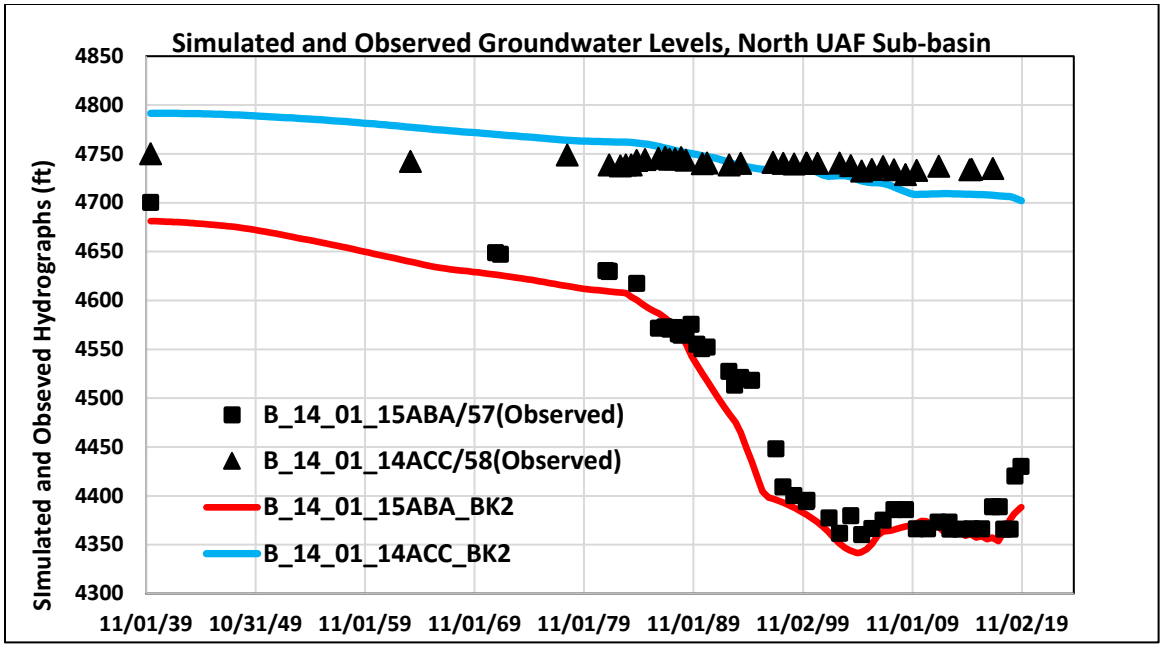

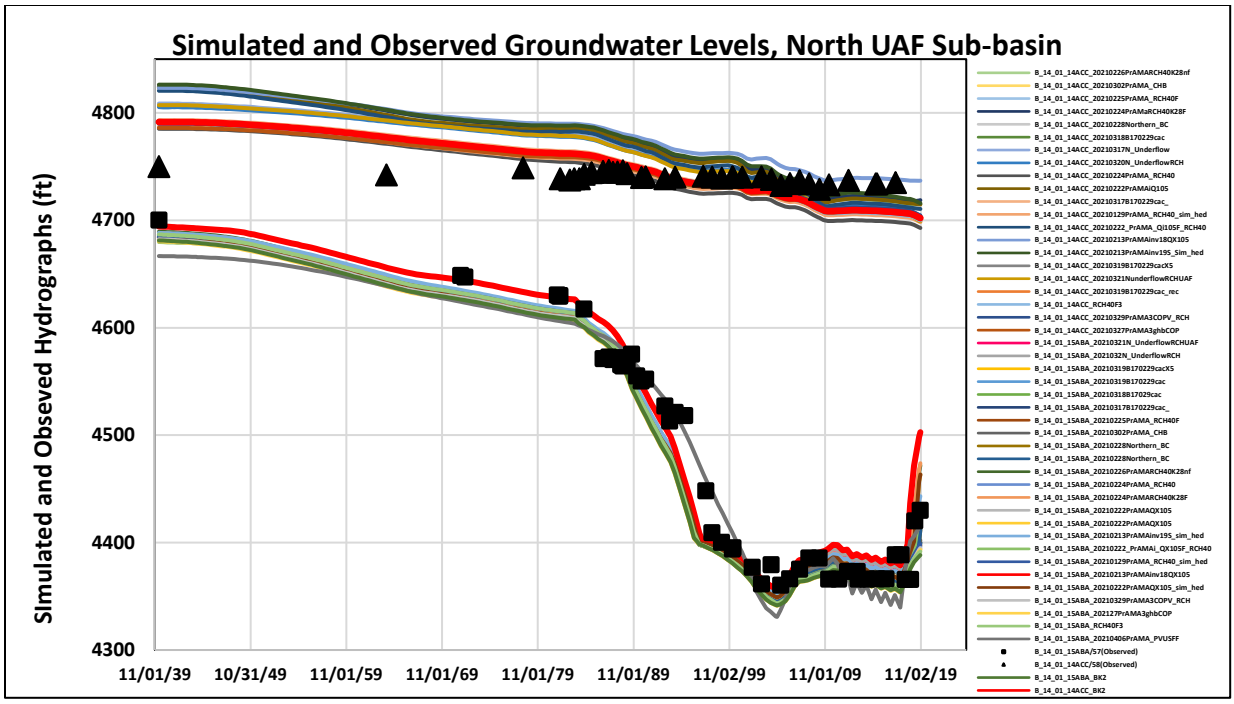

Figure 7a and **7b**. *Simulated and Observed UAU and LVU Heads, northern UAF Sub-basin; (a) Base model (top) and (b) ensemble showing range of plausible ACM solutions (bottom).*

4.2.4. Central UAF Sub-basin: Pumping declines and Induced Recharge

Groundwater pumping creates aquifer storage space in unconfined aquifer systems. Data clearly shows that in select areas, episodic streamflow induces recharge when storage space is available in unconfined aquifers.

Figures 8a and **8b** below show simulated and observed heads for well (A-14-01)28BBB and the ensemble in the central UAF Sub-basin location.

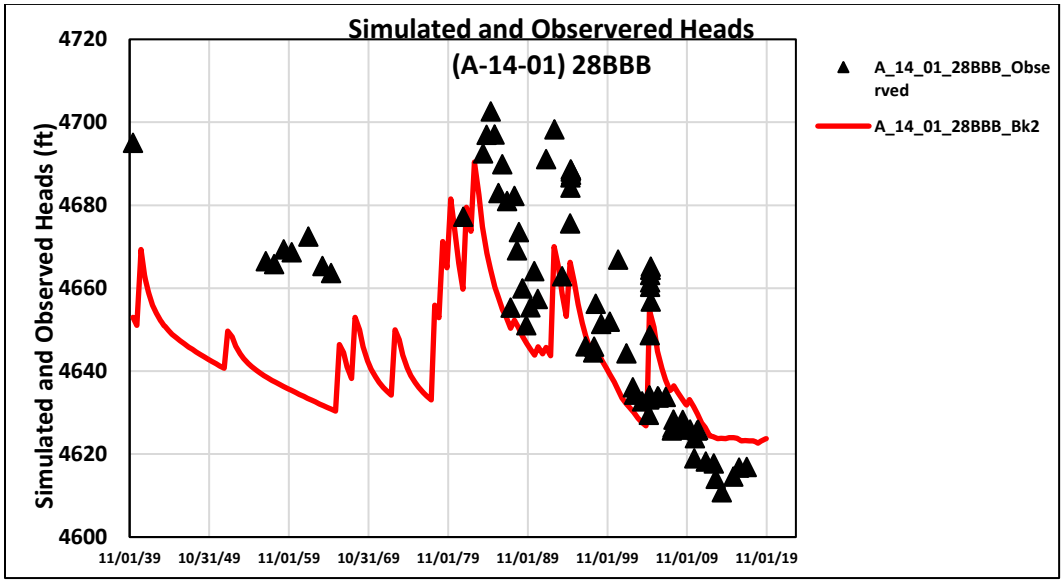

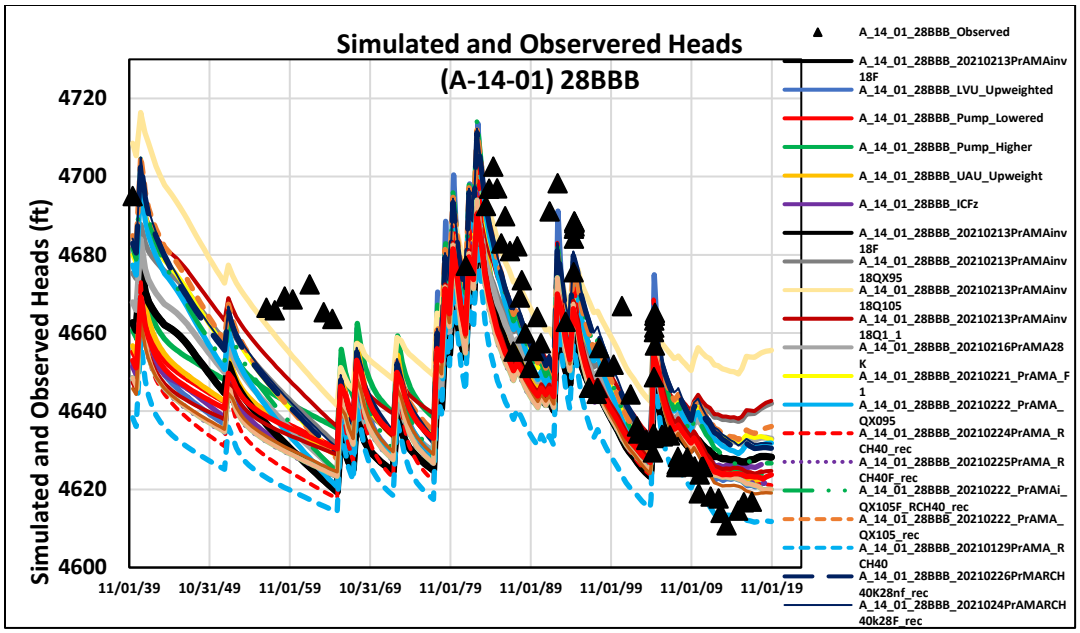

Figures 8a and **8b.** *Simulated and Observed UAU Heads, central UAF Sub-basin; (a) Base model (top) and (b) ensemble showing range of plausible ACM solutions (bottom).*

4.2.5. Williamson Valley Area (BIC / LIC Sub-basin divide)

Williamson Valley is another area where local pumping declines have been accentuated because the extent of the aquifer is limited. Similar to the Santa Fe Well Field, relatively low-K subsurface materials surround the local pumping center and limit the propagation of the cone-of-depression. Consequently the "bounding" effect results in more local dewatering and significant local drawdown. For more details, see **Appendix E**. Note that high sensitivity was associated with the "bounding" parameter, K_x6, and resulted in little variation among ACMs solutions. Because there was so little variation, an ensemble of head solutions from the various plausible ACMs is not presented for this area. See **Figure 9** below showing the simulated and observed groundwater heads.

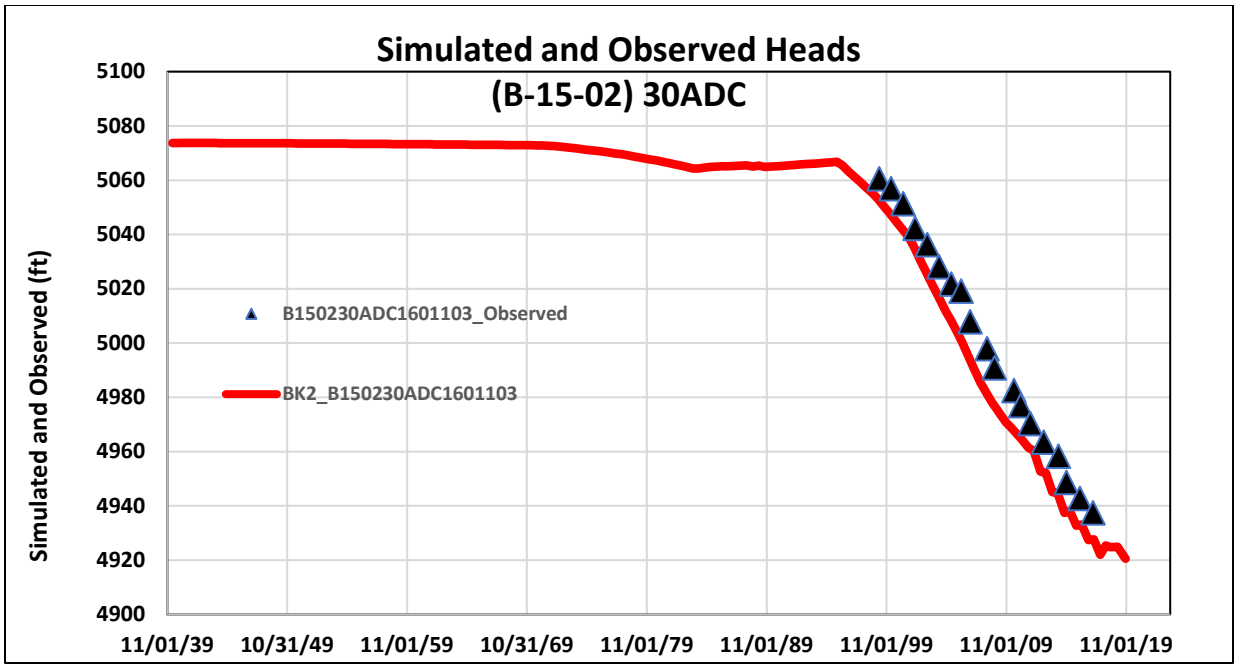

Figure 9. *Simulated and Observed heads, Williamson Valley.*

4.3. Simulated Flow

Regional-scale flow targets were used to constrain the calibration of the groundwater flow model. Assigned flow targets at Del Rio Springs and baseflow along the Agua Fria River represent systemic regional-scale groundwater discharge in the LIC and UAF Sub-basins, respectively. Located at the northern and southern model boundaries, Del Rio Springs and baseflow along the Agua Fria River represent concentrated hydrologic information associated with the upgradient groundwater flow regime in the LIC and UAF Sub-basins, respectively. **Figure 10** below shows the locations of the regional-scale flow targets. Comparison between simulated and observed groundwater discharge are shown in **figures 11a, 11b, 11c, 12a** and **12b** below. The importance of including these calibration constraints cannot be overstated. Additional information about the importance of including flow targets in groundwater flow modeling is provided in Hill (1998).

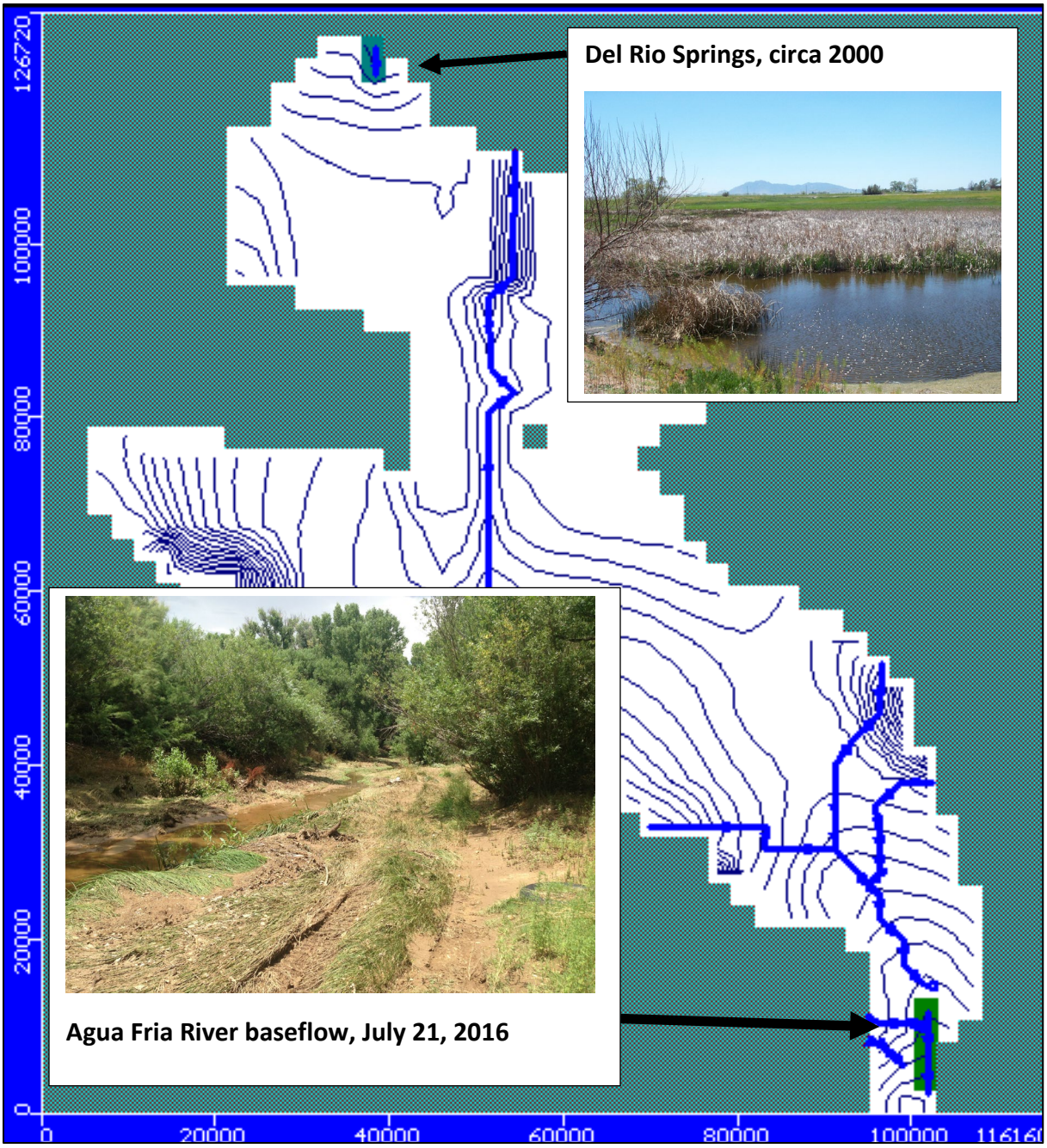

Figure 10. *Locations of regional groundwater discharge*

Simulated and observed groundwater discharge at Del Rio Springs for the base model is shown in **Figures 11a** and **11b**. To illustrate the range of simulated groundwater discharge representing Del Rio Springs, an ensemble of selected ACM's is presented in **Figure 11c**.

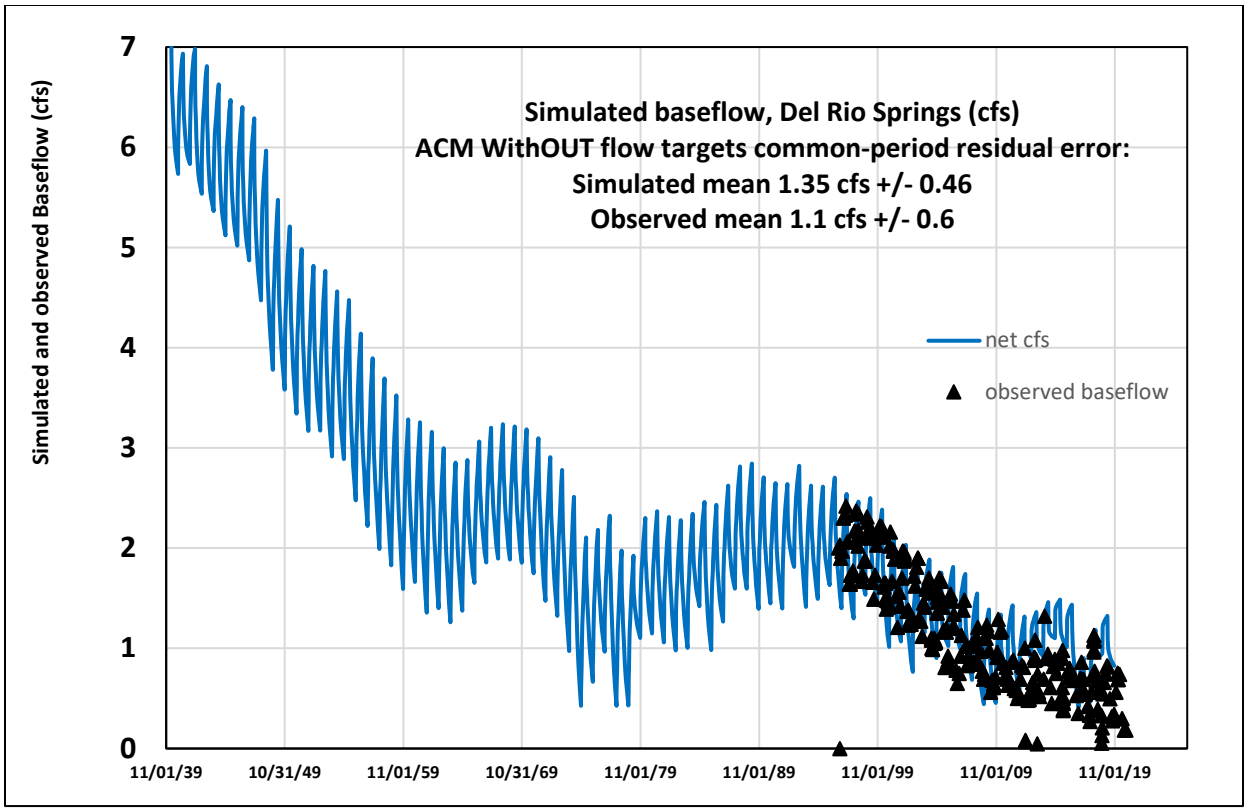

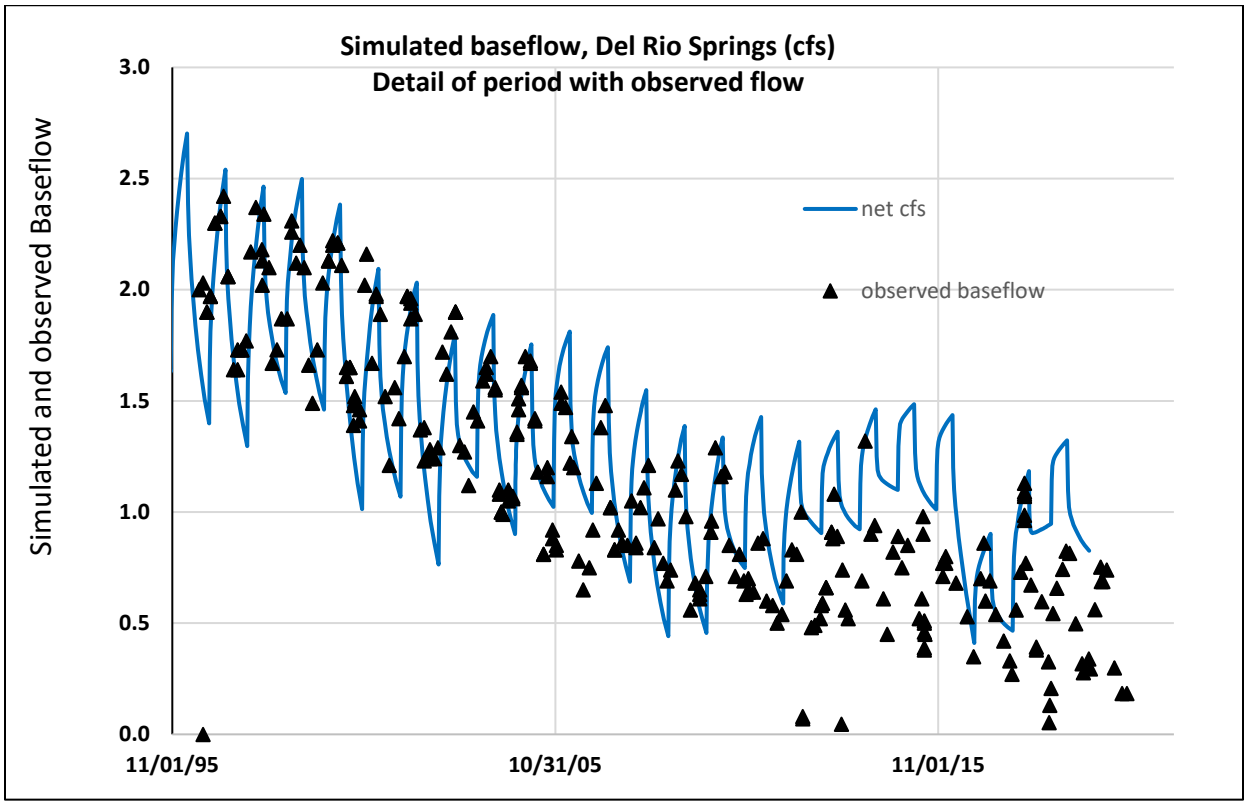

Figure 11a and 11b. *Simulated and observed flow at Del Rio Springs (top); detail showing seasonality for period with high observation sample rate (bottom).*

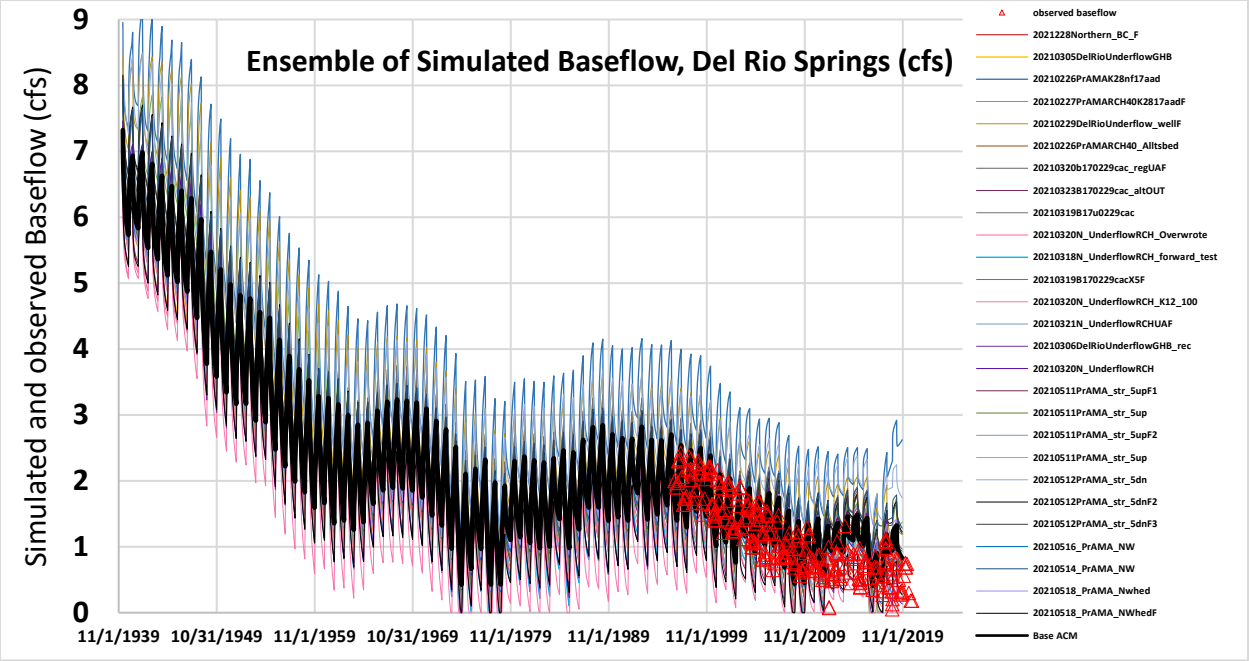

Figure 11c. *Ensemble of selected ACM's showing the range of simulated flow representing Del Rio Springs and observed flow targets (red triangles).*

Simulated and observed baseflow along the Agua Fria River for the base model is shown in **Figure 12a**. To illustrate the range of simulated baseflow along the Agua Fria River, an ensemble of selected ACM's is presented in **Figure 12b**.

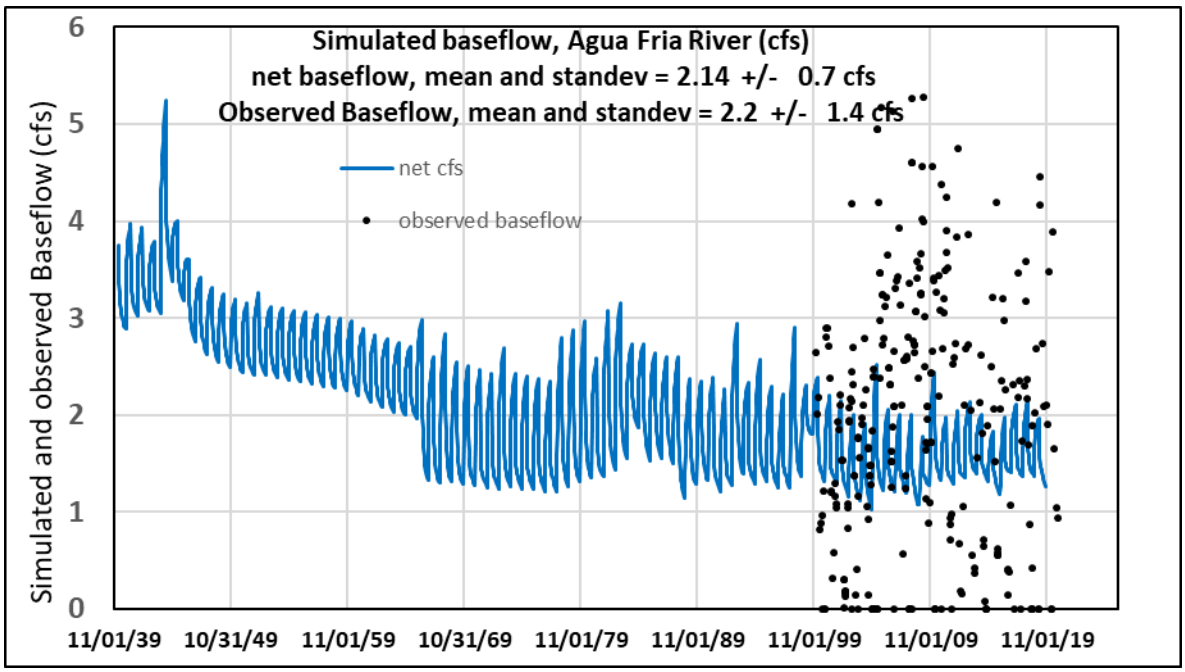

Figure 12a. *Simulated and observed baseflow along Agua Fria River*

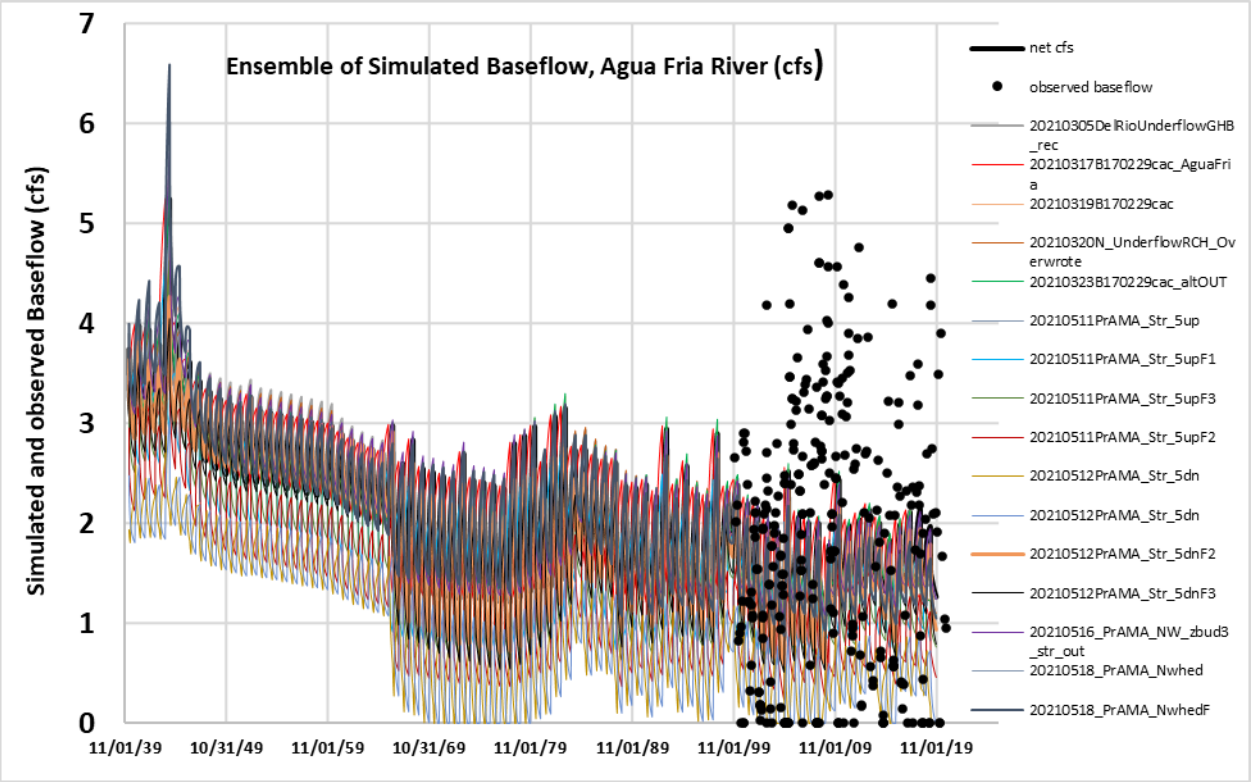

Figure 12b. *Ensemble of selected ACM's showing the range of simulated baseflow along the Agua Fria River and observed baseflow targets (black circles)*

4.4. Simulated Water Budgets

Calculated water budgets for the steady state and transient simulations are provided in **Tables 1** and **2**, respectively. Additional, detailed water budget information is provided in **Appendix B**.

***Simulated Steady State Water Budget, circa 1939**	
Inflow	**AF/yr**
Mountain Front Recharge (MFR) & Chino Valley Irrigation District (CVID) AG recharge	5,803
Granite & Lynx Creek Natural recharge	7,702
Underflow from BIC Sub-basin into the LIC Sub-basin	2,233
	15,738
Outflow	**AF/yr**
Del Rio Springs	5,301
LIC Underflow to BIC	4,017
Agua Fria Baseflow	3,605
UAF Underflow and groundwater discharge below gage	1,873
Early-development groundwater pumping; bank releases	932
	15,728
*For details see **Appendix B**.	

Table 1. *Simulated steady state water budget.*

*Simulated Transient Water Budget (long-term annualized rates)	
Inflow	**AF/yr**
Storage in	18,233
Total Recharge (RCH cells)	20,607
Granite & Lynx Creek: Natural recharge (Str cells)	865
Total Inflow ->	**39,705**
Outflow	**AF/yr**
Storage out	10,940
LIC Groundwater discharge (Del Rio Springs); str cells	1,997
UAF Groundwater discharge (Agua Fria River); str cells	4,046
LIC and UAF EVT	715
LIC Underflow (flux and GHB)	3,863
UAF underflow (flux)	500
Pumping	17,571
Total Outflow	**39,632**
Net Change-in-storage	**-7,293**
*Rates have been annualized. Long-term mean net change-in-storage rates in the LIC and UAF are 6,000 and about 1,300 AF/yr, respectively. For more budget details see **Appendix B**. GHB = general head boundary	

Table 2. *Simulated transient water budget*

5. Summary and Conclusions

5.1. Core System Features

By evaluating groundwater data (heads; flows; aquifer tests; well logs; pumping estimates, existing studies etc.), an increasingly clear picture is forming about the regional-scale groundwater flow system. With each update, regional-scale hydrologic features are being identified with greater confidence. Important regional-scale hydrologic features represented in the model include:

1) ***High values of hydraulic conductivity (K_x23 and K_x25) are associated with the LVU aquifers in the LIC Sub-basin in model layer 2.*** Wells screened in K_x23 and K_x25 are generally excellent water producers. Long-term pressure head declines associated with the LVU aquifer in the LIC Sub-basin are approximately 100 ft, and hydraulic gradients are generally flat, due to high transmissivity. Currently, groundwater levels associated with the LVU aquifer in the central LIC Sub-basin are at an elevation of 4,500 ft above sea level. The distribution of hydraulic conductivity for the base model is shown in **Appendix F**.
2) ***An aquitard separates layers 1 and 2 in the LIC sub-basin***. Historically, there was an upward vertical gradient, including artesian wells, especially in the northern LIC Sub-basin, south of Del Rio Springs. Chronic regional groundwater extraction in the LIC Sub-basin has reduced the LVU aquifer pressure head to elevations more consistent with water table elevations associated with the UAU aquifer. Modeling results suggest the "effective"

vertical hydraulic conductivity may have increased over time, possibly due to crossflow in wells screened in both the UAU and LVU aquifers in the LIC Sub-basin.

3) ***K-zone representing groundwater conditions in the general Del Rio Springs area, K_x2, and connection to BIC Sub-basin along the northern model boundary.*** A sensitive model parameter, K_x2, has been consistently estimated using non-linear regression techniques at about 10 ft/d; also see Nelson and Yunker, 2014. The resistance to vertical flow (aquitard) separating the UAU and LVU aquifers in the central portion of the LIC Sub-basin is largely absent in K_x2, thus allowing for the upwelling and emanation of groundwater discharge that forms Del Rio Springs.
4) ***Long-term groundwater pumping in the LIC Sub-basin has resulted in a significant reduction in groundwater discharge - or capture - at Del Rio Springs***, due to the direct hydraulic connection between the springs and the LIC Sub-basin aquifers (UAU and LVU).
5) ***High values of hydraulic conductivity (K_x26) are associated with the LVU aquifer(s) in the northern UAF Sub-basin in model layer 2 (Santa Fe Well Field):*** Wells screened in K_x26 are generally excellent water producers, however, the lateral extent of K_x26 is limited.
6) ***Geologic materials with lower values of hydraulic conductivity surround the LVU aquifers***, including K_x1, K_x2, K_x4, K_x9 and K_x27. Higher resistance to groundwater flow occurs outside the primary LVU aquifer zones and, consequently, impedes the lateral propagation of the cones of depression by accentuating drawdown within the productive LVU aquifers, represented by K_x23, K_x25 and K_x26.
7) ***Wells screened in layer 2 outside the LVU zones have distinct elevations, trends, and hydraulic gradients, with respect to the LVU zone patterns.***
8) ***An aquitard or aquiclude (K_z4) separates layers 1 and 2 in the northern UAF sub-basin (Santa Fe Well Field);*** both data and modeling indicate that there is very high resistance to vertical flow.
9) ***The UAU aquifer in model layer 1 is heterogeneous***, hydraulic conductivity estimates range by orders of magnitude.
10) ***Relatively high values of hydraulic conductivity are associated with stream gravels in select areas such as Agua Fria River, Lynx Creek and associated tributaries*** (Errol L. Montgomery, 2008); ***high recharge rates are observed during significant streamflow events.***
11) ***There exists a significant downward vertical gradient in the southern portions of the LIC sub-basin***. Observed groundwater levels screened in the UAU can exceed LVU heads by 200 ft. In general, groundwater levels currently observed at about 4,500 ft above sea level are mostly likely in direct hydraulic connection with the LVU aquifer in the LIC Sub-basin. Groundwater levels differing from this value are probably not in direct hydraulic connection with the LIC Sub-basin LVU aquifer.
12) ***A significant cone of depression is developing in the Williamson Valley area***. Since about 2000, groundwater level declines in the most impacted areas have exceeded 100 ft.
13) ***Long-term groundwater pumping in the UAF Sub-basin has resulted in the capture of groundwater discharge, including baseflow associated with the Agua Fria River.*** However, due to periodic flood recharge along the Agua Fria River *and* the finite storage capacity of the respective stream-aquifer system, the magnitude of baseflow continues to

reflect natural stream recharge patterns where increases and decreases in baseflow are consistent with periods of high and low rates of natural recharge. Continued capture may result in: 1) a reduction in baseflow, especially during dry periods; and/or 2) a reduction in downstream flow and subsequent recharge, due to induced recharge along upgradient areas.

14) In addition to groundwater discharge as spring flow, baseflow and riparian demand (EVT), both the northern and southern model boundaries consistently indicate underflow occurs to the BIC Sub-basin (to the north) and Agua Fria Basins (to the south). ***The magnitude of underflow simulated along these boundaries has, generally, been increasing with each successive model update.***

15) ***Episodic periods of natural recharge along Granite Creek, the Agua Fria River, Lynx Creek and other major tributaries account for approximately two thirds of all natural recharge.***

5.2. Conclusions

The Prescott AMA groundwater flow model was updated and re-calibrated to simulate hydrologic conditions in the LIC and UAF Sub-basins from 1939 to 2019. The model simulates groundwater flow conditions associated with UAU and LVU aquifers. Numerous ACMs were developed and tested for plausibility. Each ACM was optimized using non-linear regression by constraining model parameters to available target data, including observed groundwater levels and regional groundwater discharge. The calibration is consistent with the methods and guidelines established by the USGS (Hill, 1998). Although the model is generally consistent with the previous update, several areas were refined, including the Santa Fe Well field, the northern and southern boundaries, the general Williamson Valley area, and locations near present-day USFs.

Each ACM was optimized using inverse modeling techniques by constraining 3,962 head calibration targets and 248 regional-scale groundwater discharge targets. For the base model, the residual mean and absolute residual mean head errors were -1.2 ft and 12 ft, respectively, where the residual error is equal to observed minus simulated heads. All plausible ACMs had similar head residual error statistics. The model accurately represents regional-scale groundwater discharge patterns in the LIC and UAF sub-basin, both in trend and magnitude. Evaluating regional groundwater discharge patterns provides a robust measure for discriminating among ACMs. Significant rates of capture have occurred at both Del Rio Springs and baseflow along the Agua Fria River, due to long-term groundwater pumping.

At Del Rio Springs, capture has resulted in a significant decrease in groundwater discharge as spring flow. Similarly, due to the changing hydraulic gradients in the LIC Sub-basin, capture has also occurred along the northern underflow boundary. It is important to note that capture has resulted in a chronic reduction in groundwater *outflow* along the northern boundary: while the reduced outflow lessens the degree of long-term groundwater overdraft (all else equal), it does so at the expense of groundwater discharge.

While the capture of baseflow has also occurred along the Agua Fria River, floods periodically recharge (and "reset") the shallow water table aquifer. In practical terms, local groundwater pumping provides storage *space* for subsequent recharge, or induced recharge. This space (or capacity) is only replenished when large flood events occur. Given the complex nature of the

stream-aquifer system in the UAF sub-basin and continued groundwater pumping, downgradient streamflow may be subject to retraction due to induced recharge, upgradient, all else equal.

Between 1939 and 2019, the model simulated 1.4 million AF of groundwater pumping, corresponding to a long-term annualized average rate of 17,571 AF/yr. The cumulative net change-in-storage loss to the aquifer was simulated at 583,038 AF, representing a long-term annualized rate of -7,293 AF/yr.

Many ACMs were investigated during this model update and it is unreasonable to assume any one single ACM fully represents the regional-scale groundwater flow system. As a result, head solutions for plausible ACMs were grouped together to form ensembles for selected sites. The ensemble head distributions, therefore, provide a measure of uncertainty, and results showing wider or narrower head distributions can be associated with areas simulated with less or greater certainty, respectively. Analyzing ensemble results consisting of equally likely ACM's in combination with potential boundary conditions may assist in developing a more complete understanding of future groundwater conditions. This is particularly true for locations where future groundwater conditions (heads and flows) are anticipated to extend far beyond the calibration range. The resulting head and flow solutions, thus, form a distribution that can be used to better understand the groundwater flow system and associated uncertainty.

References

1. Arizona Water Atlas Volume 8: infoshare.azwater.gov/docushare/dsweb/Get/Document-10433/Volume_8_final.pdf
2. Ch2M. Iron King Mine – Humboldt Smelter Superfund Site Dewey-Humboldt, Yavapai County, Arizona. Remedial Investigation Report prepared for the US. Environmental Protection Agency, 2016. https://response.epa.gov/sites/11828/files/IKMHS%20Remedial%20Investigation%20Report%20Text%20Sept%202016.pdf
3. Corkhill, E, F. & Mason, D. Hydrogeology and Simulation of Groundwater Flow, Prescott Active management Area, Yavapai County, Arizona: Arizona Department of Water Resources. Modeling Report No. 9 ADWR, 1995. https://new.azwater.gov/sites/default/files/GMR%209-Hydrogeology_and_Simulation_of_Groundwater_Flow%20-PRAMA_0.pdf
4. Hill, M. Methods and Guidelines for effective model calibration. USGS Water Resources Investigation Report 98-4005, 1998. https://water.usgs.gov/nrp/gwsoftware/modflow2000/WRIR98-4005.pdf
5. Nelson, K. Application of the Prescott Active Management Area Groundwater Flow Model Planning Scenario 1999 – 2025: Arizona Department of Water Resources Model Report No. 12 ADWR, 2002. https://new.azwater.gov/sites/default/files/Modeling_Report_12_0.pdf
6. Timmons, D. & Springer, A. Prescott AMA Groundwater Flow Model Update Report. Prepared for Arizona Department of Water Resources, contract #2005-2592, 2006 https://new.azwater.gov/sites/default/files/Prescott_Model_Update_Report_0.pdf
7. Nelson, K. and Yunker, D. Groundwater Flow Model Update Report for the Prescott Active management Area, Yavapai County, Arizona Model Report No. 25 ADWR, 2014. https://new.azwater.gov/sites/default/files/Prescott_AMA%20GW%20model%20report_3_31_2014_0.pdf
8. Iron King Mine EPA. https://response.epa.gov/site/doc_list.aspx?site_id=11828
9. Errol L. Montgomery. Evaluation of Pumping-Induced Stream Depletion in the Vicinity of Young's Farm and the Agua Fria River Yavapai County, Arizona, 2008. *Report submitted to ADWR with Yavapai Land Holdings, LLC application for analyses of water supply number 28-402259.0000.*
10. Pool, D.R. et. al. Regional Groundwater-Flow Model of the Redwall-Muav, Coconino, and Alluvial Basin Aquifer Systems of Northern and Central Arizona. Scientific Investigations Report 2010-5180, v. 1.1, USGS, 2011. https://pubs.usgs.gov/sir/2010/5180/
11. Corkhill, Remick, Norton and Nelson, Prescott Active Management Area 2000-2001 Hydrologic Monitoring Report, ADWR, 2001. https://new.azwater.gov/sites/default/files/HMR_PrescottAMA_00_01.pdf
12. Pool, D.R. Simulation of Groundwater Withdrawal Scenarios for the Redwall-Muav and Coconino Aquifer Systems of Northern and Central Arizona, Scientific Investigations Report 2016–5115, USGS 2016 https://pubs.usgs.gov/sir/2016/5115/sir20165115.pdf.

Appendix A: Inverse Model Statistics

In general, the model is well constrained, and the reliability of model parameters is good. There are, however, some parameters that are more subject to lower reliability due to either low sensitivity and/or parameters that have some degree to dependence or parameter correlation. Notwithstanding noted non-linearity assumptions about optimized values or conducting a full-scale global sensitivity analysis, the 95% confidence provide a meaningful measure of parameter uncertainty.

A byproduct of non-linear regression, the composite scale sensitivities (CSS) generally provide a metric regarding how individual parameter calibration adjustments result in systemic observation responses; in situations where no parameter correlation is present, the CSS can provide a ranking of how parameters influence (or don't influence) the calibration, all else equal.

Because different ACMs generally have consistent cumulative head-residual error statistics (typically, within several percent), systemic flow was generally a more distinct measure of ACM differences.

Figure A1 is an excerpt from the non-linear regression "record" file for the base model showing optimized parameter values and the upper-and-lower 95% CI's. **Figure A2** shows the composite sensitivity (CSS) for all estimated parameters associated with the base model. **Figure A3** shows the CSS's greater than 0.01 for estimated base model parameters. Model parameters having higher sensitivity exhibit more influence on controlling simulated flow (and targeting observations), and are thus more conducive to calibration process, all else equal.

However sometimes two (or more) model parameters may counter-act each other and result in parameter correlation; this can occur even when their individual sensitivities are relatively large. Thus, highly correlated parameters can be thought of as another form of low sensitivity between two (or more) system model parameters. For example, modest spatial parameter correlation (-0.78) exists between natural recharge sources associated with upper Lynx Creek (par006) and Glassford Hill recharge (par008); that is, there is modest (not extreme) uncertainty regarding the specific location of natural recharge between upper Lynx Creek and nearby Glassford Hill.

OPTIMISATION RESULTS

Adjustable parameters ----->

Parameter	Estimated value	95% percent confidence limits lower limit	upper limit
kx_19	2.02272	0.401010	10.2027
kx_23	325.000	271.503	389.038
kz_23	2.317580E-03	1.864248E-03	2.881149E-03
kx_24	0.385241	7.456436E-02	1.99037
kx_25	101.120	87.3611	117.046
kx_26	149.077	30.8514	720.355
kz_26	1.518050E-07	2.058385E-10	1.119555E-04
kx_27	20.0062	6.71198	59.6319
kx_28	0.625669	0.499817	0.783210
kx__2	10.1986	9.21325	11.2893
kx_31	0.517438	8.008529E-02	3.34321
kx_34	4.345360E-02	2.036126E-02	9.273568E-02
kx_35	1.00000	0.908820	1.10033
kx_36	0.350000	0.242512	0.505130
kx__3	0.500000	0.385626	0.648297
kz__3	5.000000E-03	4.018120E-03	6.221815E-03
kx__4	0.440000	0.392230	0.493588
kz__4	6.193020E-04	5.274616E-04	7.271335E-04
kx__5	4.65834	0.522797	41.5078
kx__6	7.022650E-02	6.020590E-02	8.191491E-02
kx__7	11.8544	0.912286	154.038
kx__8	2.43871	1.32025	4.50469
kx__9	5.375840E-03	4.853114E-03	5.954868E-03
kz__9	2.105960E-02	3.440261E-03	0.128917
kx_10	5.729560E-02	3.179626E-02	0.103244
kx_11	3.31370	2.82329	3.88930
kx_13	2.12226	1.82840	2.46335
kx_14	42.2989	36.1168	49.5392
kx_15	4.226010E-03	9.326407E-04	1.914903E-02
kx_16	0.341256	0.223481	0.521100
kx_17	0.418386	0.240035	0.729256
kx_18	120.926	59.5800	245.436
par010	1.00000	0.902636	1.10787
par011	1.00000	0.854744	1.16994
par012	1.00000	0.145433	6.87600
par013	1.00000	0.318063	3.14403
par002	1.00812	0.929687	1.09317
par001	0.859345	0.269503	2.74014
par014	1.00000	1.588263E-71	6.296187E+70
par015	1.00000	0.849993	1.17648
par003	1.00000	0.899396	1.11186
par018	0.903385	0.757120	1.07791
par019	1.18844	0.925569	1.52597
par027	1.06327	0.557147	2.02916
par005	1.00000	0.828640	1.20680
par007	1.00000	0.102177	9.78689
par008	1.00000	0.844717	1.18383
par006	0.984263	0.682879	1.41866
sy__2	0.149706	0.117818	0.190224
sy__3	7.451470E-02	6.739671E-02	8.238445E-02

Figure A1. *Optimized solution BK2_inv.rec {Par cross-reference: par010=CVID canal recharge; par011=LIC AG recharge;par012=CVID+LIC AG recharge; pa r002=Granite Creek recharge; par001=UAF underflow; par014=Underflow, Watson Lake; par015=upper Lynx recharge; par003=MFR-NW; par018=low Lynx recharge; par019=LIC underflow, NW; par027=LIC inflow from BIC; par005=MFR-SE; par007=Williamson Valley recharge; par008=Glassford Hill recharge; par006=Upper Lynx recharge recharge.} K_x1 omitted from NL regression*

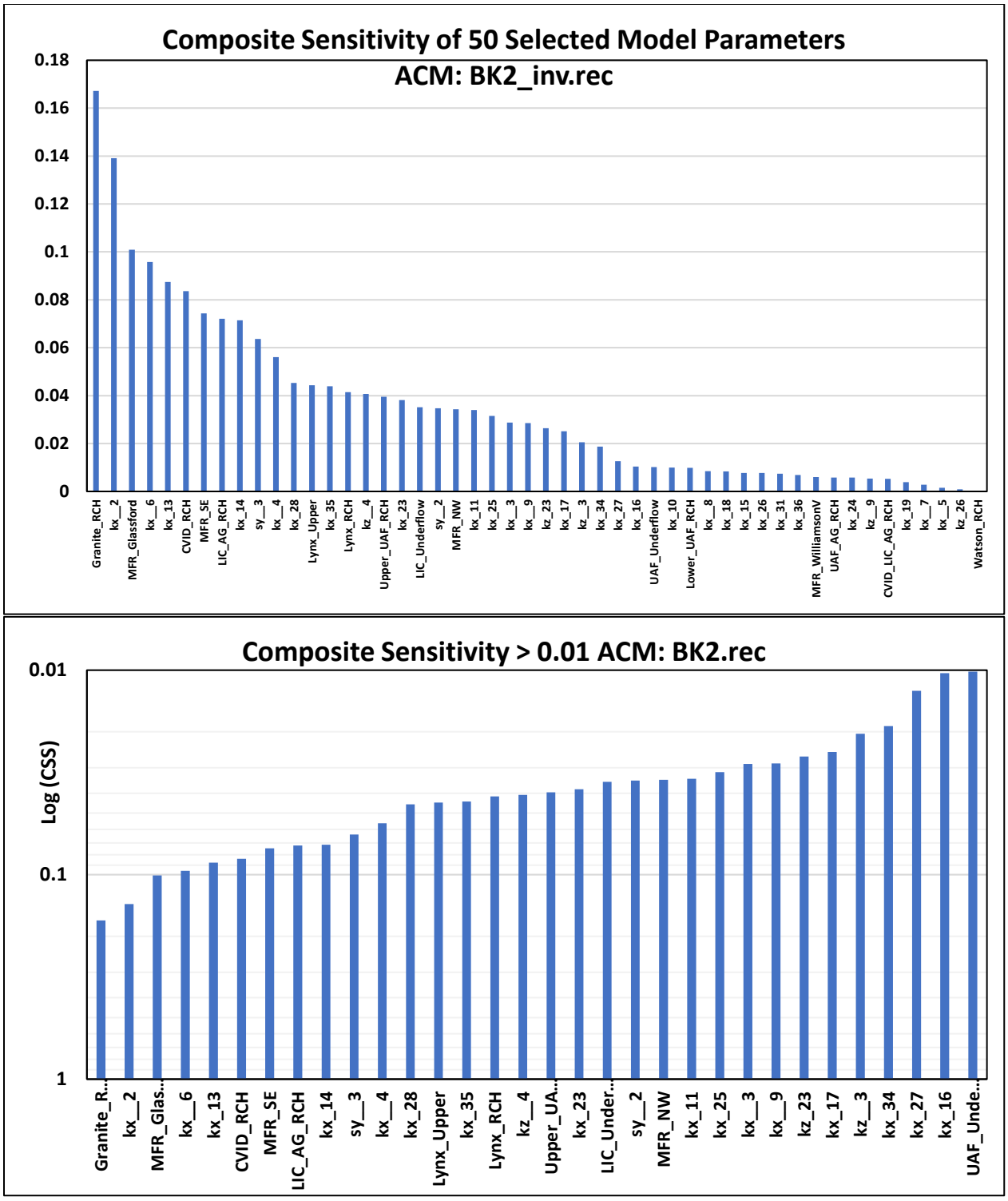

Figures A2 and **A3.** *Composite sensitivities for the 50-parameter solution, arithmetic scale (top); CSS > 0.01, log-scale (bottom). For both figures, parameter sensitivity decreases from left-to-right.*

As mentioned above there is modest parameter correlation between recharge applied along upper Lynx Creek (par006) and Glassford Hill (par008), shown below in [48,47]. Further inspection also shows modest correlation also exist between the receiving hydraulic conductivity zone, K_x16 (**Figure A4**).

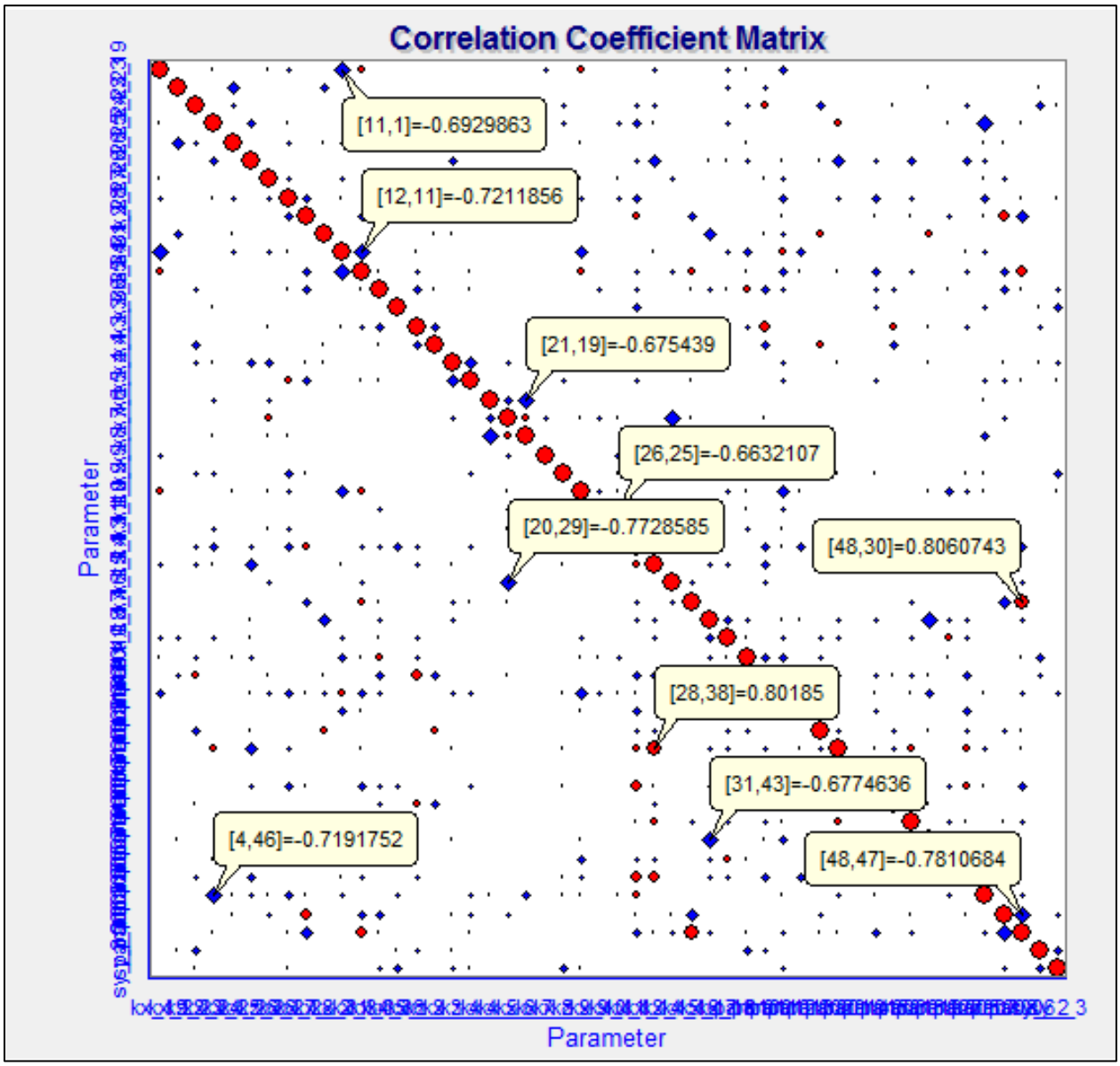

Figure A4. *Parameter Correlation Coefficient Matrix. Note: P-4=>Kx24; P-20 => Kx6; P-28 => Kx14; P-29 => Kx15; P-30 =>Kx16; P-38=>UAF underflow;P-49=>RCH6; P-47=>RCH7; P-48=> RCH8*

Functional dependence between these three terms is also evident in the normalized eigenvectors of the parameter covariance matrix in **Figure A5**. Much of the variance linked to those terms can be explained by their orthogonal relations of the eigenvectors, expressed through the eigenvalues; note that the larger eigenvalues represent more parameter (co)variance (uncertainty).

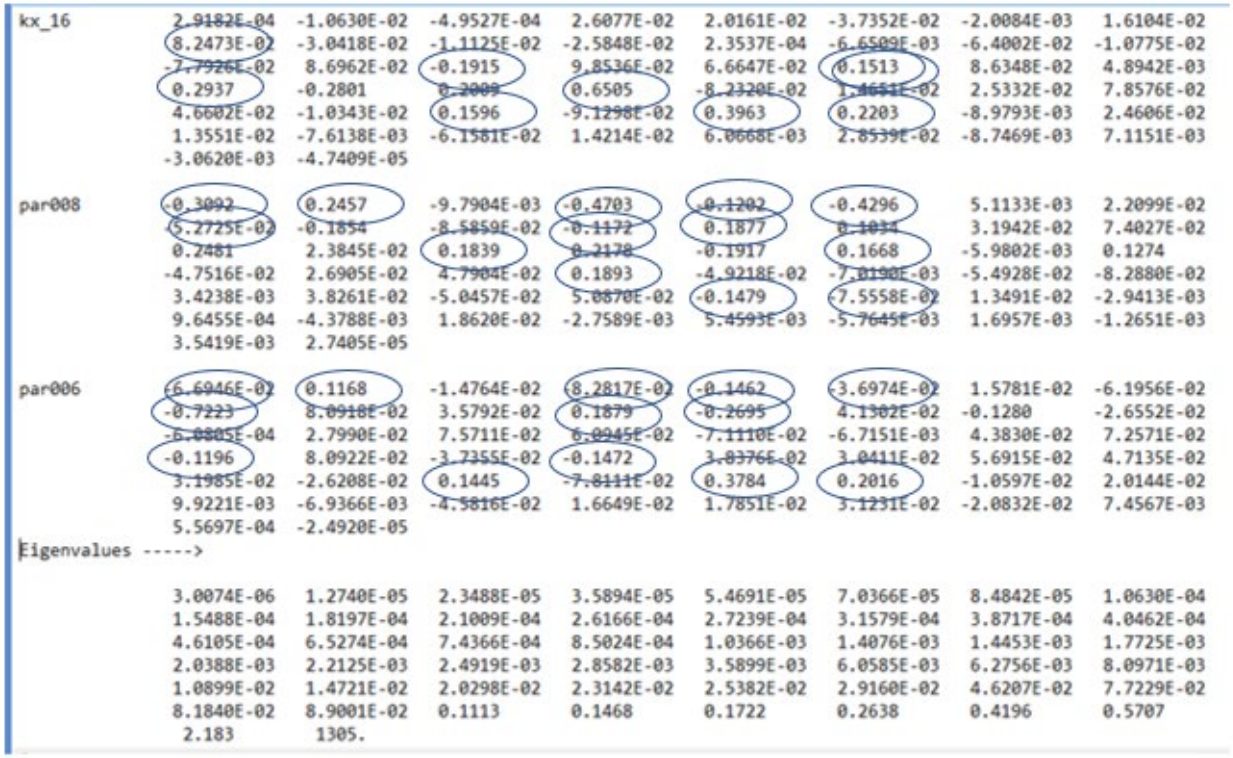

kx_16	2.9182E-04	-1.0630E-02	-4.9527E-04	2.6077E-02	2.0161E-02	-3.7352E-02	-2.0084E-03	1.6104E-02
	8.2473E-02	-3.0418E-02	-1.1125E-02	-2.5848E-02	2.3537E-04	-6.6509E-03	-6.4002E-02	-1.0775E-02
	-7.7926E-02	8.6962E-02	-0.1915	9.8536E-02	6.6647E-02	0.1513	8.6348E-02	4.8942E-03
	0.2937	-0.2801	0.2009	0.6505	-8.2320E-02	1.4651E-02	2.5332E-02	7.8576E-02
	4.6602E-02	-1.0343E-02	0.1596	-9.1298E-02	0.3963	0.2203	-8.9793E-03	2.4606E-02
	1.3551E-02	-7.6138E-03	-6.1581E-02	1.4214E-02	6.0668E-03	2.8539E-02	-8.7469E-03	7.1151E-03
	-3.0620E-03	-4.7409E-05						
par008	-0.3092	0.2457	-9.7904E-03	-0.4703	-0.1202	-0.4296	5.1133E-03	2.2099E-02
	5.2725E-02	-0.1854	-8.5859E-02	-0.1172	0.1877	0.1034	3.1942E-02	7.4027E-02
	0.2481	2.3845E-02	0.1839	0.2178	-0.1917	0.1668	-5.9802E-03	0.1274
	-4.7516E-02	2.6905E-02	4.7904E-02	0.1893	-4.9218E-02	-7.0190E-03	-5.4928E-02	-8.2880E-02
	3.4238E-03	3.8261E-02	-5.0457E-02	5.0870E-02	-0.1479	-7.5558E-02	1.3491E-02	-2.9413E-03
	9.6455E-04	-4.3788E-03	1.8620E-02	-2.7589E-03	5.4593E-03	-5.7645E-03	1.6957E-03	-1.2651E-03
	3.5419E-03	2.7405E-05						
par006	6.6946E-02	0.1168	-1.4764E-02	8.2817E-02	-0.1462	3.6974E-02	1.5781E-02	-6.1956E-02
	-0.7223	8.0918E-02	3.5792E-02	0.1879	-0.2695	4.1302E-02	-0.1280	-2.6552E-02
	-6.0805E-04	2.7990E-02	7.5711E-02	6.0945E-02	-7.1110E-02	-6.7151E-03	4.3830E-02	7.2571E-02
	-0.1196	8.0922E-02	-3.7355E-02	-0.1472	3.8376E-02	3.0411E-02	5.6915E-02	4.7135E-02
	3.1985E-02	-2.6208E-02	0.1445	-7.8111E-02	0.3784	0.2016	-1.0597E-02	2.0144E-02
	9.9221E-03	-6.9366E-03	-4.5816E-02	1.6649E-02	1.7851E-02	3.1231E-02	-2.0832E-02	7.4567E-03
	5.5697E-04	-2.4920E-05						
Eigenvalues ----->								
	3.0074E-06	1.2740E-05	2.3488E-05	3.5894E-05	5.4691E-05	7.0366E-05	8.4842E-05	1.0630E-04
	1.5488E-04	1.8197E-04	2.1009E-04	2.6166E-04	2.7239E-04	3.1579E-04	3.8717E-04	4.0462E-04
	4.6105E-04	6.5274E-04	7.4366E-04	8.5024E-04	1.0366E-03	1.4076E-03	1.4453E-03	1.7725E-03
	2.0388E-03	2.2125E-03	2.4919E-03	2.8582E-03	3.5899E-03	6.0585E-03	6.2756E-03	8.0971E-03
	1.0899E-02	1.4721E-02	2.0298E-02	2.3142E-02	2.5382E-02	2.9160E-02	4.6207E-02	7.7229E-02
	8.1840E-02	8.9001E-02	0.1113	0.1468	0.1722	0.2638	0.4196	0.5707
	2.183	1305.						

Figure A5. *Normalized Eigenvectors of the parameter covariance matrix. Note that the full eigenvector display (50 terms) has been collapsed to show only Kx16 (30), par006/RCH8/Lynx_RCH and par008/RCH7_Glassford_Hill*

Regarding Kx16, RCH8 and RCH7, the percentage of total system variance explained by the common terms (blue ovals) is about 75%. Nonetheless, most of the variance is expressed through eigenvalues having relatively low magnitudes. While some parameter dependence exists (parameter uncertainty), extreme parameter correlation does not exist.

Another complex relation exists between the stream alluvium in the lower UAF Sub-basin (Kx14) and underflow out of the UAF Sub-basin. When only head data is used to constrain parameter estimates, the Jacobian Matrix shows modest observation response symmetry, inferring parameter correlation exists (**Figure A6**). However, when groundwater discharge targets are included, the flow terms provide observation markers that increase parameter sensitivity and uniqueness (**Figure A7**). With inclusive flow data, the parameter correlation, +0.8, is well below problematic levels (Hill, 1998). Nonetheless, modest dependence among some estimated parameters, inevitably, results in uncertainty for some variables included in the non-linear regression.

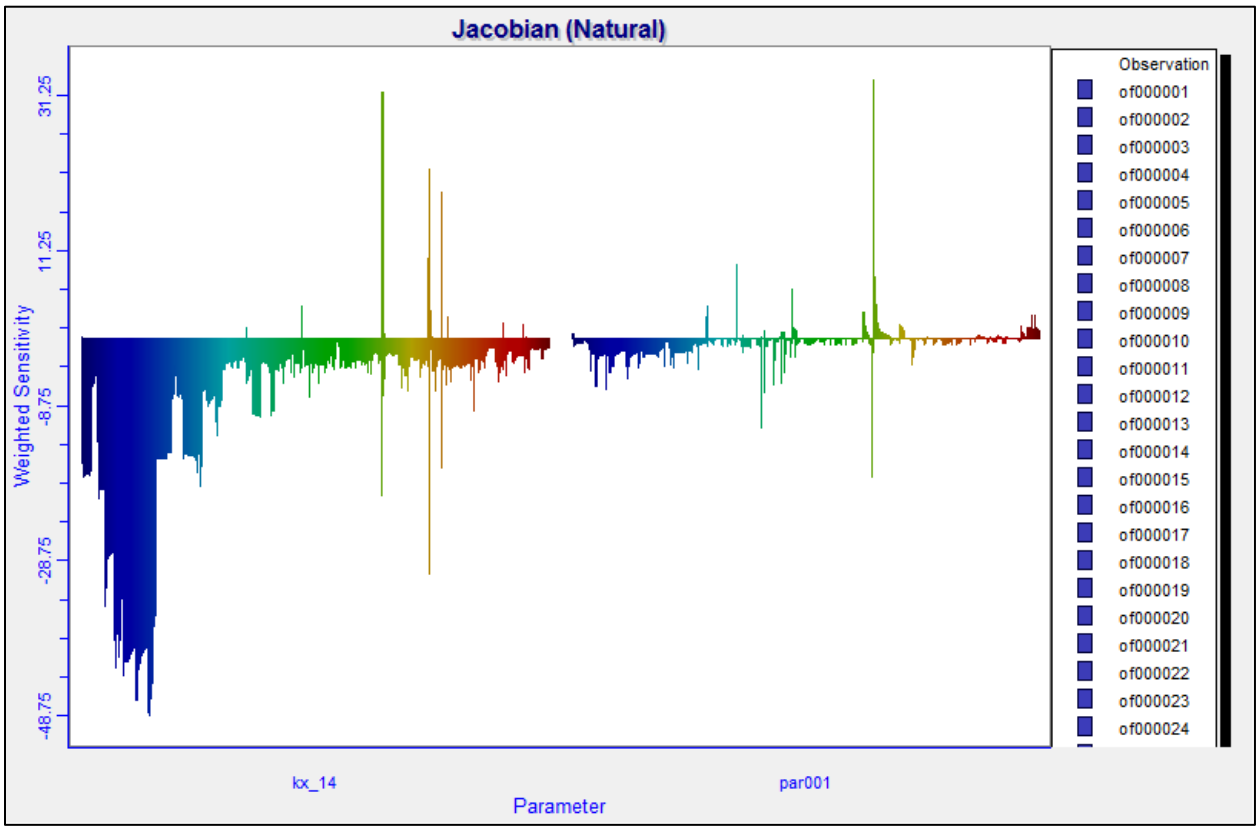

Figure A6. *Jacobian Matrix displaying weighted head sensitivity.*

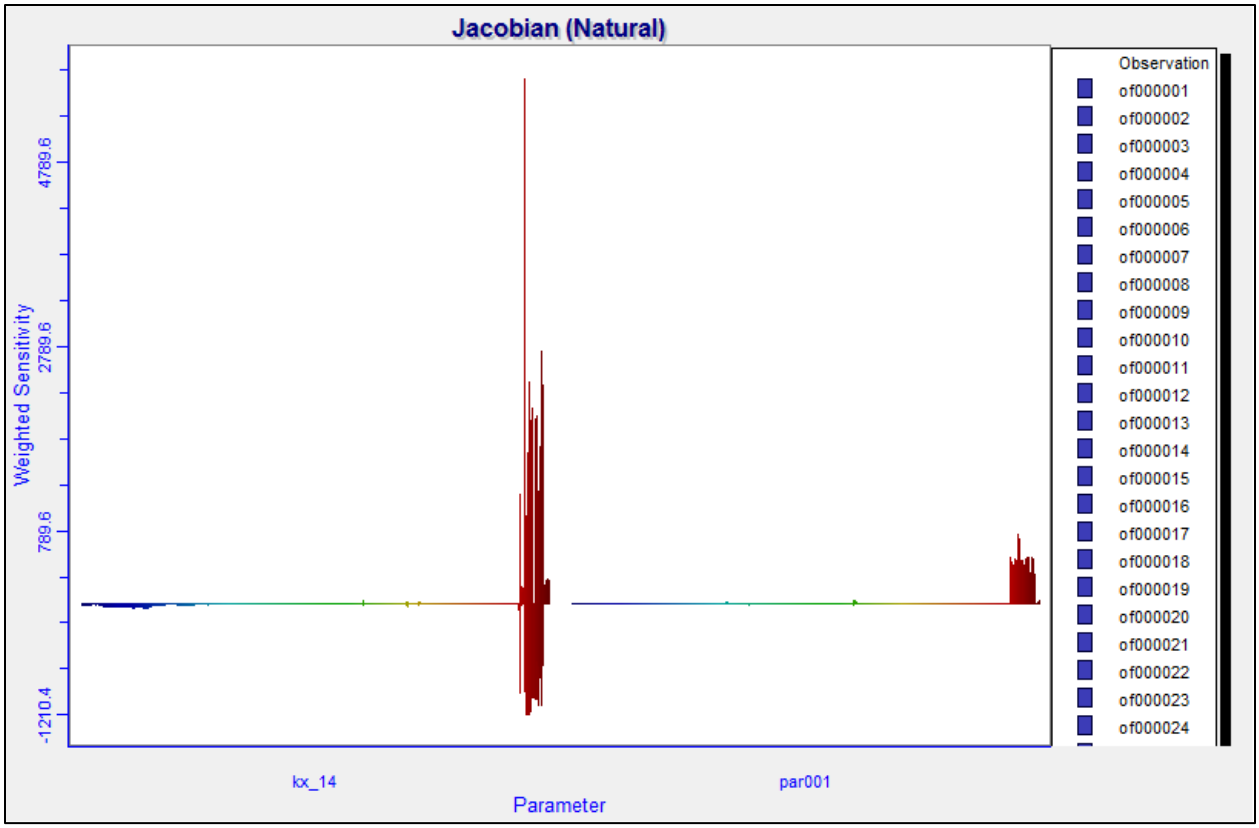

Figure A7. *Jacobian Matrix displaying weighted head and flow sensitivity*

However, when flow is added in combination with heads, the flow terms provide observation markers that both increase sensitivity and parameter uniqueness. With inclusive flow data, the parameter correlation +0.8, well below problematic levels (see Hill, 1998).

Appendix B: Miscellaneous Simulated Water Budget Information

*Simulated Steady State Water Budget, circa 1939			
Inflow Component	**AF/yr**	**Inflow**	**AF/yr**
LIC: CVID AG + MFR	1,977	MFR & CVID AG recharge	5,803
UAF: Agua Fria RCH: R=135+Str=896	1,031		
LIC: Del Rio downstream re-infiltration	10		
LIC & UAF: Broad MFR	2,311		
LIC: CVID RCH	474		
LIC: Granite Creek recharge	3,977	Granite & Lynx Creek Natural recharge	7,702
UAF: Lynx Creek & Agua Fria recharge	3,725		
LIC: BIC underflow to LIC (limestones)	2,233	Underflow from BIC	2,233
Total Inflow	**15,738**		**15,738**
Outflow Component	**AF/yr**	**Outflow**	**AF/yr**
LIC: Del Rio Springs	5,301	Del Rio Springs	5,301
LIC: Underflow to the NXNE	1,051	LIC Underflow to BIC	4,017
LIC: Underflow to the NXNW)	2,966		
UAF: Agua Fria Baseflow reach)[1]	3,605	Agua Fria Baseflow	3,605
UAF: Underflow: -Rch=499+Str=1,374[2]	1,873	UAF Underflow 1,873	1,873
UAF: Agua Fria & Lynx, bank release[3]	548	Early-development groundwater pumping; bank releases	932
LIC: Granite Creek bank release[4]	194		
LIC & UAF minor discharge balance	10		
LIC: groundwater pumping	180		
Total Outflow	**15,728**		**15,728**

*Rates have been annualized. Although recharge cells represented most of the periodic recharge occurring along the major tributaries of Granite Creek, Lynx Creek and the Agua Fria River, stream cells remained active (even though *no* surface water flow was introduced at upstream segments), the conditioned steady state solution resulted in some minor groundwater discharge near shallow areas. ACMs that assume early-time pumping in the UAF (see Nelson and Yunker, 2014) results in different solutions, where some of the net groundwater discharge out would be categorized as wells, but the total outflow is, generally, consistent. Regarding net groundwater targets (which *are* the calibration targets), subtract str seepage inflow. Simulated groundwater discharge may represent flow discharge below USGS gauge near Humboldt. Along the southern boundary, when head-dependent boundaries (GHB; lower Str reach) are replaced with specified flux, optimize underflow rates are generally greater than 1,000 AF/yr.

[1] Groundwater discharge above gauge.

[2] Groundwater discharge and underflow below gauge. It should be noted that when the str boundary along the lowest portion of the Agua Fria River boundary was omitted, underflow rates out of the UAF sub-basin using specified flux increased to ~ 1K AF/yr

("20210531PrAMA_GHB_N_S.rec"). Thus, as with underflow beneath the northern boundary, underflow out of the UAF was necessary to reduce groundwater discharge flow bias, based on available data.

[3] Minor groundwater upgradient of baseflow reach using str cells.

[4]Minor groundwater discharge (bank release) along Granite Creek following significant flood recharge events, i.e., 1980; 1993 etc. Note that ACM's were developed, where independent model parameters representing dispersed, natural recharge in the basin valley center (excluding Granite Creek, Lynx Creek and the Agua Fria River) were optimized to evaluate the magnitude of recharge that might occur away from proven, efficient natural recharge zones (e.g., Granite Creek; lower Lynx Creek, etc.). Non-linear regression results indicate low rate of natural recharge occur in basin-center area. Thus, conveyance of precipitation-based runoff away from in valley center areas (where most of the water simply evaporates) towards areas having efficient recharge could augment recharge and help balance the long-term over-draft.

Table B1. *Simulated Steady State Water Budget.*

Most of the inflow and outflow terms associated with the simulated transient water budget change over time. As a result, the rates shown in **Table B1** represent annualized averages. Furthermore, due to spatial and temporal resolution limitations, some individual model cells have multiple types of uses. For example, in terms of simulated pumping, some individual model cells are subject to exempt, municipal and/or agricultural demands. In addition, there are also individual cells that receive multiple forms of recharge including natural flood recharge, agricultural and artificial recharge. Examples of recharge are shown in **Photographs B1** and **B2**. Thus, some components of the transient water budget reflect multiple water-use types.

Photograph B1. *Recharge along Granite Creek, 2008.Photo courtesy of Doug McMillan. Highway 89A in foreground; photo faces to the north.*

Photograph B2. *Stream recharge along losing reach, Agua Fria River, Dewey-Humboldt AZ March 17th, 2017; photo facing south.*

A transient water budget is presented in **Table B2** showing simulated water budgets terms for the LIC and UAF Sub-basins.

*Simulated Transient Water Budget (long-term annualized rates)			
Inflow Component	**AF/yr**	**Inflow / notes**	**AF/yr**
LIC: Storage in	14,556	Total Storage in	18,233
UAF: Storage in	3,677		
LIC Sub-basin Recharge, RCH cells[5]	14,244	Total Recharge (RCH cells)	20,607
UAF Sub-basin Recharge, RCH cells	6,363		
str recharge, losing reaches, str cells	12	Granite & Lynx Creek Natural recharge (Str cells)	865
str recharge, baseflow re-infiltration, Agua Fria River (str) [2]	853		
str recharge, baseflow re-infiltration, Del Rio Springs (str)	0		
Total Inflow	**39,705**		**39,705**
Outflow Component	**AF/yr**	**Outflow / notes**	**AF/yr**
LIC: Storage out	8,560	Total Storage out	10,940
UAF: Storage out	2,380		
LIC: Groundwater discharge, Del Rio*	1,997	LIC Str = 1,997	6,044
UAF: Groundwater discharge_baseflow [1]	2,385	UAF Str = 4,046	
UAF: Str_Out_UAF_Lower Baseflow 2014 [2]	1,661		
UAF: EVT	456	Total_EVT ->	715
LIC: EVT	259		
UAF: Underflow_rch [2]	500	Recharge cells	500
LIC: Underflow_rch_NE_to_Verde_Baseflow[3]	1050		3,863
LIC: Underflow_GHB_NW_to_BIC[4]	2,813	GHB cell	
LIC Sub-basin simulated pumping	14,703	Total pumping	17,571
UAF Sub-basin simulated pumping[1]	2,868		
Total Outflow	**39,632**		**39,633**
Net Change-in-storage	**-7,293**		

*Rates have been annualized. Rates representing Del Rio Springs show a strong decreasing trend over time. Long-term mean net change-in-storage rates in the LIC and UAF are 6,000 and about 1,300 AF/yr, respectively. To obtain cumulative volumes simulated during the transient period, the mean rates can be integrated over time (79.945 years). Note that the ACMs and water budgets presented in this report assume there was no early-time pumping in the UAF; for a description of plausible ACMs that assume early-time pumping and surface water diversion in the UAF Sub-basin, see Nelson and Yunker (2014)

1. Simulated groundwater discharge may represent flow discharge below USGS gauge near Humboldt.

2. Mass balance error =0.0019, or 73 AF/yr: 39,705AF/yr. When Hclose was reduced from 10 to 1 ft, mass balance was 0.001; the resulting solution was effectively identical. Although recharge cells represented most of the periodic recharge occurring along the major tributaries of

Granite Creek, Lynx Creek and the Agua Fria River, stream cells remained active (even though *no* surface water flow was introduced at upstream segments.

[2]There are several groundwater discharge outflow terms associated with the southern boundary including net 1) baseflow above the gauge (net str, representing baseflow along the Agua Fria River); 2) below the gage (another net str, representing groundwater discharge below the gauge, which in this case is strictly str_out); 3) underflow as specified flux (-RCH) and 4) EVT. It should be noted that when the str boundary along the lowest portion of the Agua Fria River boundary was omitted, underflow rates out of the UAF sub-basin using specified flux increased to ≥ 1K AF/yr ("20210531PrAMA_GHB_N_S.rec").

[3 & 4]There are several groundwater discharge outflow terms associated with the northern boundary including net 1) baseflow above the gauge (representing Del Rio Springs); 2) underflow to the NE (specified flux), underflow to the northwest (NW GHB) and 4) EVT.

[5] Includes a "new" inflow component from the BIC sub-basin; this term along with contributions from the LIC sub-basin (in addition to the NE underflow), combine and exit through the NW GHB. [3]When specified flux (to the NE) was replaced with a GHB (applying plausible external-elevation-distance controls as well as conductance values consistent with adjacent *K_x2)*, underflow rates to the BIC/Verde Headwaters area increased, in order to reduce model bias. With respect to previous estimates, higher underflow contributions from the LIC sub-basin to the BIC sub-basin/Verde are not inconsistent with recent data in the BIC, which show only modest flood recharge along the Big Chino Wash; that is, it is more likely that that there is another *non* BIC Sub-basin contribution associated with groundwater discharge to the Verde River Headwaters; independent of groundwater modeling, steep hydraulic gradients from the northern boundary towards both the NE and NW suggest that LIC sub-basin provides subsurface flow to the BIC. Different configurations of the northern and southern boundaries provide similar results over the calibration period. With respect to the model calibration, flow calibration targets are more sensitive - and discriminating - than head calibration for discerning and ranking ACM's. Thus, for evaluating the groundwater flow system into the future, it is strongly suggested that users employ boundary condition configurations that are consistent in function with the calibration period.

Table B2. *Simulated transient state water budget K_x2.*

The cumulative net change-in-storage loss was simulated at 583,300 AF during the 80-year transient simulation, resulting in an annualized mean net change-in-storage loss of 7,300 AF/yr. The cumulative simulated pumping was 1.4 million AF, equaling an average annualized mean of 17,565 AF/yr. The distribution of selected water budget components is provided below in **Figures B1 through B6**.

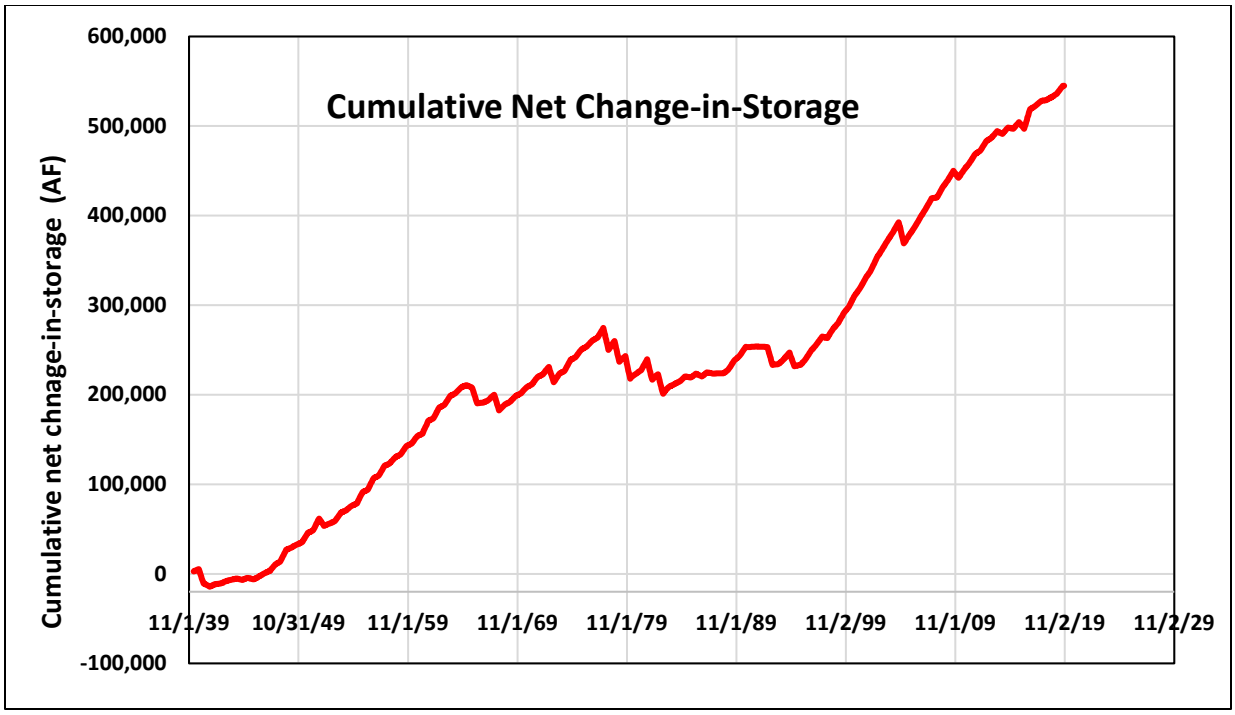

Figure B1. *Simulated cumulative net change-in-storage.*

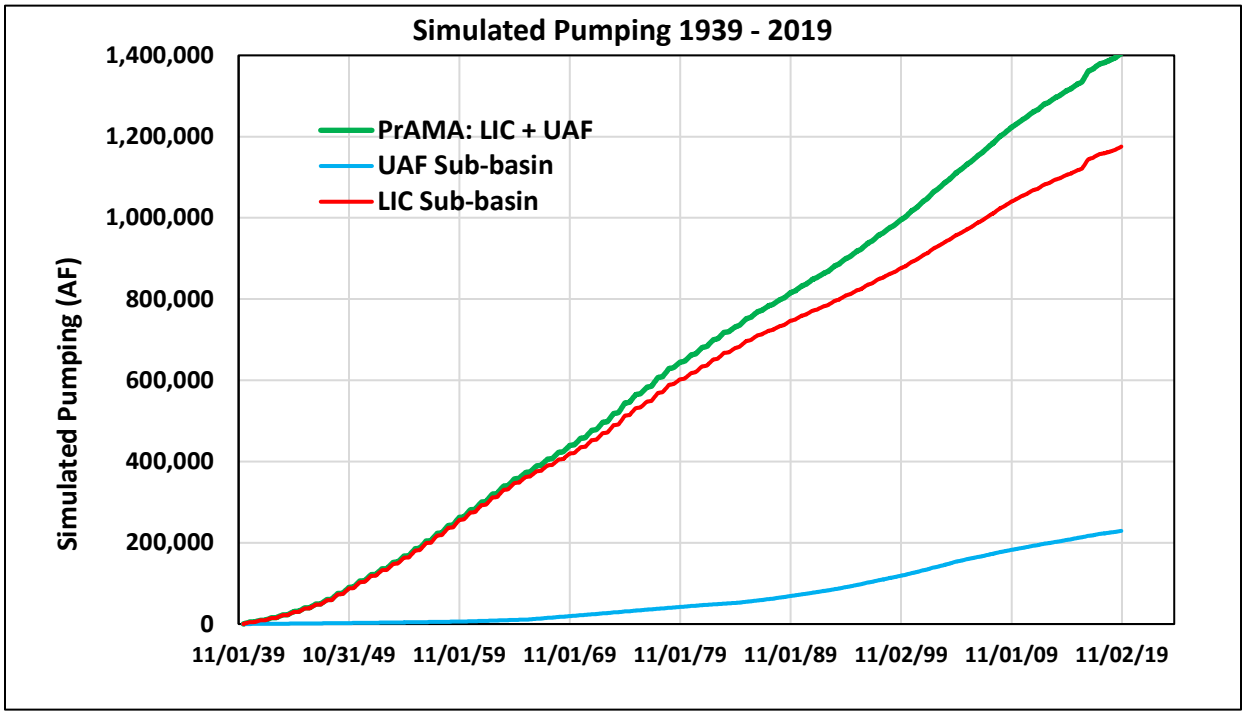

Figure B2. *Simulated pumping 1939-2019.*

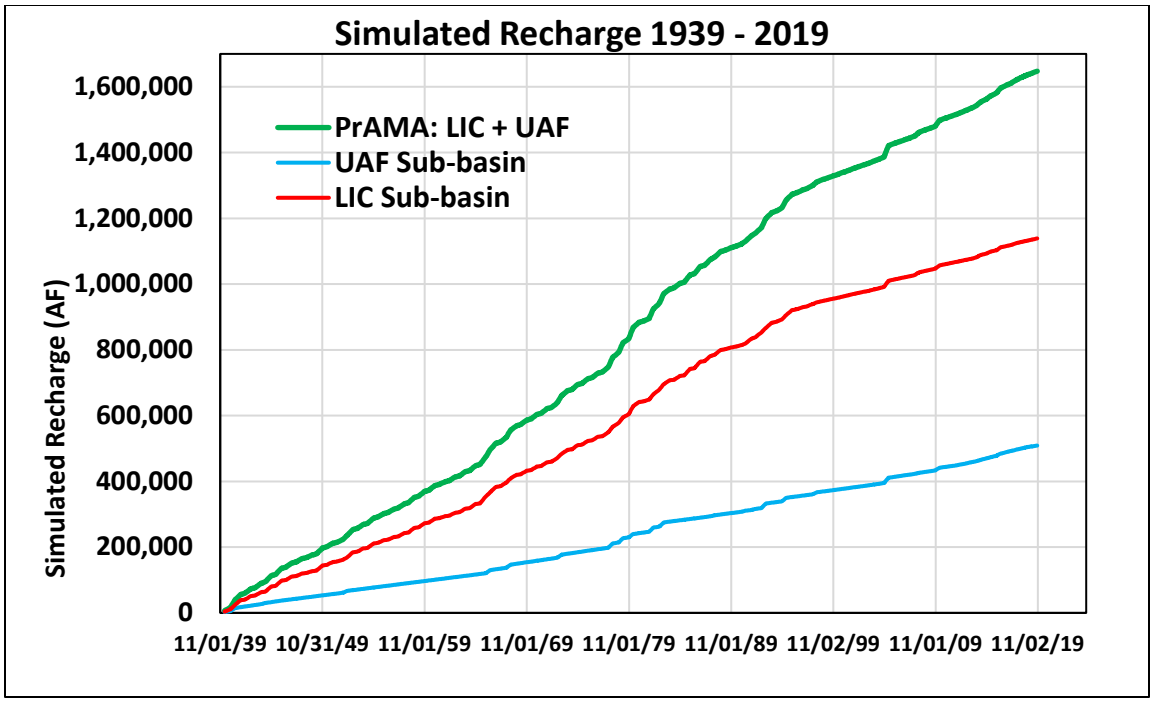

Figure B3. *Simulated recharge 1939-2019.*

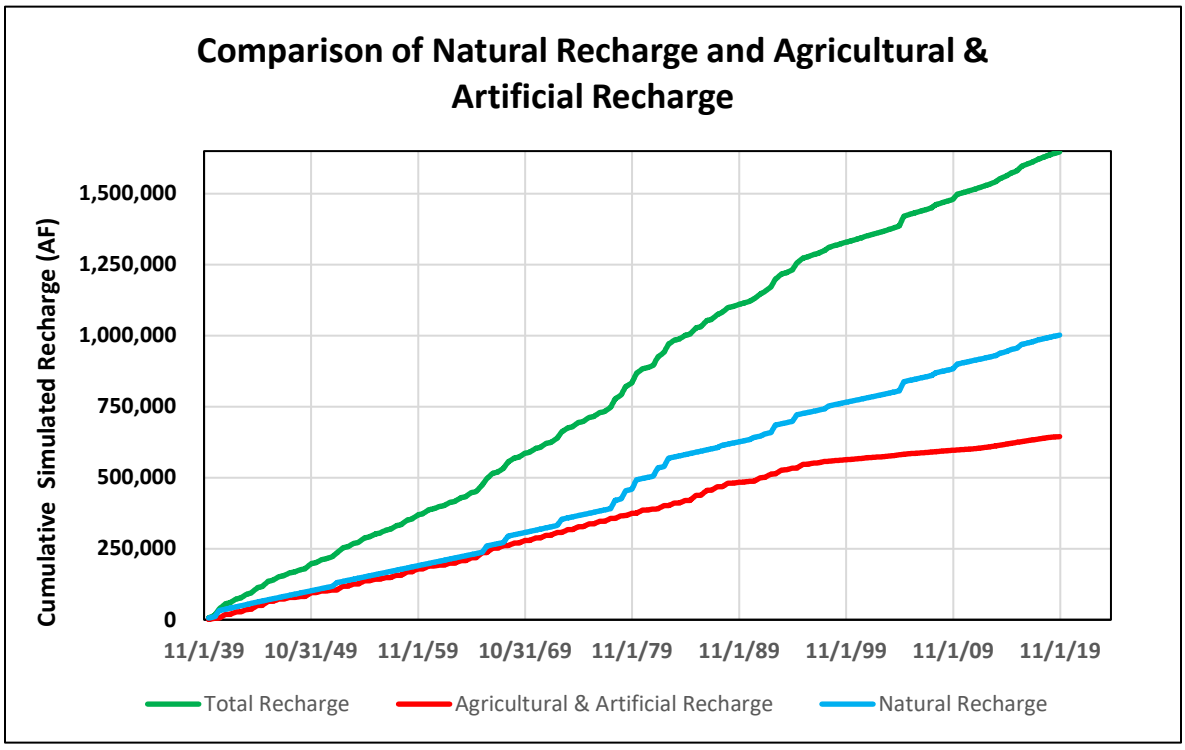

Figure B4. *Comparison of natural, agricultural, and USF recharge.*

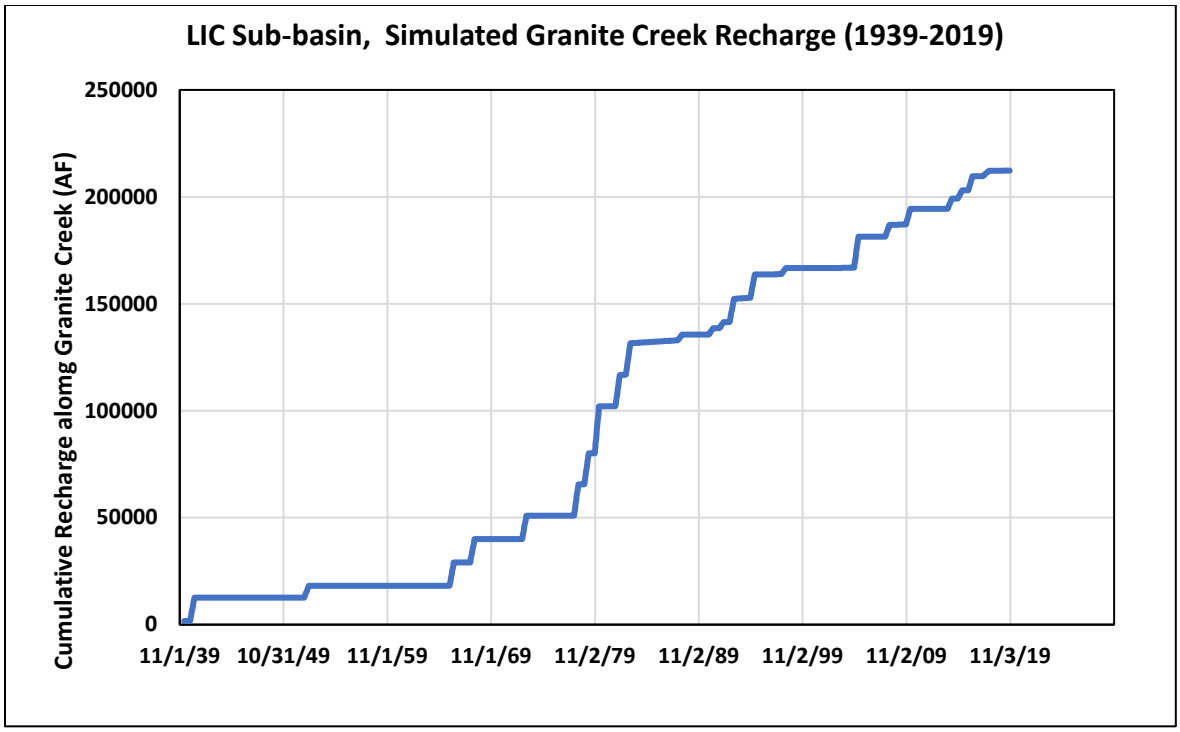

Figure B5. *Simulated natural recharge along Granite Creek.*

Cumulative simulated recharge totaled 212,270 AF, resulting in an average of about 2,655 AF/yr. The steady state recharge rate along Granite Creek was estimated at 3,977 AF/yr using non-linear regression techniques. Steady state recharge along Granite Creek represents a transitional, quasi-steady flow rate, that reflects the groundwater flow system prior-to and after, construction of Watson and Willow Creek Dams. That steady state recharge along Granite Creek was optimized to be higher than transient-period rates and is consistent with the conceptual model, which assumes impounding of surface water would reduce the overall recharge along Granite Creek, all else equal. It should be noted that after the construction of Watson and Willow Creek Dams, incidental agricultural recharge associated with the delivery of surface water by Chino Valley Irrigation District (CVID) effectively displaced a component of natural recharge that would have, otherwise, resulted in natural recharge along nearby Granite Creek. Similarly, during later phases of the transient simulation, impounded surface waters were redirected toward the City of Prescott's artificial recharge site, located near the airport (**Figure B1**).

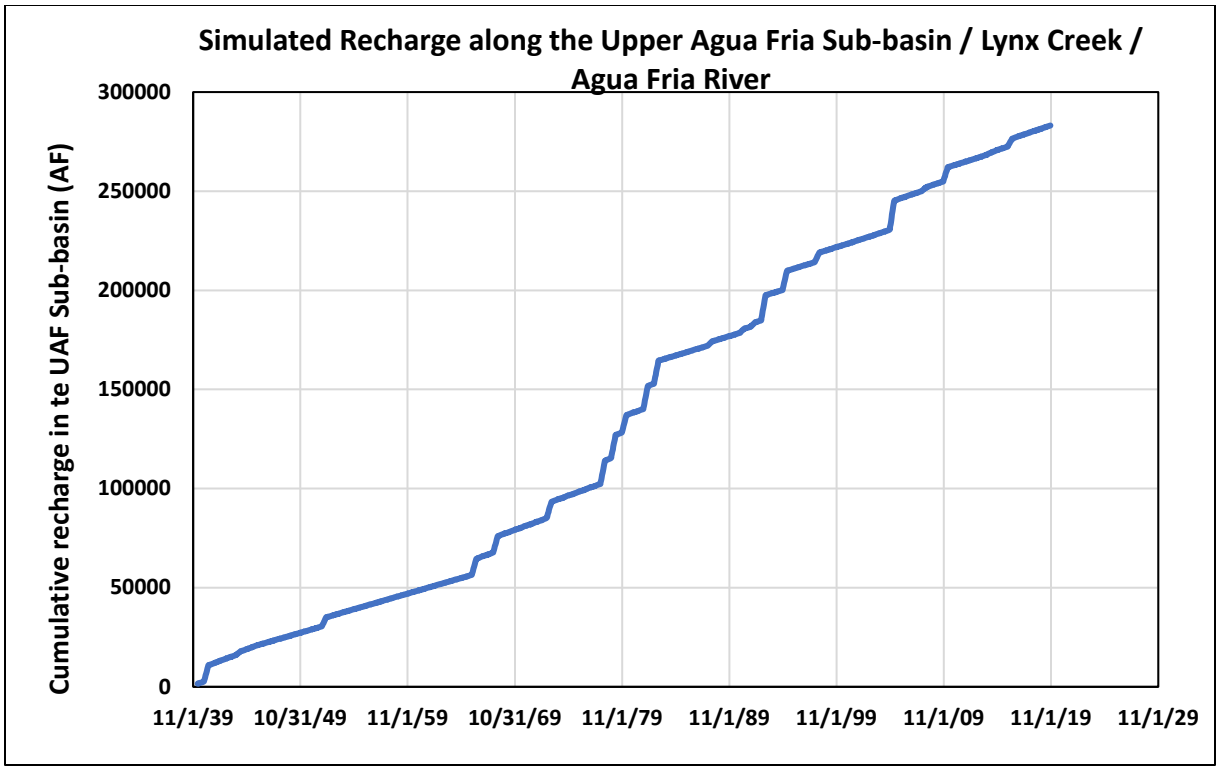

Figure B6. *Simulated natural recharge in the UAF Sub-basin.*

Cumulative simulated recharge in the UAF Sub-basin totaled 283,130 AF, resulting in a long-term annualized average rate of about 3,542 AF/yr. The steady state natural recharge in the UAF Sub-basin was independently estimated using non-linear regression techniques at 3,725 AF/yr. This result is consistent with the conceptual model, which assumes minimal surface water diversion and only minor evaporation from Lynx Lake, all else equal.

Appendix C: The Northern and Southern Model Boundaries

Northern Boundary

With respect to previous Prescott AMA regional groundwater flow model updates, a group of high-ranking ACMs consistently yielded solutions that had higher underflow rates from the LIC to BIC Sub-basin. Subsequent investigation revealed groundwater levels consistent with elevations associated with wells perforated in limestones including, (B-17-03)29CAC and (B-17-02)29ADC, found more commonly in the BIC Sub-basin, and ultimately, in direct hydraulic connection with the headwaters of the Verde River. This newly identified underflow component out of the LIC Sub-basin is generally directed to north and northwest (NW underflow) is assumed to occur in addition to the underflow, assumed to generally flow to northeast (NE underflow); thus in this model update, there are two underflow components associated with the northern boundary.

The (existing) NE underflow term was optimized as a specified flux and retained at a constant rate of 1,050 AF/yr; the 95% $CI_{(log)}$ range between 820 AF/yr and 1,350 AF/yr.

Underflow exiting the NW boundary is represented as a general head boundary (GHB), and the conceptual model assumes groundwater flow contributions originating from both the LIC (in addition to NE underflow) and BIC sub-basins. The influx rate from the BIC was determined using non-linear regression and was estimated at 2,230 AF/yr and the 95% $CI_{(log)}$ range was from 1,180 AF/yr to 4,260 AF/yr. For steady state conditions, the NW underflow simulated through the GHB was estimated at 2,966 AF/yr, inferring the balance, or 736 AF/yr, originated from the LIC Sub-basin.

Finally, the total steady state underflow rate simulated from model, including both the NW and NE boundaries, totals 4,017 AF/yr. During the transient simulation, capture of underflow directed towards the Verde River baseflow simulated through the GHB, was calculated at 241 AF/yr. This is addition to the capture of groundwater discharge that has occurred at Del Rio Springs. The northern boundary is illustrated in **Figure C1** below.

Inspection of the inverse model statistics indicate that most of variance associated with constraining the northern boundary is influenced by "local" parameters, such as K_x2, K_x17, K_x18, underflow out (RCH31), and BIC underflow in (RCH47). However, inspection of normalized eigenvectors of the parameter covariance matrix also indicates that there is interdependence among these parameters. When another ACM was tested assuming underflow through the NE boundary be represented by a GHB instead of a specified flux boundary (ACM NE_{GHB}), the collective steady state underflow rate *from* the LIC sub-basin *to* the BIC sub-basin and Verde headwaters area exceeded 6,000 AF/yr. It should be noted that resulting solution to ACM NE_{GHB} is plausible (*20210531PrAMA_GHB_N_S.rec*). Thus, parameters and underflow rates associated with the northern boundary are subject to uncertainty. However, based on available data, less model bias occurs - especially when discriminating with flow targets and head targets in the extreme northwestern portion of the model domain - when substantial underflow rates are simulated *from* the LIC sub-basin *to* the BIC Sub-basin and Verde Headwaters area.

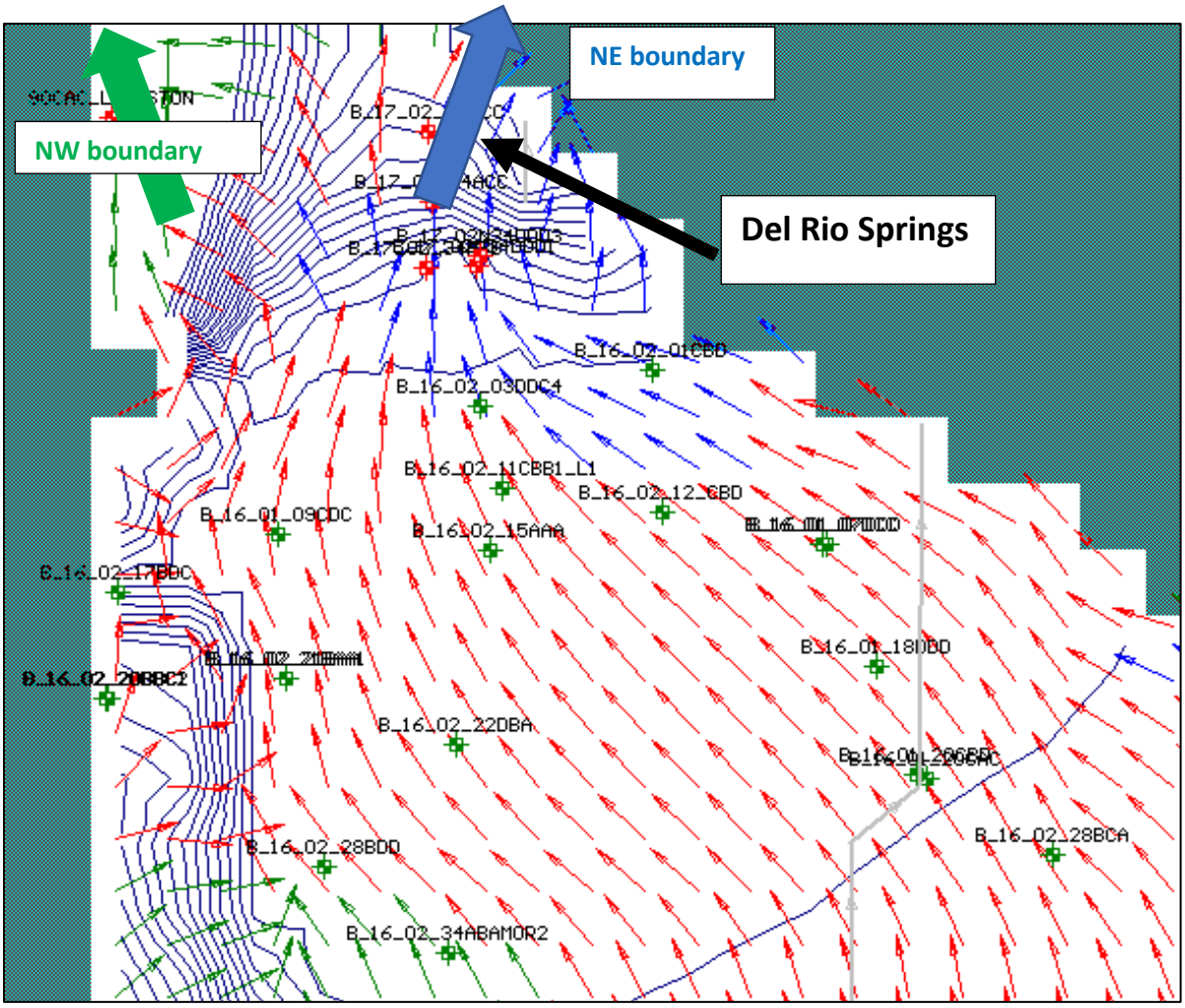

Figure C1. *Simulation of groundwater flow in model layer 2 along the northern model boundary, steady state conditions, 1939.*

The large blue and green arrows represent underflow directed towards the NE and NW, respectively. The small arrows represent regional-scale groundwater where the red, green and blue arrows represent downward, horizontal and upward flow, respectively. Note how the model represents artesian flow conditions, circa 1939.

The Southern Boundary

In the southern portion of the model, two additional model rows were activated in UAF Sub-basin in order to extend the distance between the southern boundary and simulated model stresses to the north. Furthermore, to better represent potential regional influences in the lower UAF Sub-basin, selected model cells in layer 2 were activated. Due to the uncertainty in defining contact elevations between the stream alluvium, the Hickey Formation and bedrock, as well as the observed existence of fracture flow in bedrock (CH2M Hill, 2016), a generalized thickness of 300 ft was assigned. Most underflow is assumed to occur in relatively shallow coarse-grain stream sediments and deeper preferential flows through fractures and faults.

Near the southern model boundary, data also show that wells screened in the alluvium and Hickey Formation respond to flood recharge events (GWSI, 2021; CH2M Hill, 2016), further supporting the existence of underflow and thin zones of high hydraulic conductivity. The relocation of the southern boundary one mile to the south (to model row 48) and the activation of layer 2 cell in portions of the UAF Sub-basins, is assumed to further attenuate potential adverse boundary affects associated with regional-scale groundwater flow in the UAF Sub-basin. The transmissivity of the newly activated area was expected to be low and subsequent testing confirmed this.

In the UAF Sub-basin, the highest groundwater flow rates occur in the course stream sands and gravels associated with the Agua Fria River and its major tributaries. **Figure C2** below illustrates the magnitude of relative flow in the subsurface.

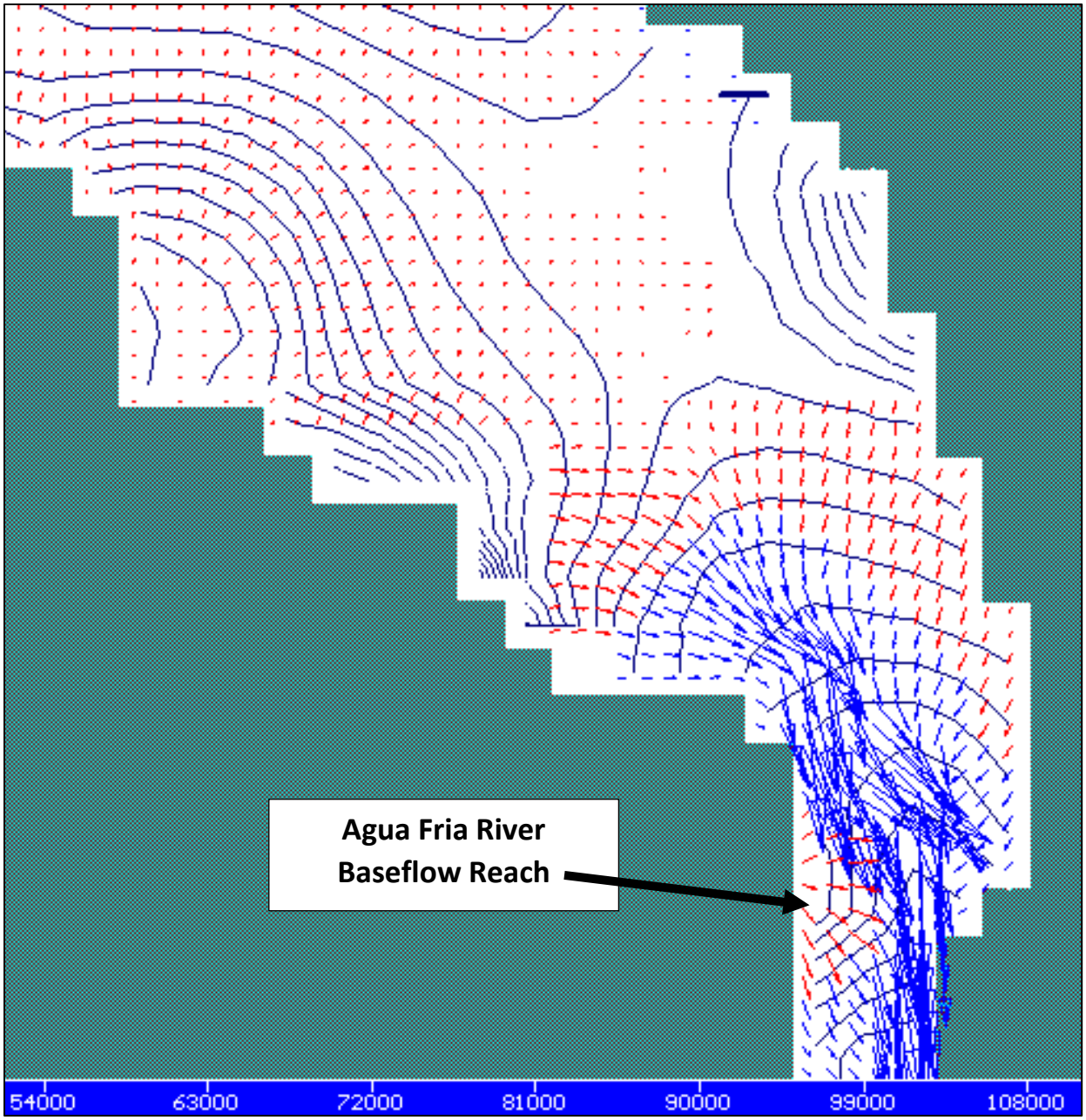

Figure C2. *Simulated groundwater flow in the UAF Sub-basin, circa 1939.*

The arrows represent regional-scale groundwater flow direction where the red, green and blue arrows represent downward, horizontal and upward flow. The magnitude of the arrows is proportional to the relative velocity of groundwater flow, most concentrated in the course stream-aquifer sands and gravels.

Appendix D: Alternative Conceptual Model Testing

Many plausible ACMs were investigated during this model update and it is unreasonable to assume any one single ACM fully represents the regional-scale groundwater flow system. Simulated as a groundwater flow system, the Prescott Model is non-unique. However, the range of plausible parameters and resulting solutions is relatively narrow. For example, when starting values were arbitrarily assigned non-calibrated values then optimized by non-linear regression (*BK2_Alt_Start.rec*), the resulting solution converged to estimated parameter values, consistent with the model (*Bk2.rec*). **Figure D1** below shows the objective function vs, iteration for model (*BK2_Alt_Start.rec*). Of the 50 variables estimated by non-linear regression (BK2_Alt_Start.rec), only two parameters (K_x27 and K_x36) were clearly outside the 95% confidence interval range of parameters associated with, Bk2.rec, and those two parameters had relatively low composite sensitivity, and thus provided little traction in the calibration.

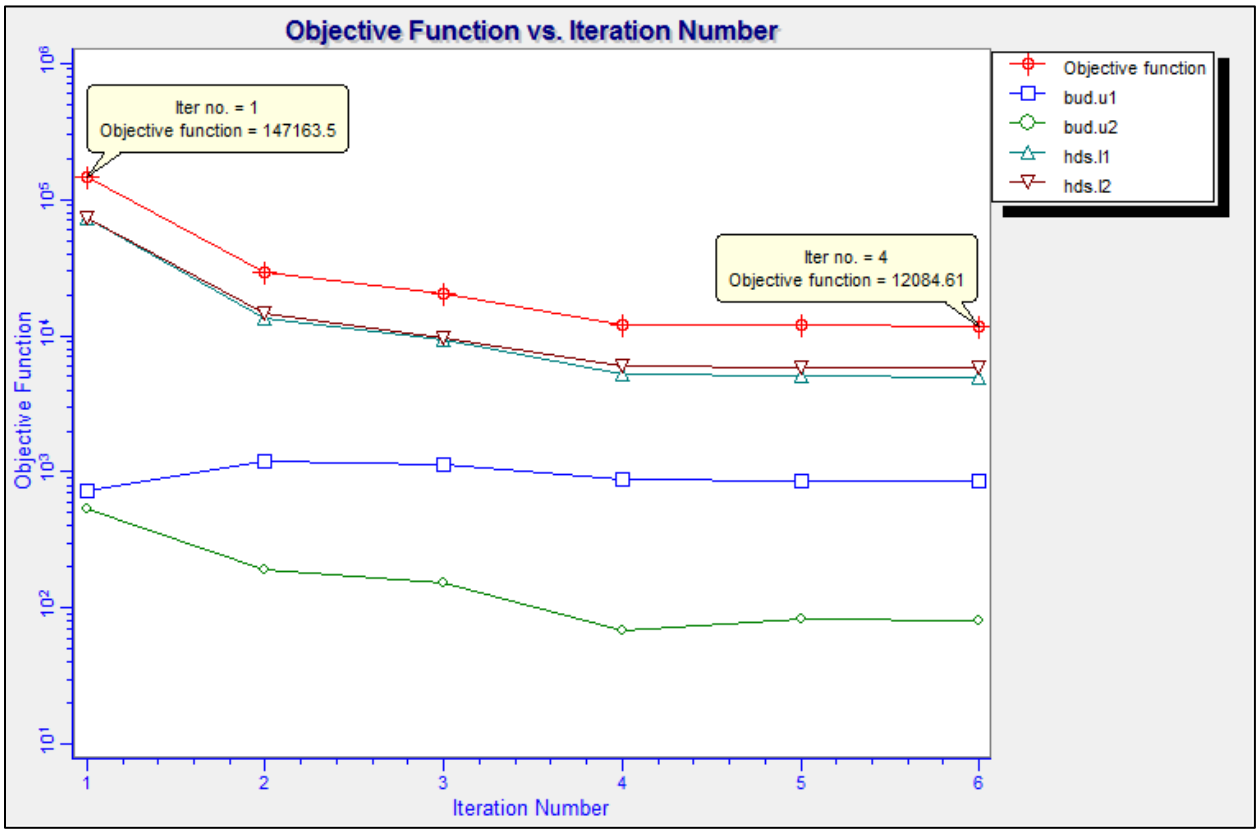

Figure D1. *Optimization of "BK2_Alt_Start.rec"*

Accordingly, results from numerous viable ACMs were developed to show the range of plausible solutions and provide a measure of how the model is constrained, with respect to location and over time. For brevity, however, simulated water budgets are provided for only base model.

Like all models, the Prescott Model is inherently non-unique. However, the range of head and flow solutions associated with plausible ACMs is relatively narrow. Furthermore, the range of viability associated with most parameter estimates are directed toward core, central tendencies.

Appendix E: Simulated Head Distribution for Selected Local Areas

The purpose of this appendix is to present head residual error statistics for select areas, using the base model. In general, the model error statistics for select locations are consistent with the collective mean and absolute mean of -1.2 ft and 12 ft, respectively.

Location	Mean Head Error, ft	Abs mean Head Error, ft	Number of Head Observations
North of LIC-UAF Sub-basin divide	-7.3	12	280
Southwest LIC Sub-basin / Williamson Valley	-5.1	8.6	329
Northern LIC Sub-basin	-3.7	9.2	407
LIC Sub-basin, adjacent to Granite Creek	1.3	19	110
General UAF Sub-basin	0.71	12	548
Northern UAF Sub-basin	-4.4	20	318
General LIC Sub-basin	0.09	11	1,556

Figures E1 through E28 below show locations of select wells and their hydrographs of simulated versus observed heads within selected local areas:

- **North of Little Chino–Upper Agua Fria Sub-basin Divide**
- **Southwest Little Chino Sub-basin & Williamson Valley**
- **Northern Little Chino Sub-basin**
- **Little Chino Sub-basin adjacent to Granite Creek**
- **General Upper Agua Fria Sub-basin**
- **Northern Upper Agua Fria Sub-basin, Santa Fe Well Field**
- **General Little Chino Sub-basin**

North of Little Chino-Upper Agua Fria Sub-basin Divide

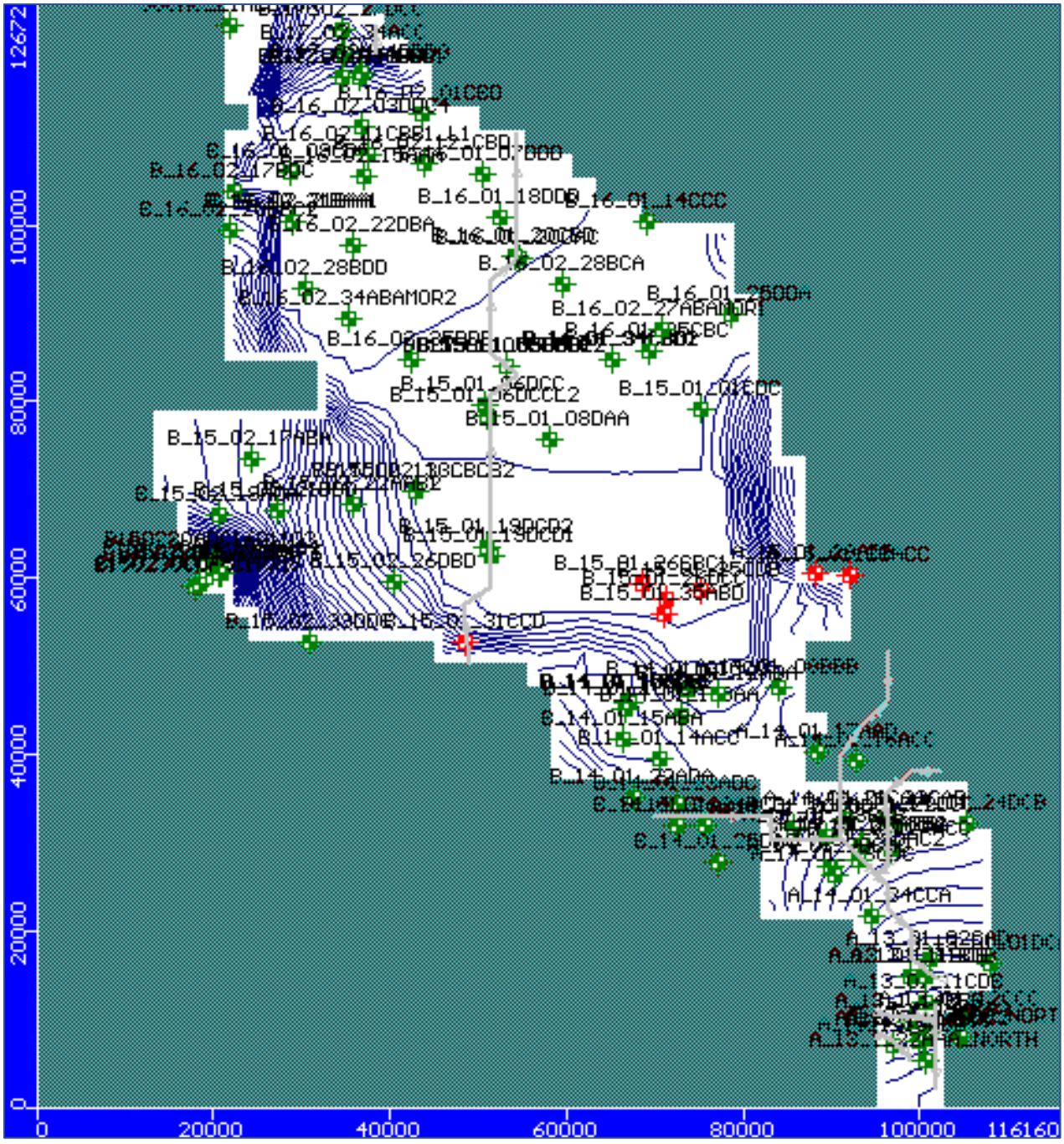

Figure E1. *Simulated and observed heads, north of LIC-UAF Sub-basin divide (in red).*

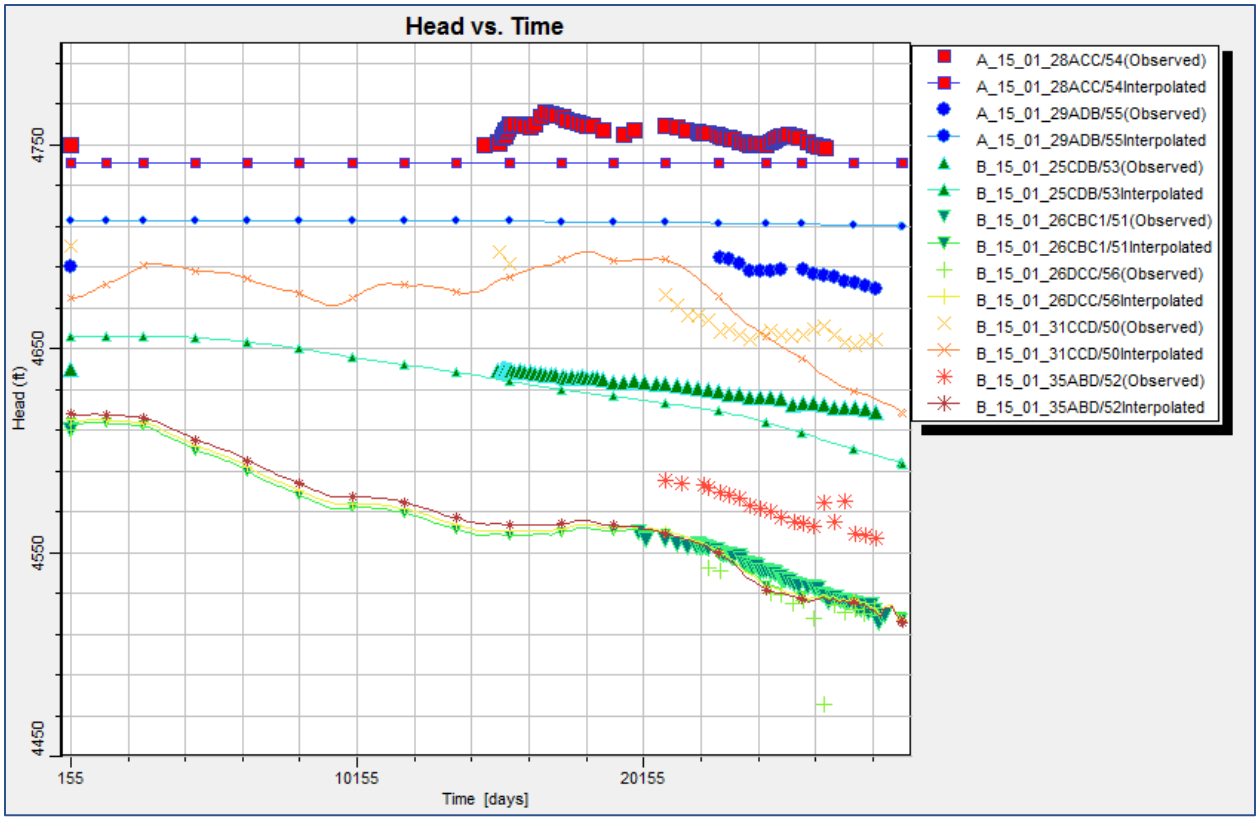

Figure E2. *Comparison of simulated and observed heads, north of LIC-UAF Sub-basin divide. Mean and absolute mean head residual error -7.3 and 12 ft, respectively (sample size = 280).*

Southwest Little Chino Sub-basin & Williamson Valley

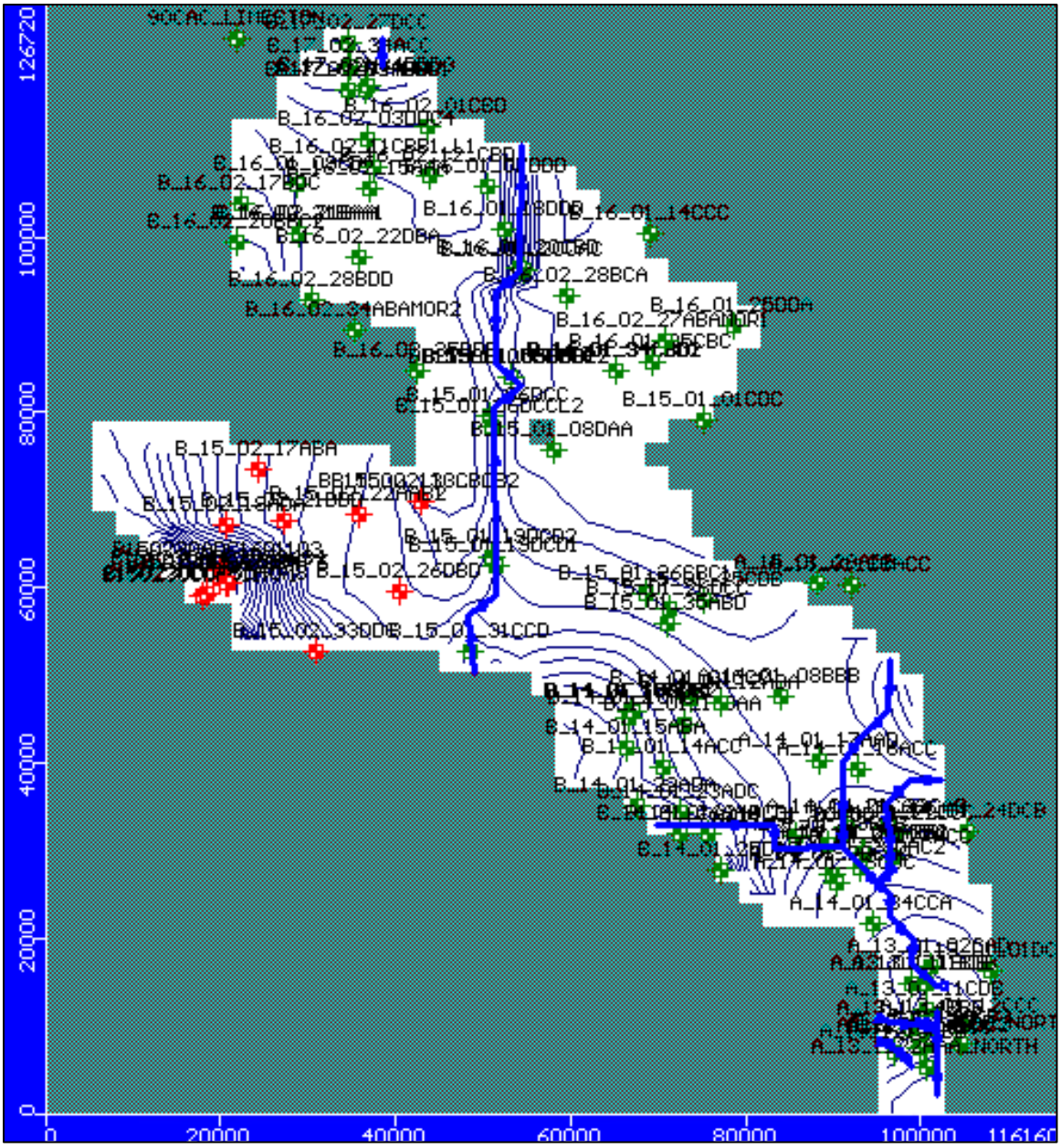

Figure E3. *Simulated and observed heads, north of LIC-UAF Sub-basin divide (in red).*

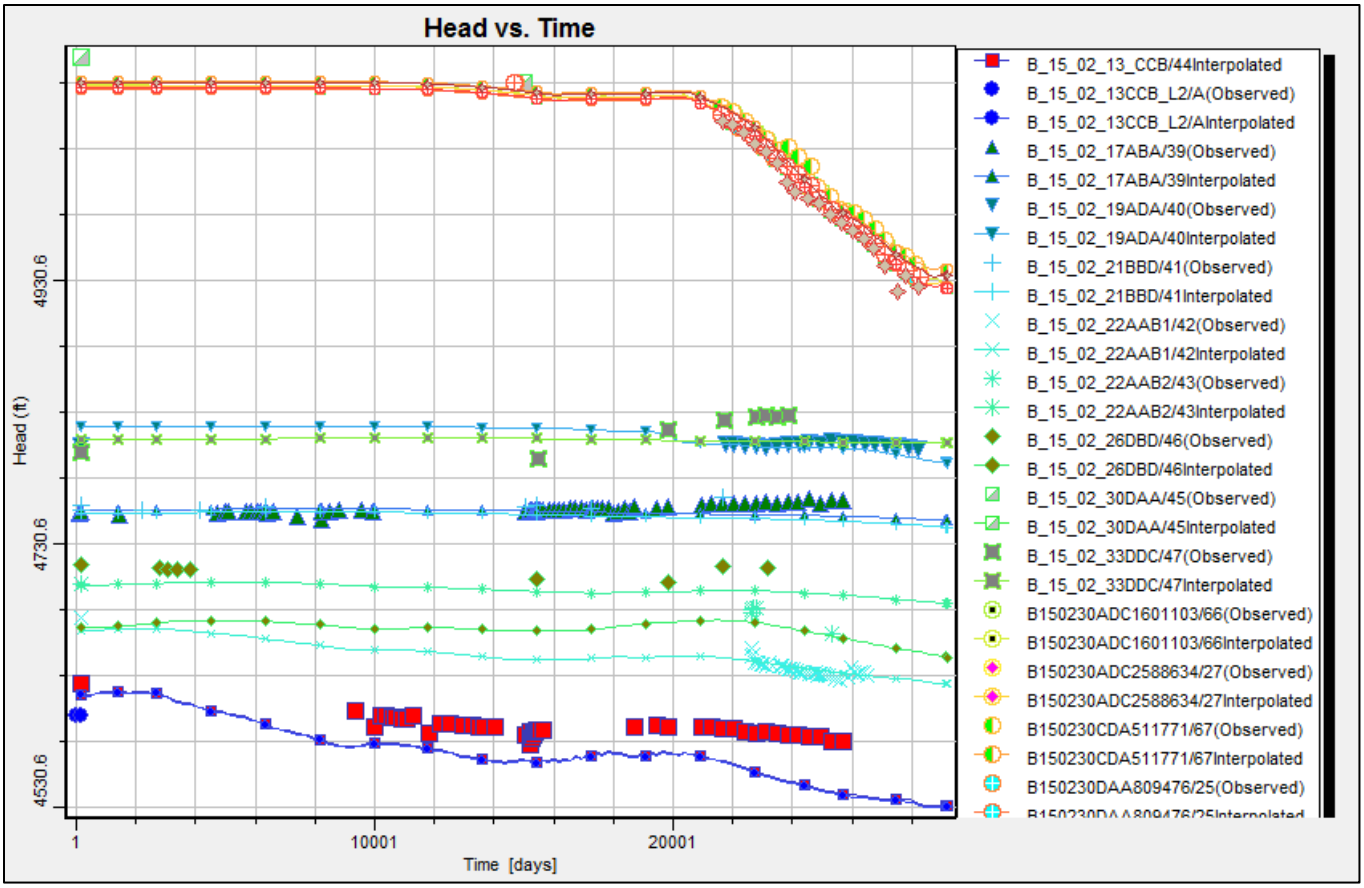

Figure E4. *Comparison of simulated and observed heads, southwest LCI Sub-basin and Williamson Valley area. Mean and absolute mean head residual error -5.1 and 8.6 ft, respectively (sample size = 329).*

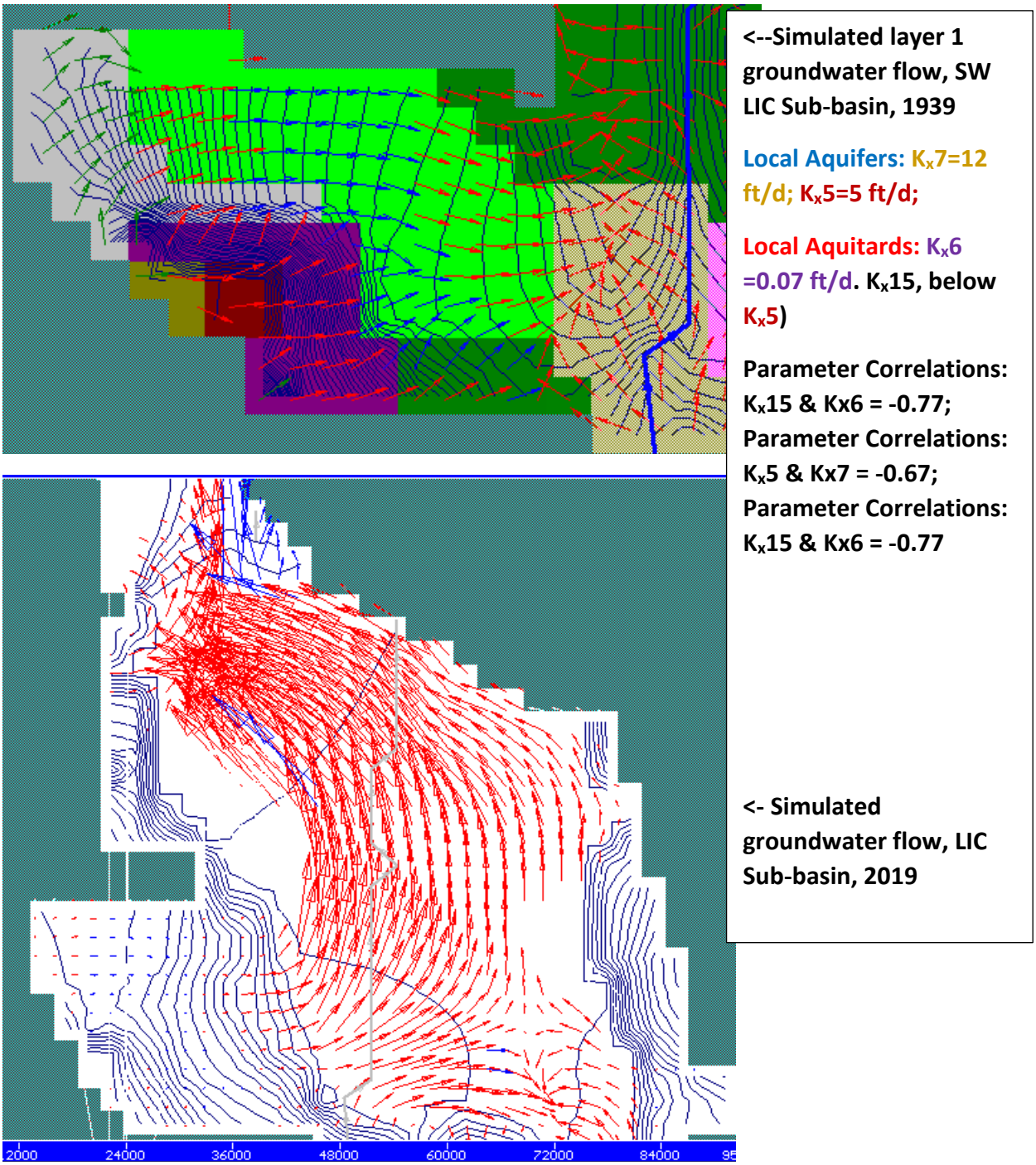

Figure E5. *Lack of recharge (outside on Mint Wash and steep hydraulic gradient support the inverse model solution. Despite the steep hydraulic gradient, groundwater flow contributions from the southwestern portion of the LIC Sub-basin are relative minor, consistent with empirical data and modeling results.*

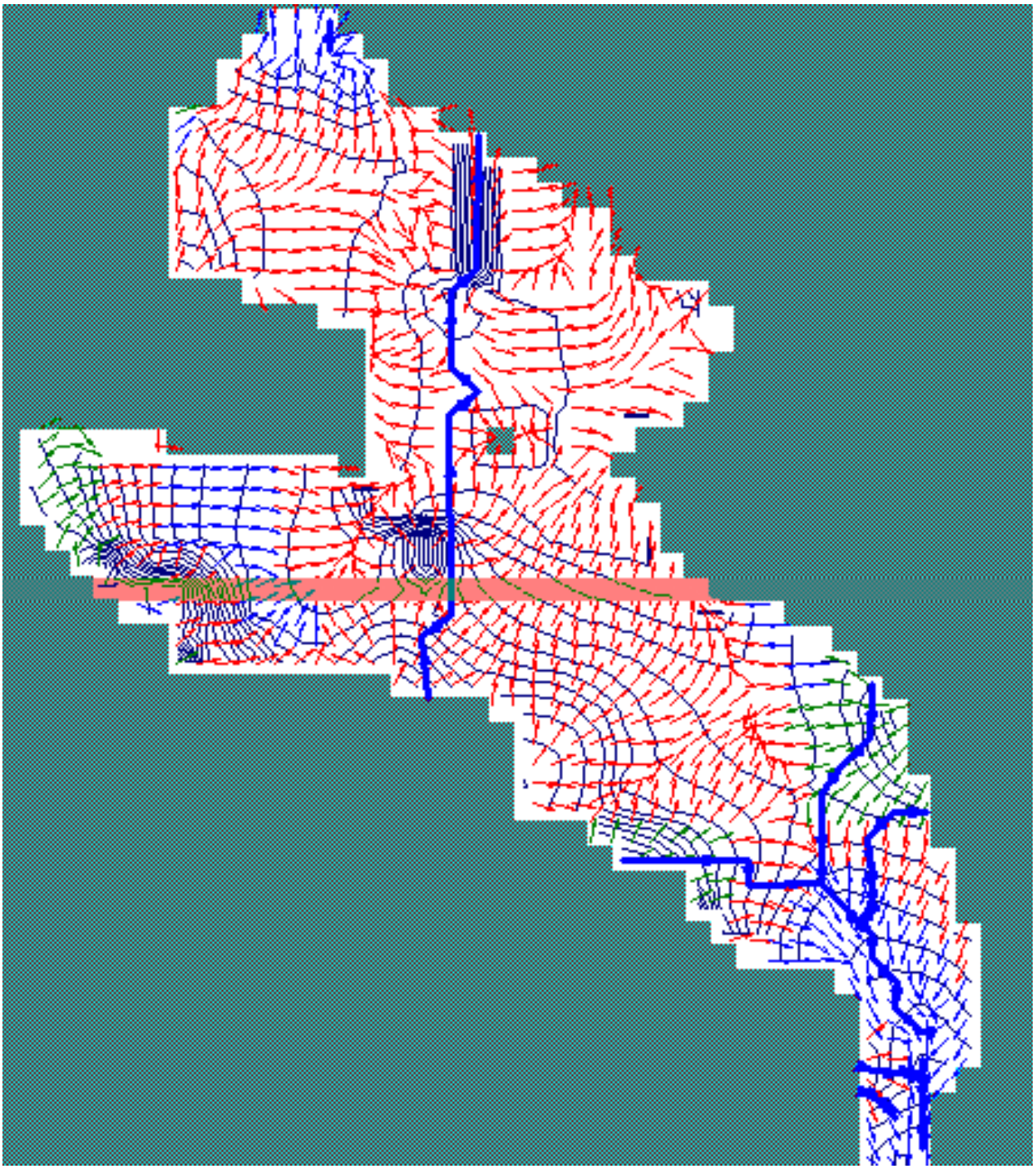

Figure E6. *Prescott AMA Groundwater Flow Model, Row 25 Highlighted.*

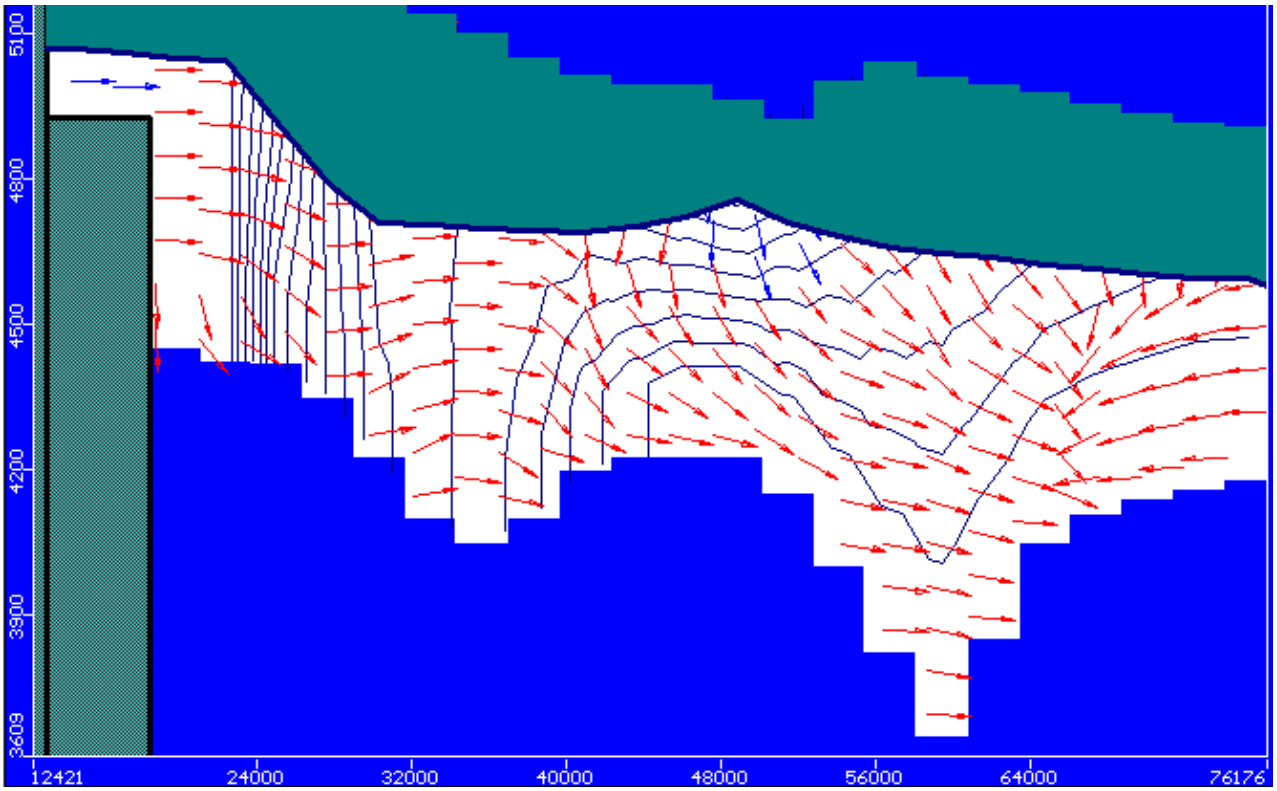

Figure E7. *Cross-sectional simulated groundwater flow in 1939 along row 25.*

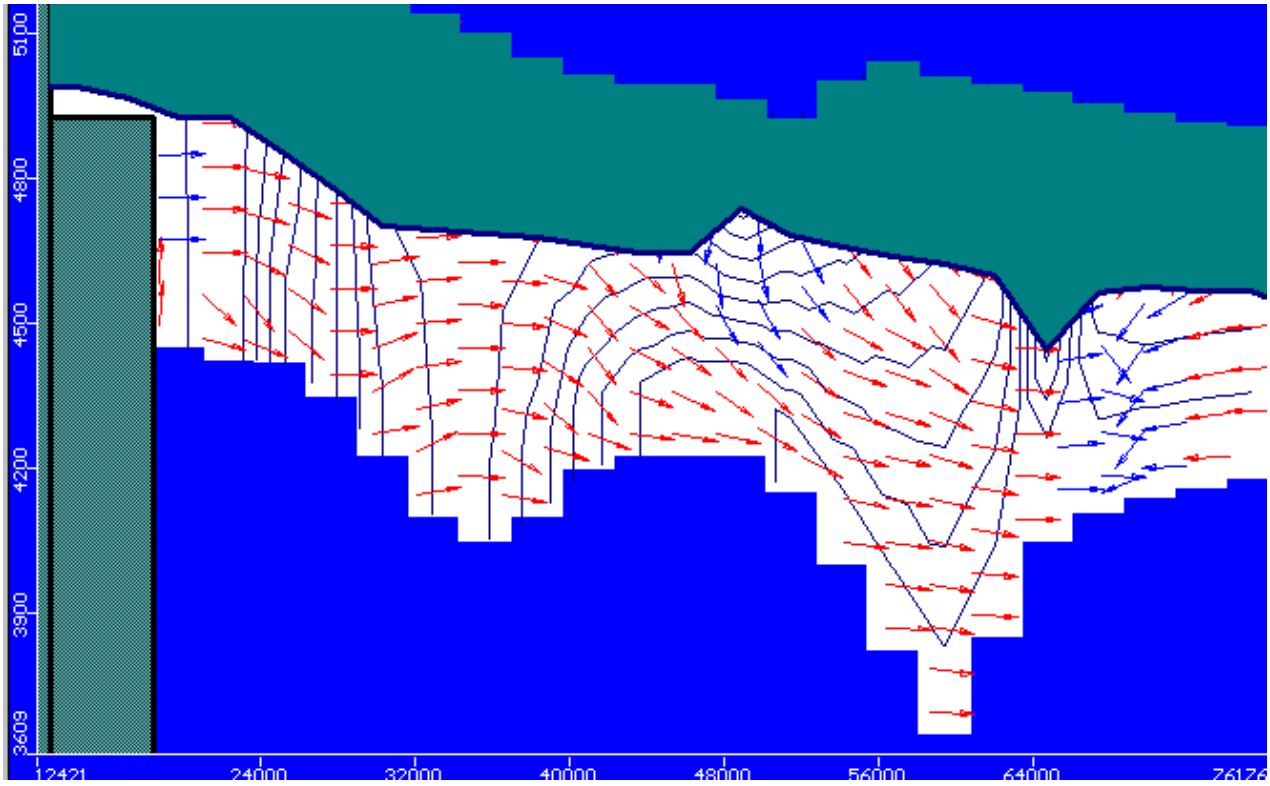

Figure E8. *Cross-sectional simulated groundwater flow in 2019 along row 25.*

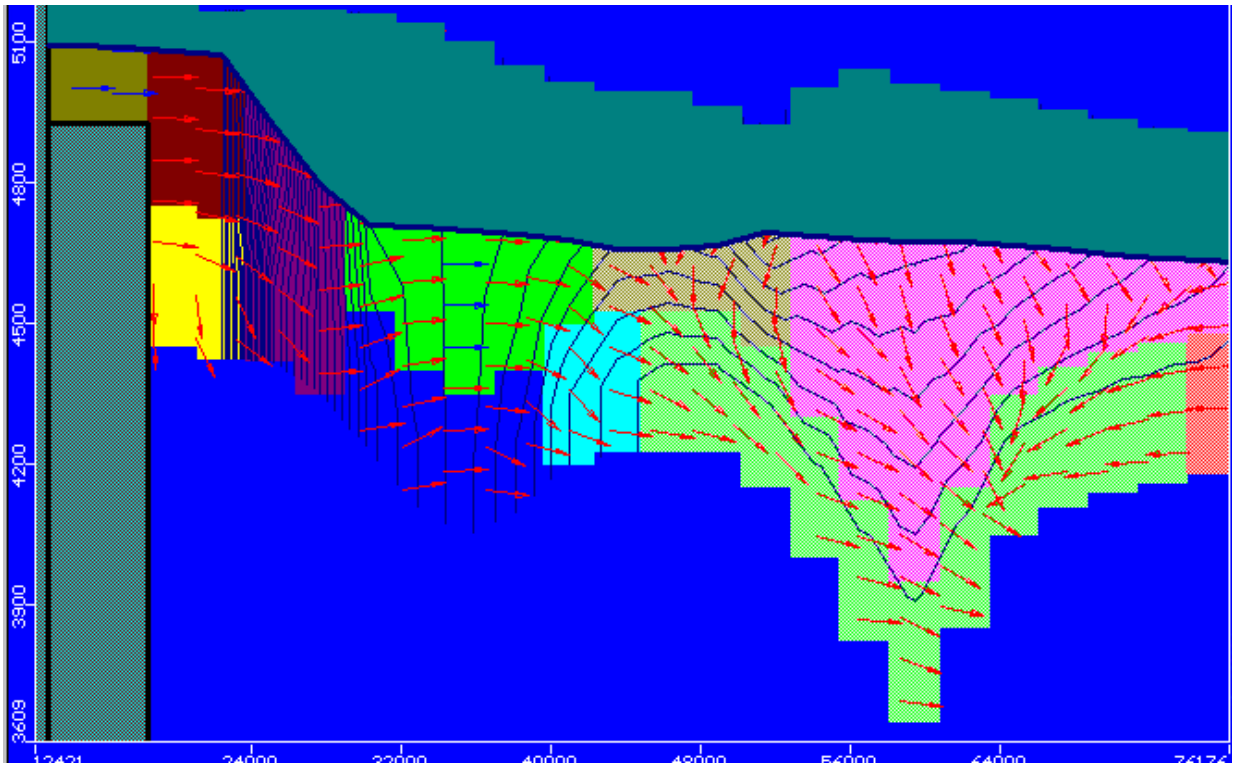

Figure E9. *Cross-sectional simulated groundwater flow in 1939 along model row 25 including hydraulic conductivity zones.*

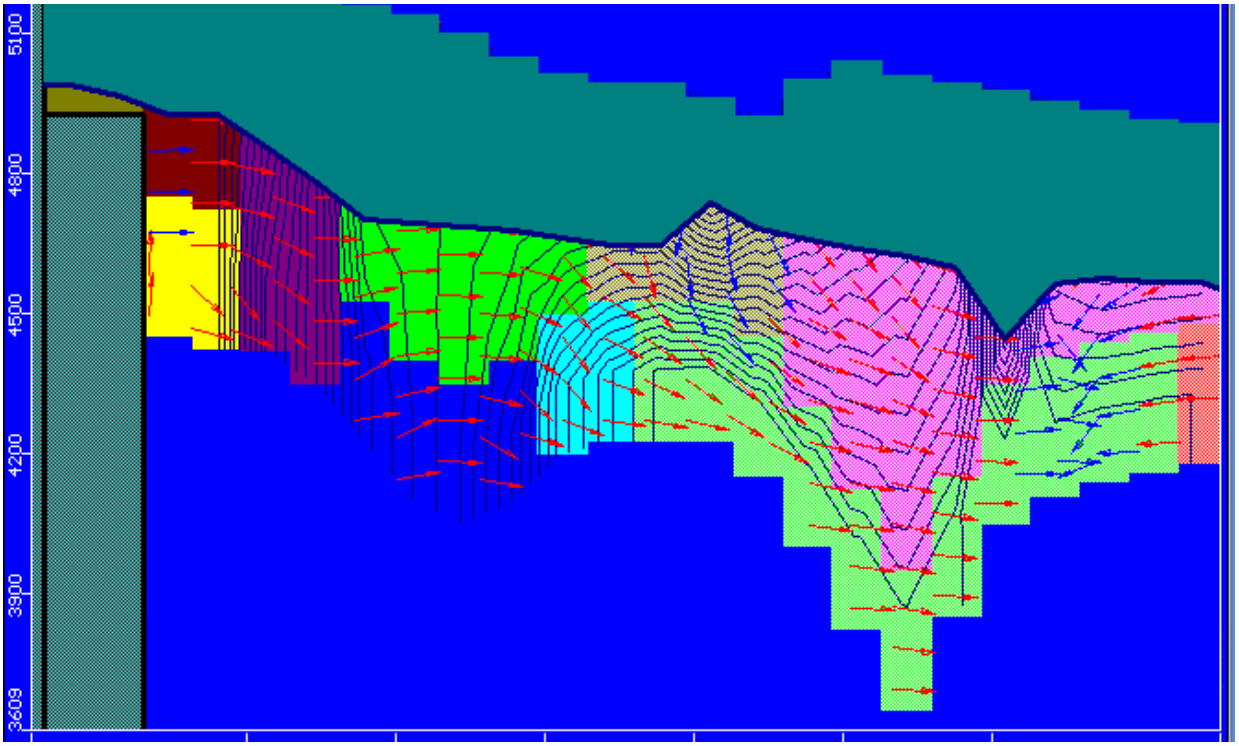

Figure E10. *Cross-sectional simulated groundwater flow in 2019 along model row 25 including hydraulic conductivity zones.*

Northern Little Chino Sub-basin

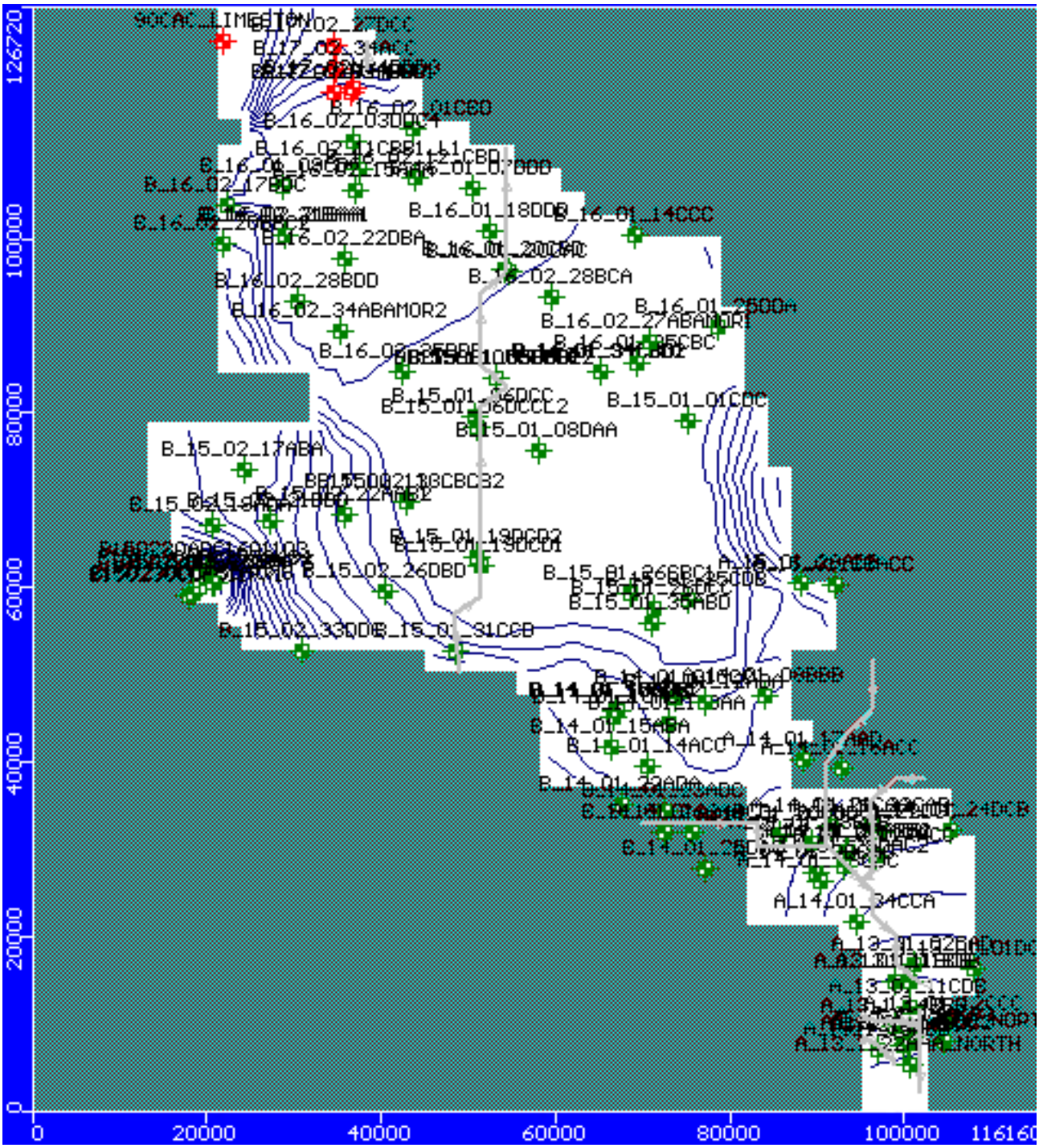

Figure E11. *Simulated and observed heads, norther LIC Sub-basin (in red).*

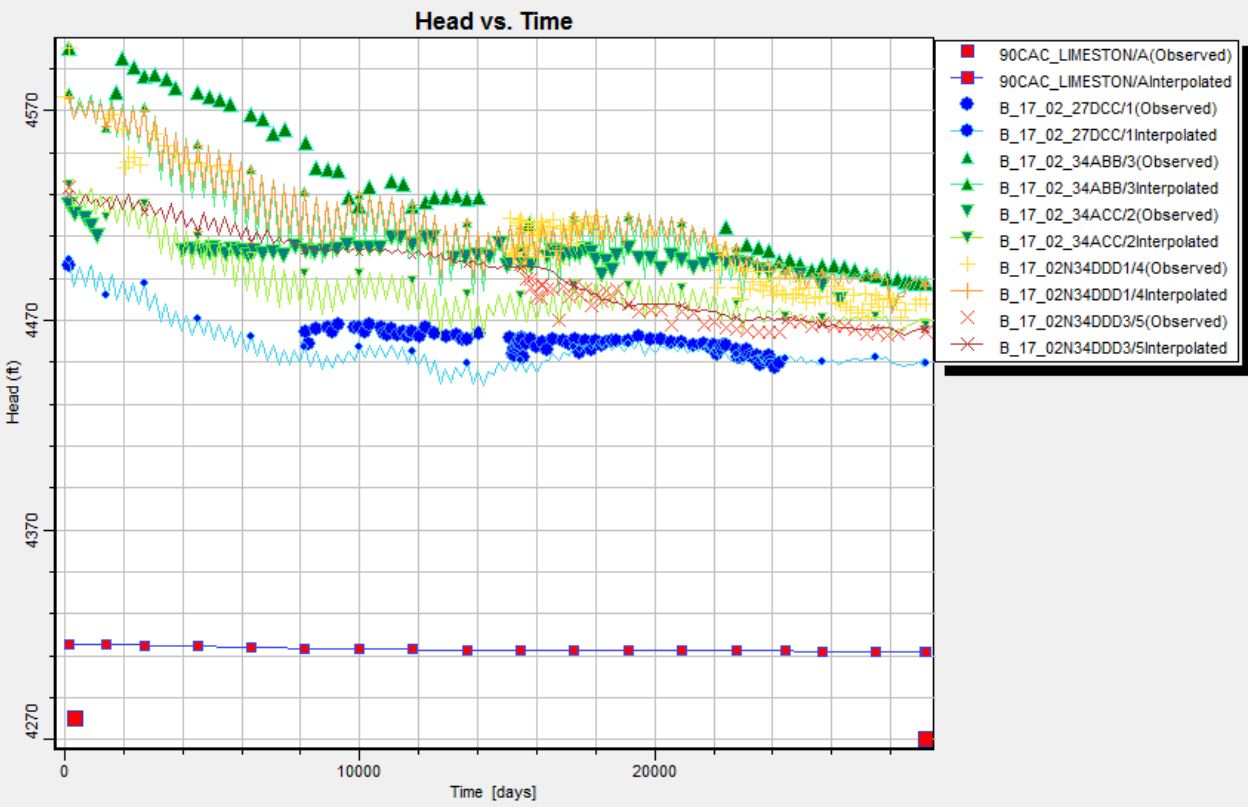

Figure E12. *Comparison of simulated and observed heads, northern LIC Sub-basin. Mean and absolute mean head residual error -3.7 and 9.2 ft, respectively (sample size = 407).*

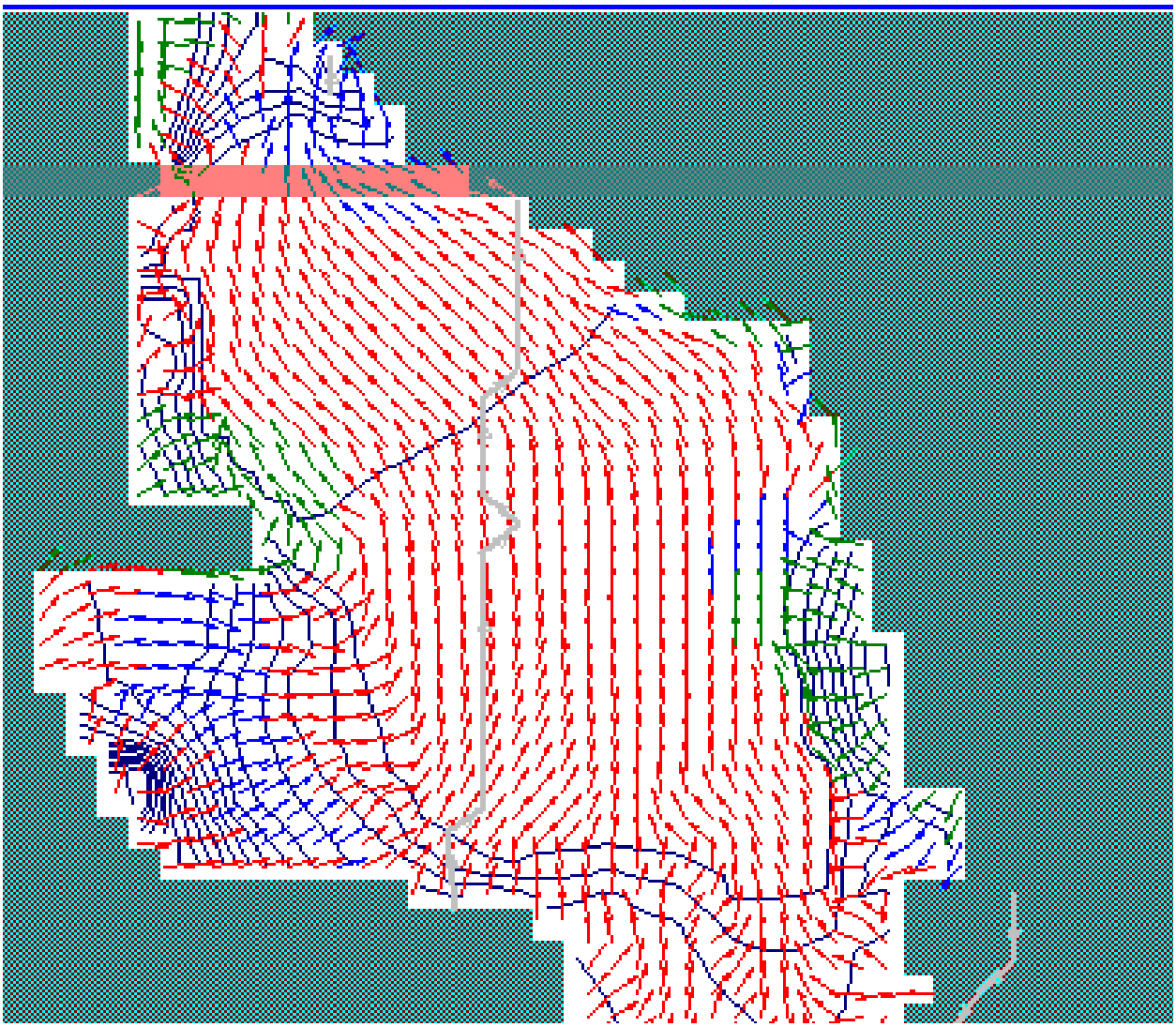

Figure E13. ***Prescott AMA Groundwater Flow Model, Row 6 Highlighted*** *Simulated groundwater flow in model layer 2, 1939, row 6 highlighted representing the northern LIC Sub-basin in cross-section; see Appendix C. Green, red and blue arrows represent horizontal, downward and upward flow, respectively.*

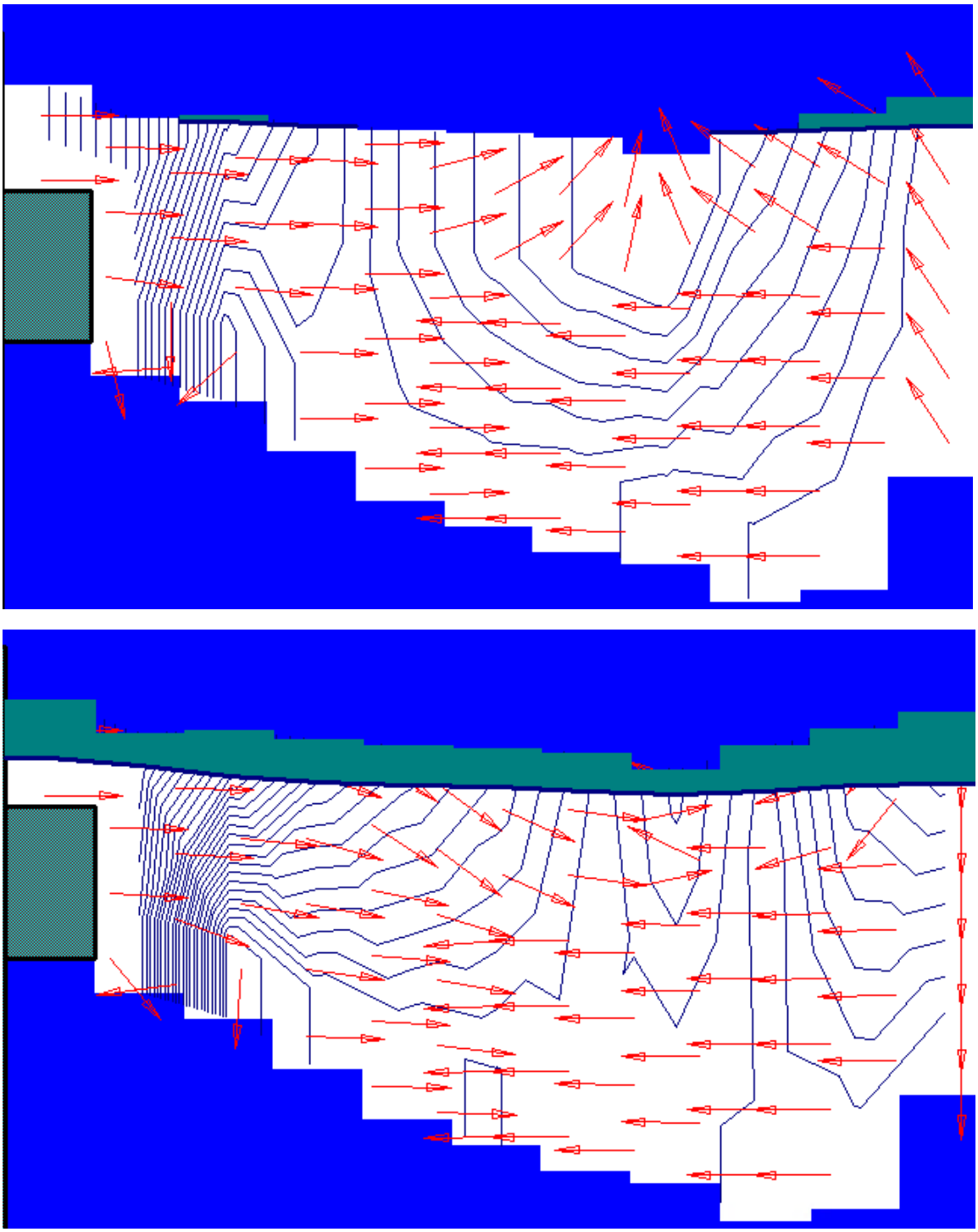

Figures E14 and E15. *Simulated groundwater flow in cross-section at model-row 6 in 1939 (top) showing an upward vertical gradient and 2019 (bottom). After 80 years of continuous pumping, the LVU pressure head had been reduced by about 100 ft, effectively eliminating upward vertical gradient. Vertical exaggeration 15X.*

Little Chino Sub-basin adjacent to Granite Creek

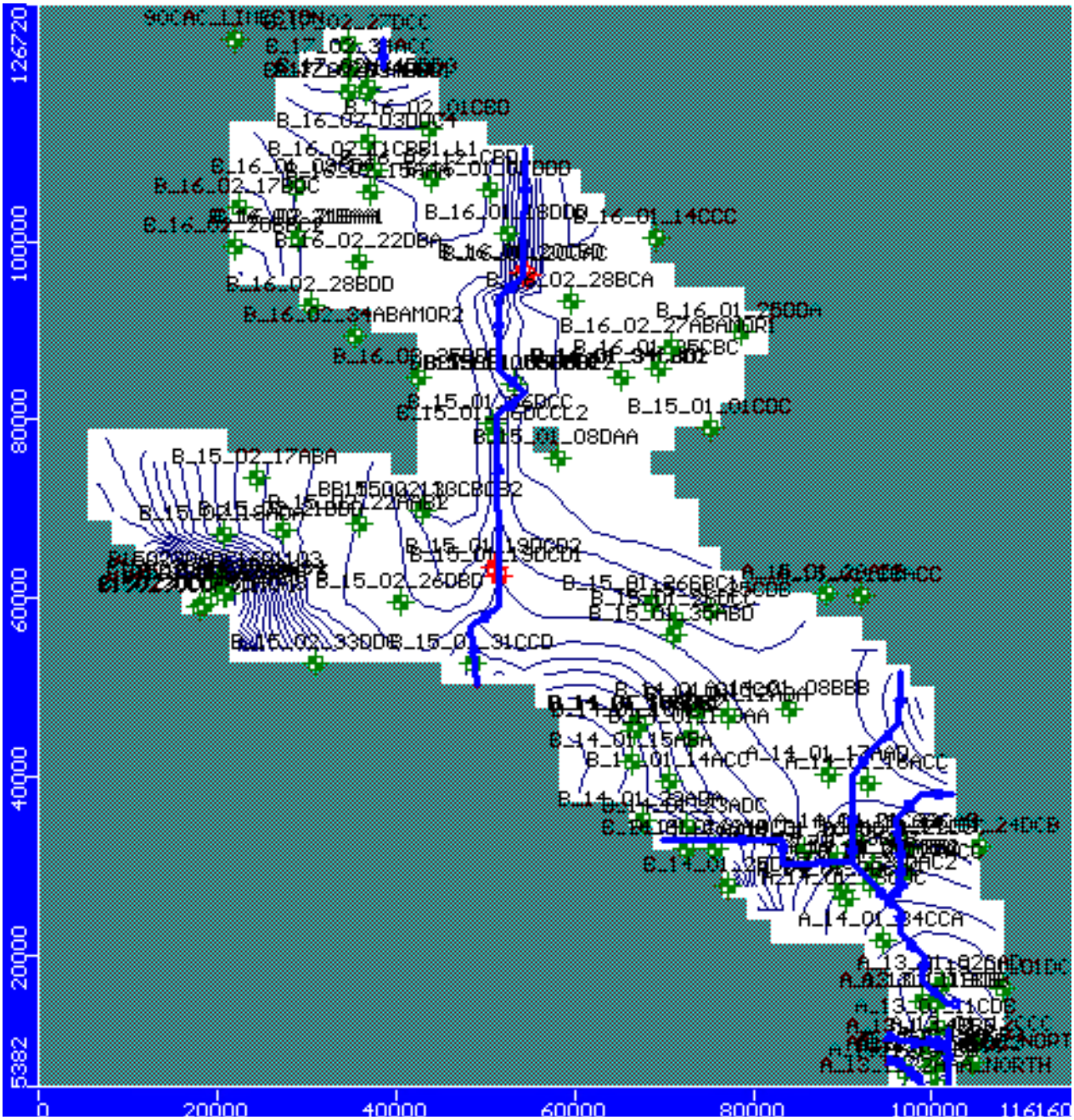

Figure E16. *Simulated and observed heads, LIC-UAF Sub-basin adjacent to Granite Creek (in red).*

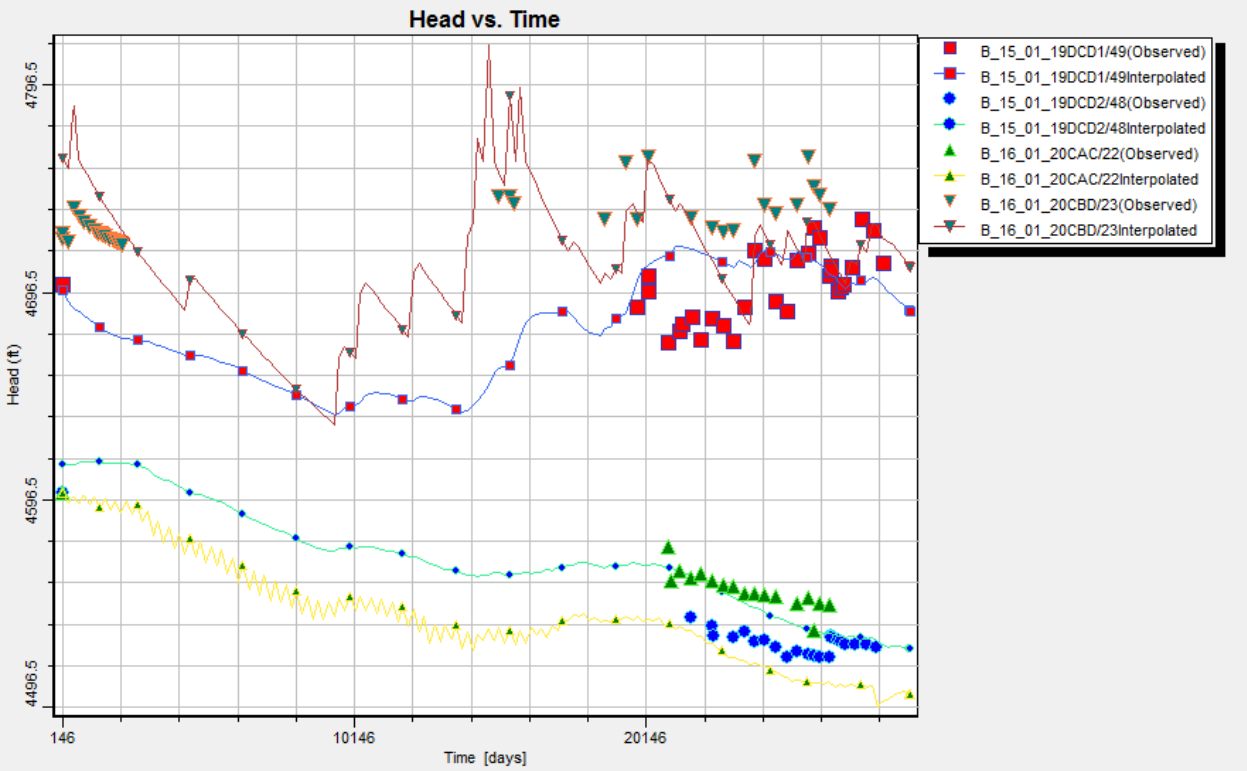

Figure E17. *Comparison of simulated and observed heads, LIC Sub-basin adjacent of Granite Creek. Mean and absolute mean head residual error 1.3 and 19 ft, respectively (sample size = 110).*

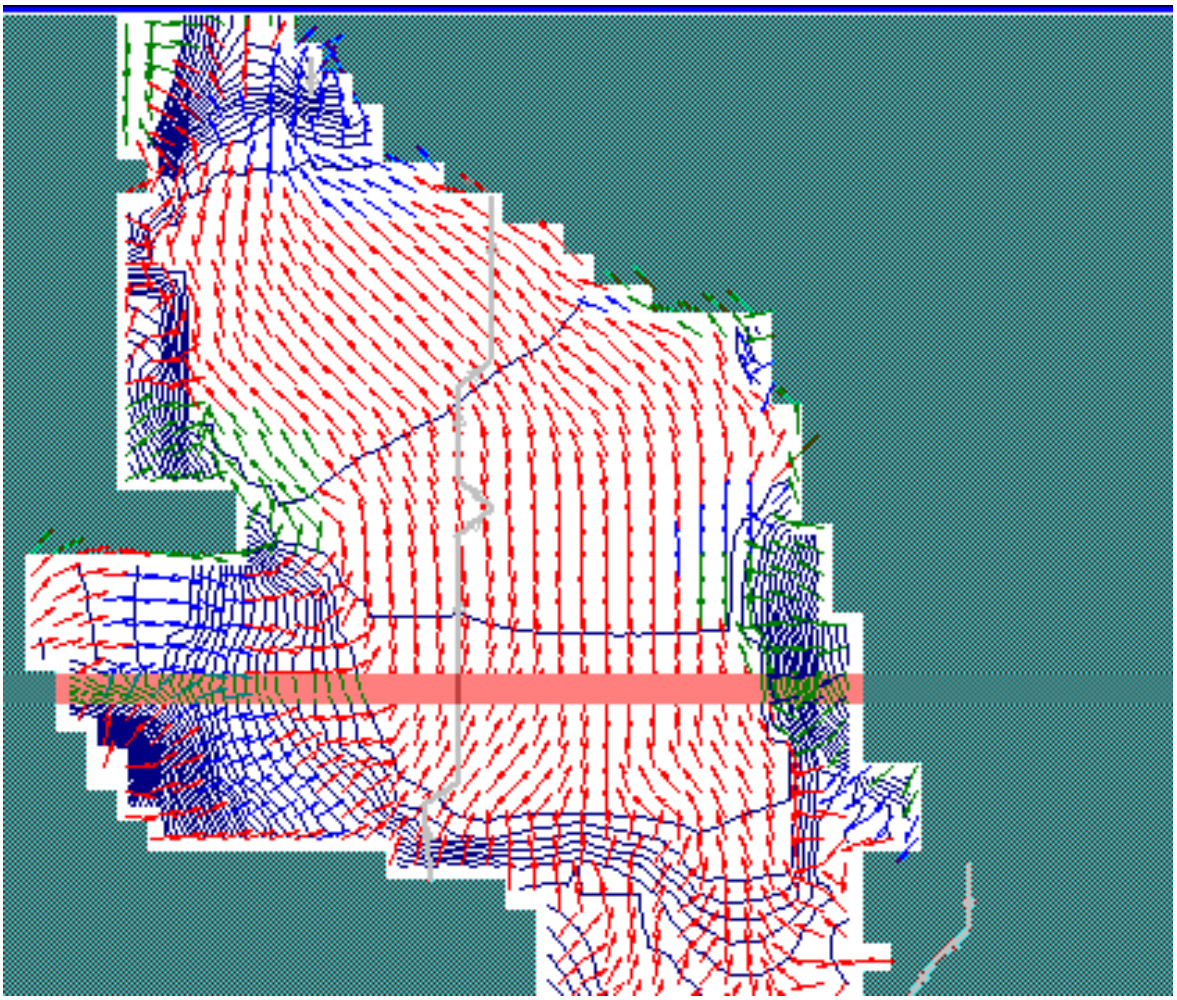

Figure E18. Prescott AMA Groundwater Flow Model, Row 23 Highlighted *Simulated groundwater flow in model layer 2, 1939, row 23 highlighted representing the southern LIC Sub-basin in cross-section. Green, red and blue arrows represent horizontal, downward and upward flow, respectively.*

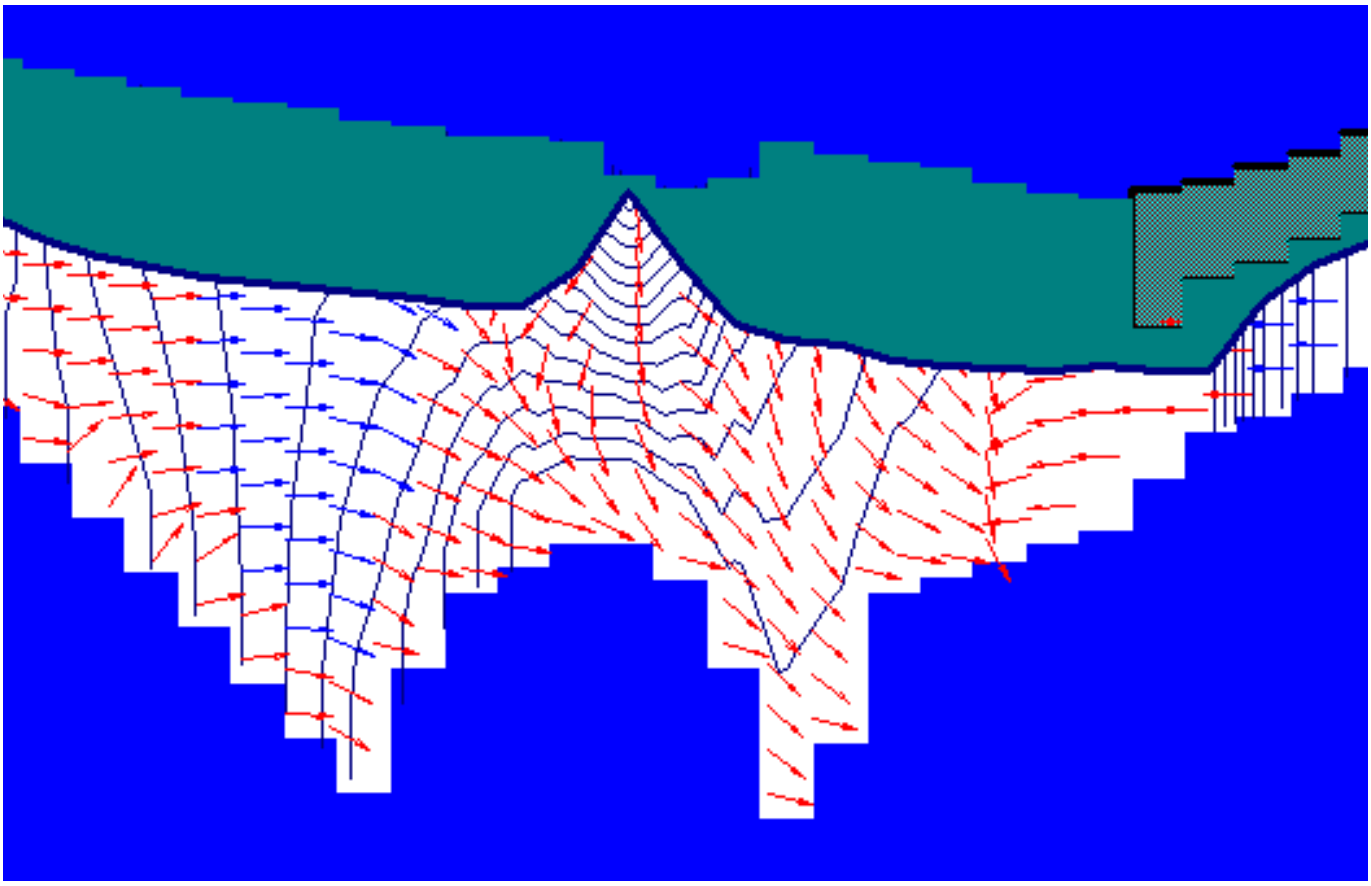

Figure E19. *Simulated groundwater flow in cross-section along row 23 showing impact of both natural and artificial recharge after the 2005 flood recharge (model-day 24,245). Vertical exaggeration 25X.*

General Upper Agua Fria Sub-basin

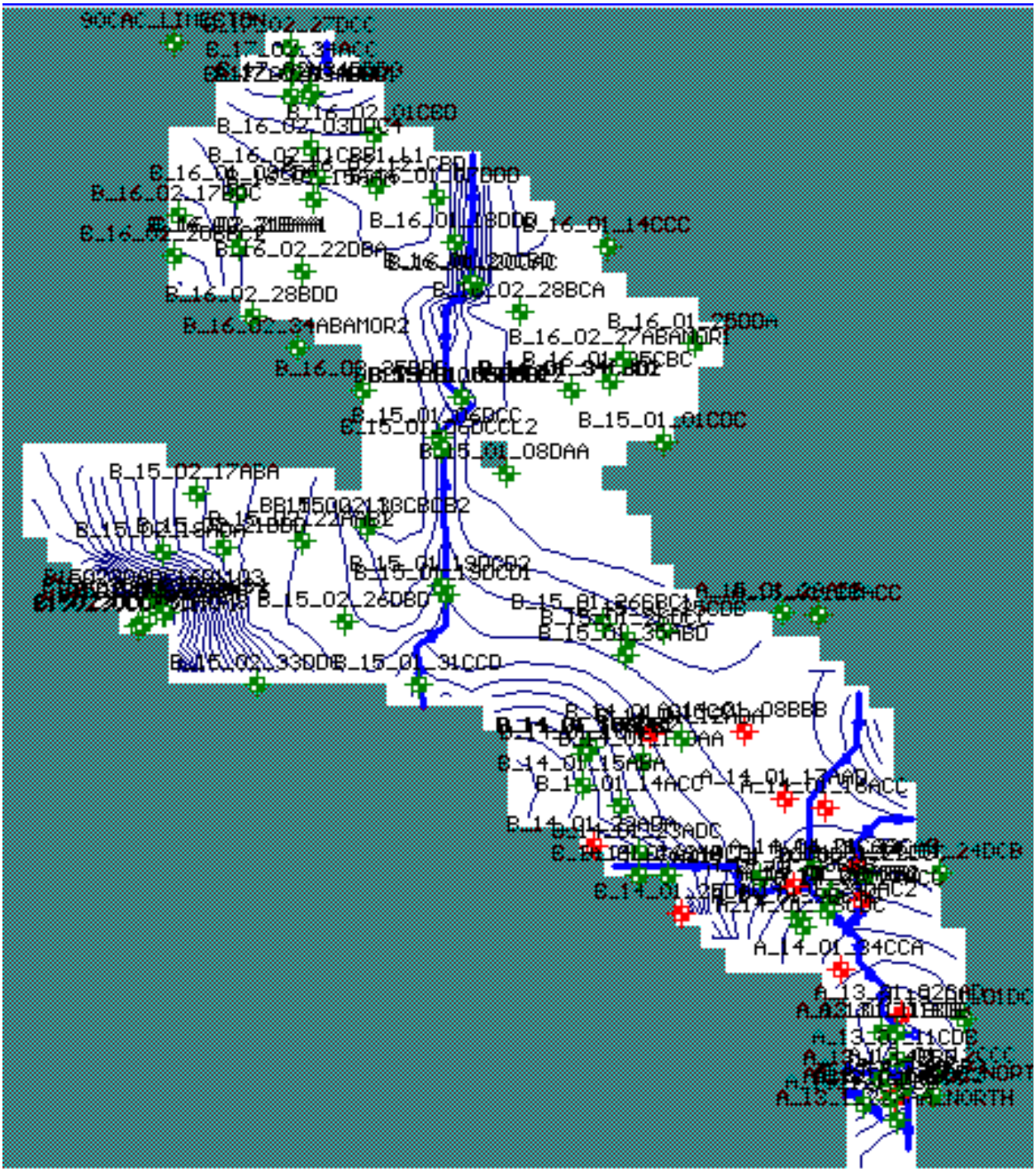

Figure E20. *Simulated and observed heads in the general UAF Sub-basin (in red).*

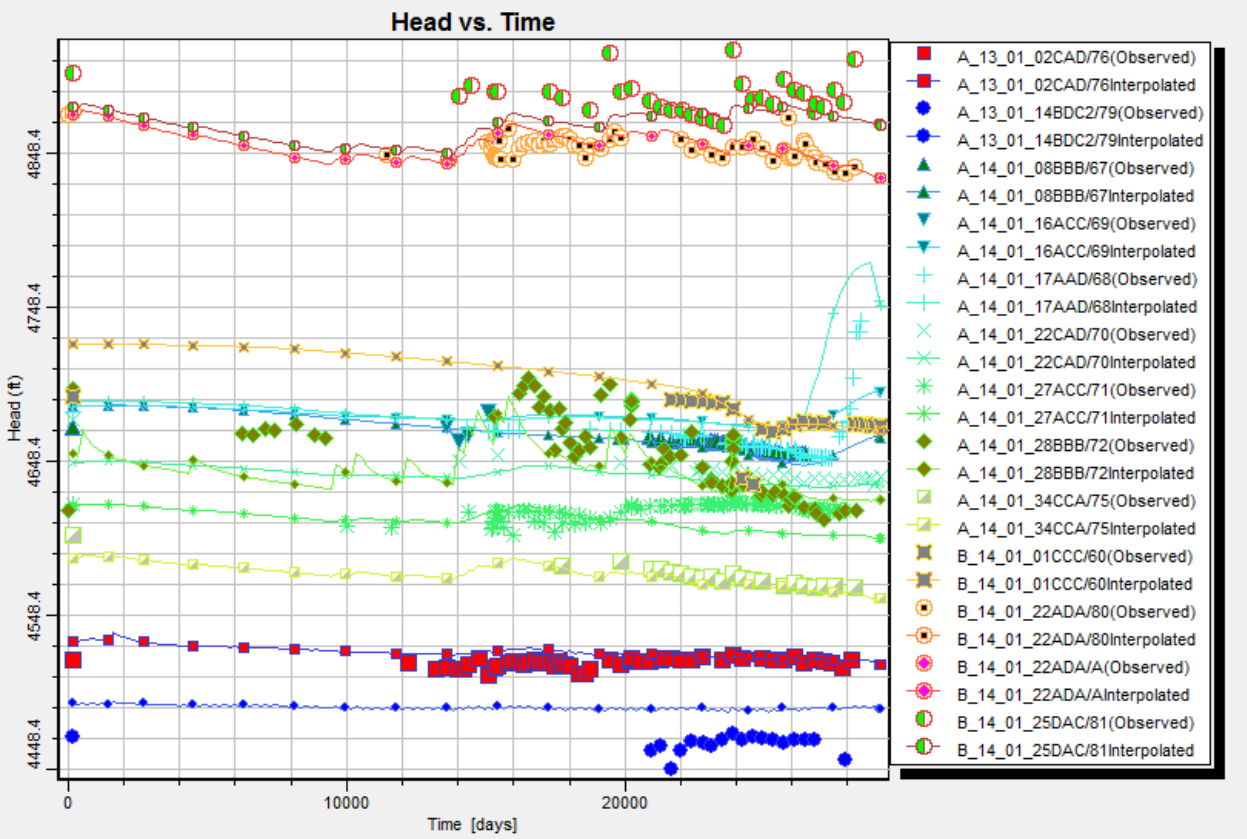

Figure E21. *Comparison of simulated and observed heads in the general UAF Sub-basin. Mean and absolute mean head residual 0.71 and 12 ft, respectively (sample size = 548).*

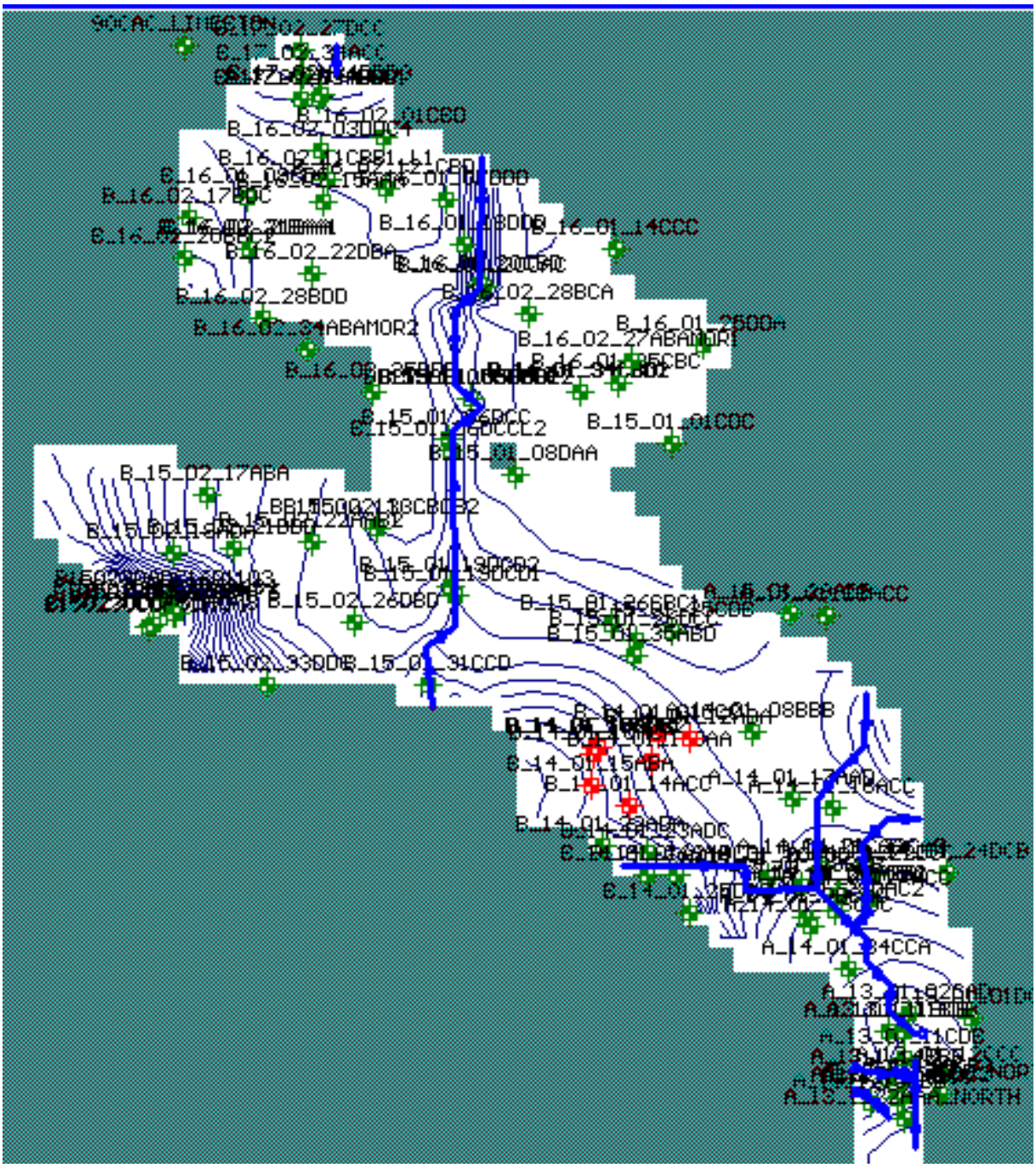

Figure E22. *Simulated and observed heads in the Northern UAF Sub-basin (in red).*

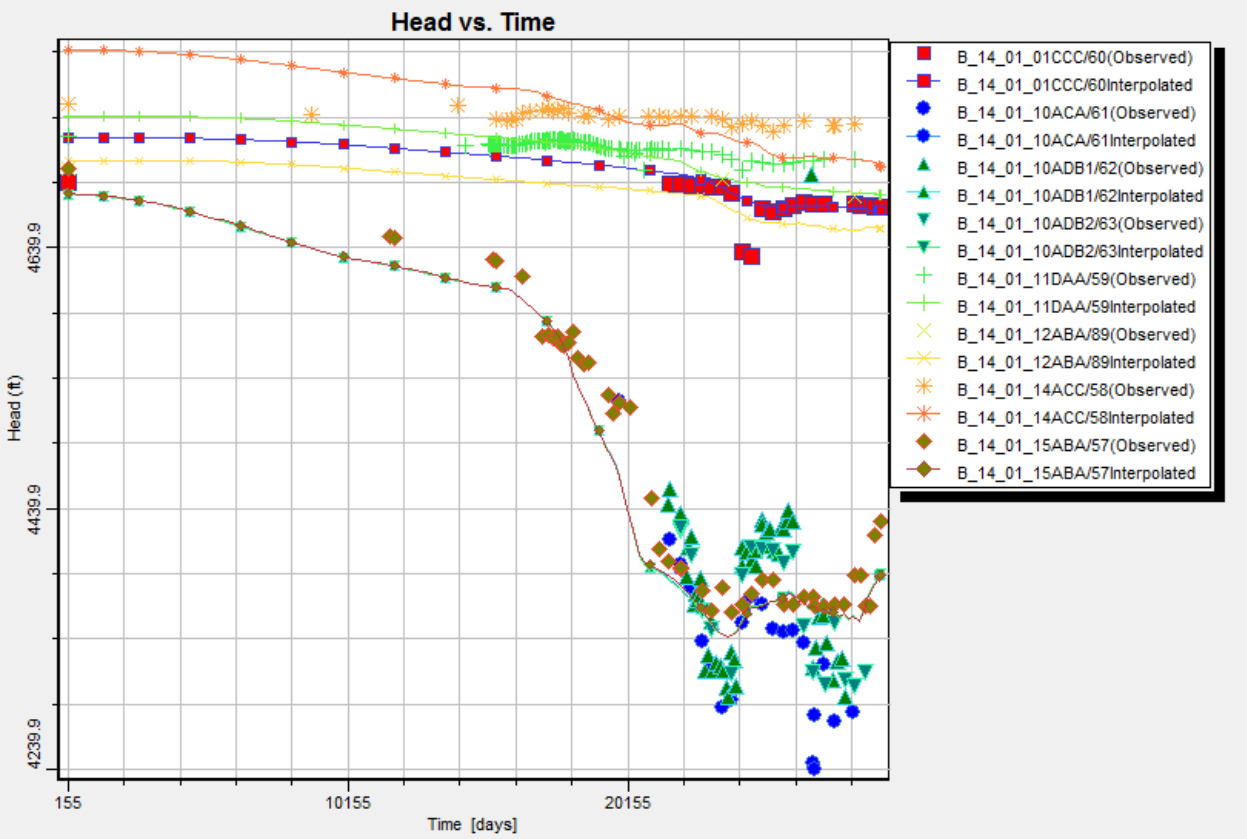

Figure E23. *Comparison of simulated and observed heads in the Northern UAF Sub-basin. Mean and absolute mean head residual -4.4 and 20 ft, respectively (sample size = 318).*

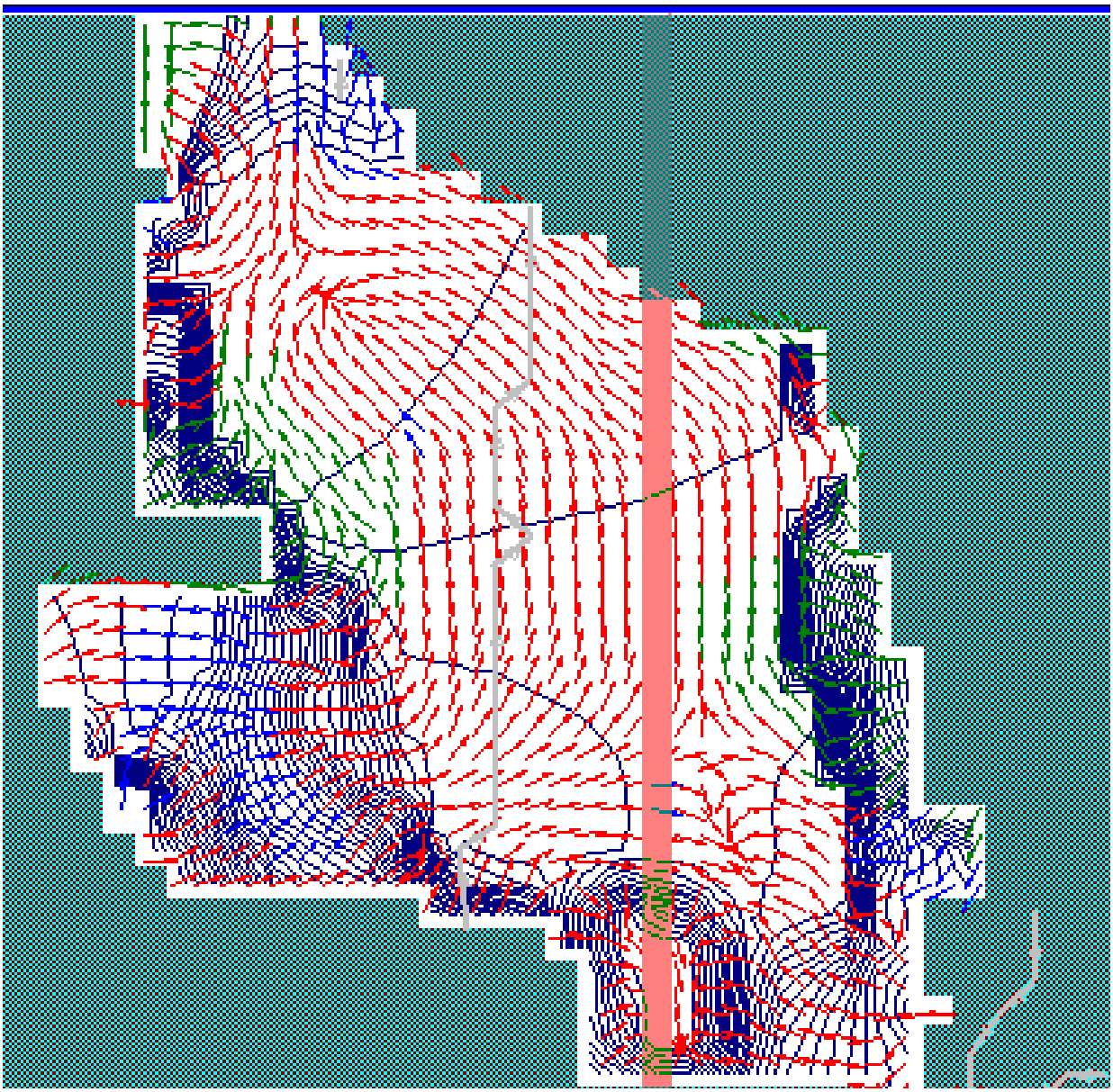

Figure E24. Prescott AMA Groundwater Flow Model, Column 25 Highlighted *Simulated groundwater flow in model layer 2, 2019, column 25 highlighted. Green, red and blue arrows represent horizontal, downward and upward flow, respectively.*

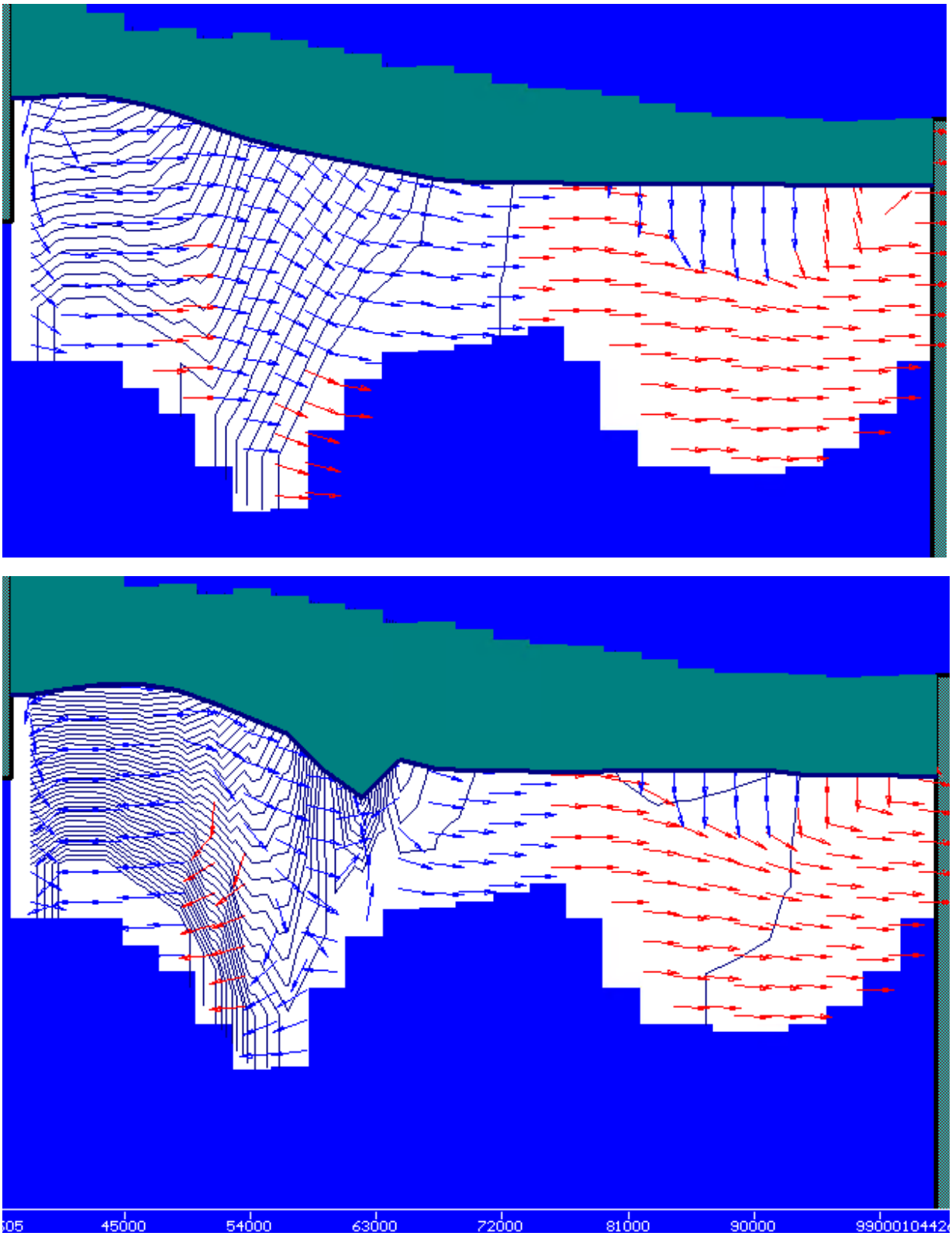

Figures E25 and E26. *Simulated groundwater flow in cross-section at model-column 25 in 1939 (top) and 2019 (bottom). Vert exaggeration 25X.*

General Little Chino Sub-basin

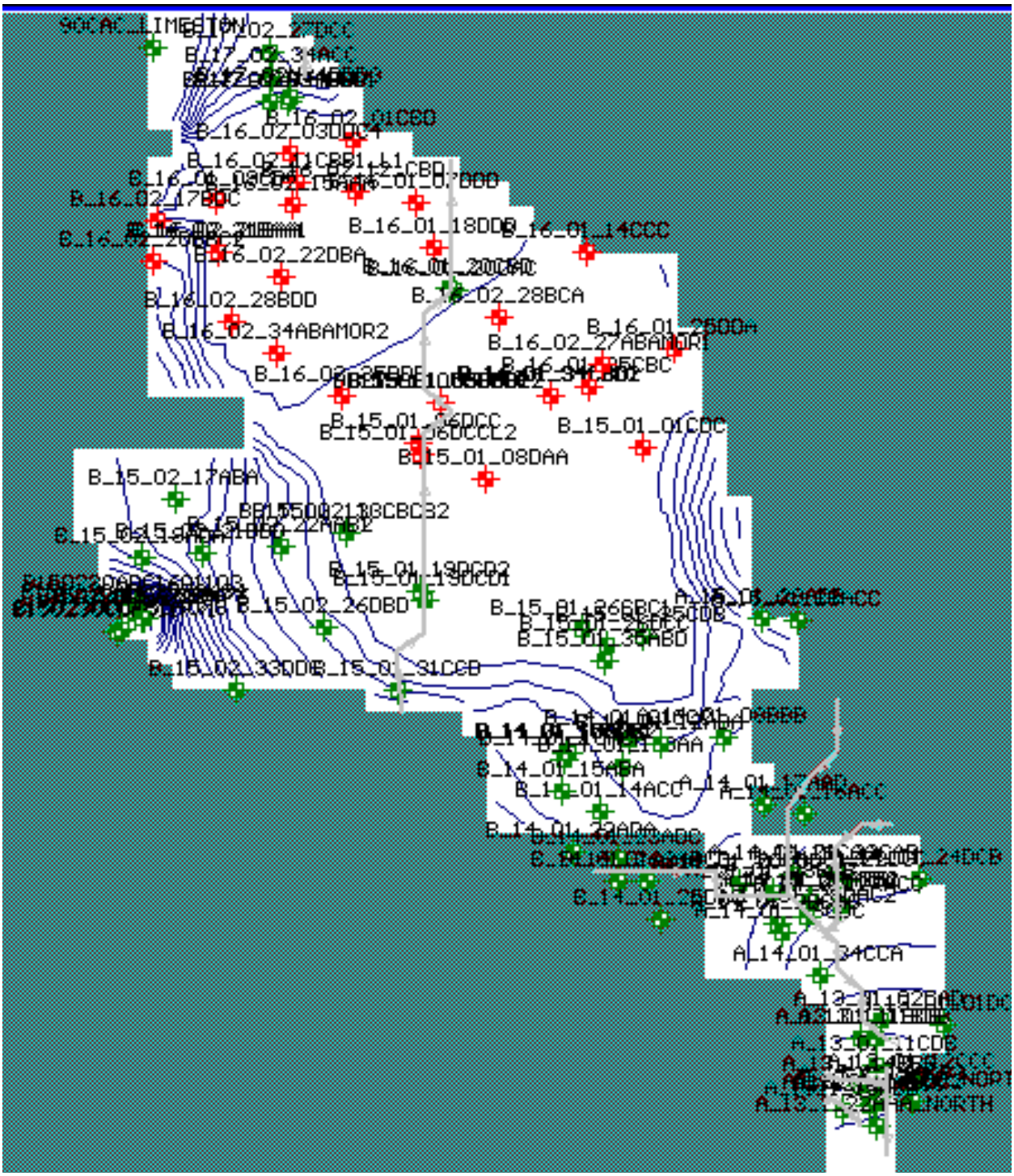

Figure E27. *Simulated and observed heads in the general LIC Sub-basin (in red).*

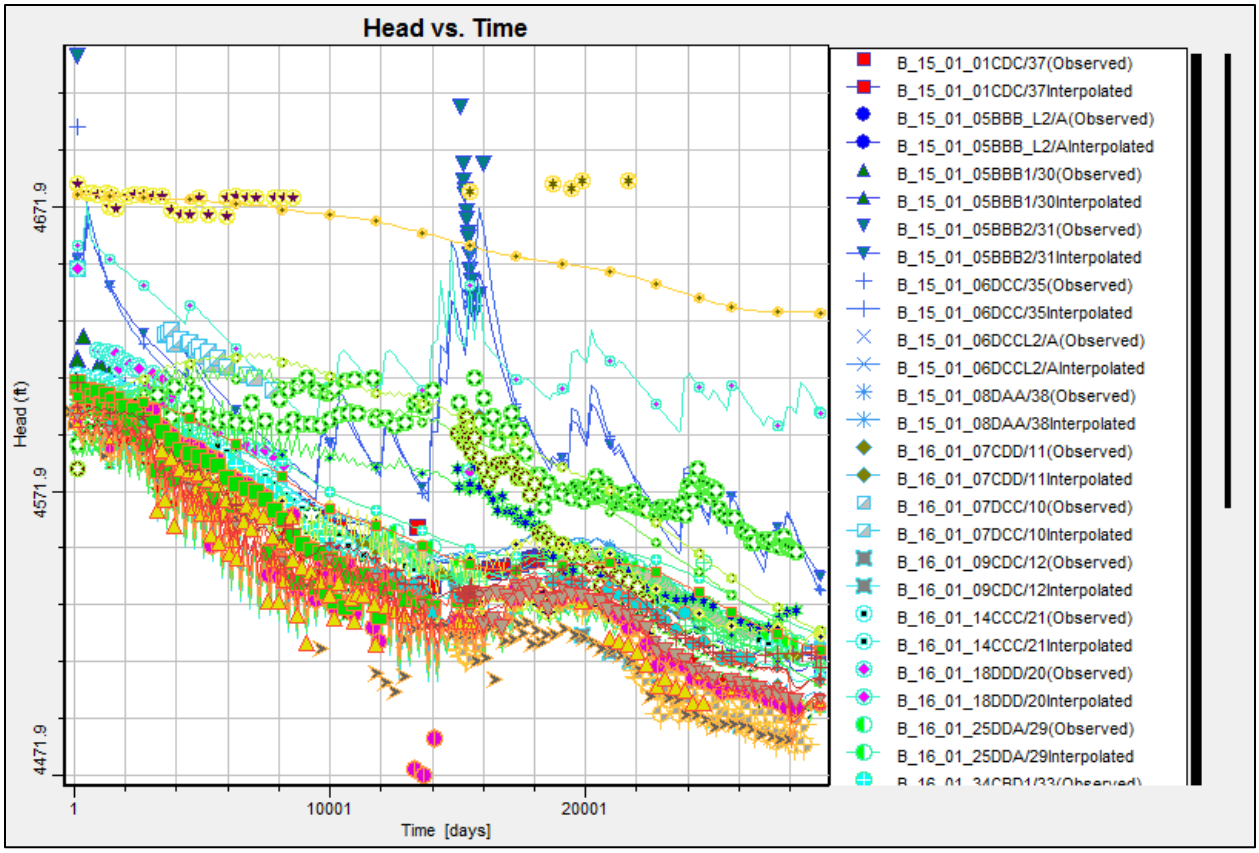

Figure E28. *Comparison of simulated and observed heads in the general LIC Sub-basin. Mean and absolute mean head residual 0.09 and 11 ft, respectively (sample size = 1,556).*

Appendix F – Distribution of Hydraulic Conductivity

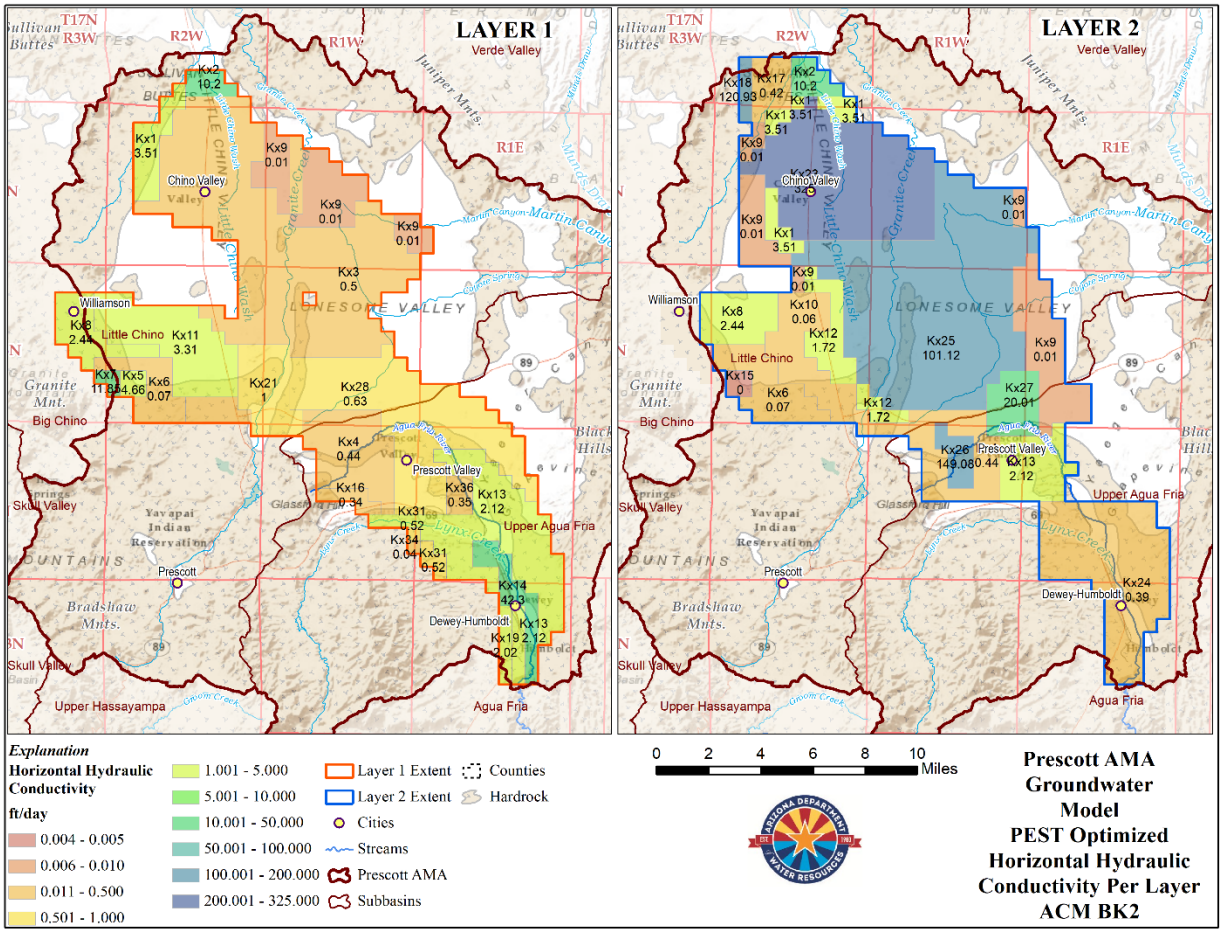

Figure F1. *Distribution of horizontal hydraulic conductivity (K) for model Layers 1 and 2.*